

國立臺灣大學理學院地質科學系

博士論文

Department of Geosciences

College of Science

National Taiwan University

Doctoral Dissertation



Earthworm 平台應用於臺灣地震速報預警研究

Development and Study of Earthworm Platform  
for Earthquake Early Warning in Taiwan

陳達毅

Da-Yi Chen

指導教授：吳逸民 博士

Advisor: Yih-Min Wu, Ph.D.

中華民國 104 年 7 月

July 2015

# 國立臺灣大學博士學位論文 口試委員會審定書

論文中文題目

Earthworm 平台應用於臺灣地震速報預警研究

論文英文題目

Development and Study of Earthworm Platform  
for Earthquake Early Warning in Taiwan

本論文係陳達毅君 (D99224002) 在國立臺灣大學地質學系、所完成之博士學位論文，於民國 104 年 07 月 13 日承下列考試委員審查通過及口試及格，特此證明

口試委員：

(簽名)

(指導教授)

張國彬

蔡瑞·徐璞峻

蕭乃琪

郭陳皓

張建興

金台齡

系主任、所長

(簽名)

(是否須簽章依各院系所規定)

## 誌 謝



感謝吳逸民老師帶領學生進入地震預警研究領域。在學期間隨老師到菲律賓、印度、越南及韓國等地，參觀地震觀測機構並進行地震觀測技術交流，讓學生增廣見聞，受益匪淺。謝謝吳老師的照顧和教導，學生銘記於心。感謝溫國梁老師與郭陳澔老師在口試時細心的指導與中肯的建議，讓學生明白論文不足之處，瞭解未來發展方向。感謝金台齡老師在電腦程式上的幫助，讓學生了解如何撰寫網路程式。感謝樂鐸老師從在台大當博士後期間開始到現在到成大任教，一直給予研究上的建議與協助。

感謝中央氣象局提供在職進修機會，讓我能夠兼顧工作與學業。氣象局提供的環境與資源是這篇論文能夠完成的最主要因素。特別感謝蕭乃祺簡正、張建興簡正與蕭文啟技正的指導與照顧。時常在生活上、工作上與學業上提供的協助，讓我一路走來從一個氣象局地震中心的菜鳥，變成一個能夠獨當一面的學者。

感謝研究室同學們的幫忙，讓口試過程一切順利。感謝研究室助理們辛苦的維護系統，安排每次研究室 meeting 時的大小事宜。感謝吳老師提供場地，在七堵 meeting 時，熱烈的學術討論、清淨舒服的環境、好吃的烤鴨與竹筍湯以及溫暖的氣氛，讓我發現原來做研究也可以這麼怡人。


最後，感謝父母的養育之恩，讓我從小到大都能一路順利的念書與學習。感謝太太宜峰的體諒與支持，讓我可以做喜歡的事情，安心地念書，做研究。

## 摘要



地震預警系統在中央氣象局運作超過十年，過去僅有少數特定機構接收此系統產生的預警訊息。從 2012 年起中央氣象局使用 Earthworm 平台整合來自不同種類的即時觀測資料，並且以此系統進行臺灣地震活動監測。本研究發展的 Earthworm Based Earthquake Alarm Reporting (*e*BEAR) 系統與過去系統相比，能夠縮短資料處理時間並且提升預警資訊的精準度。*e*BEAR 系統中包含三個於 Earthworm 環境下新開發的模組。這些新的模組可以處理：P 波到時挑選、波相組合、地震定位、規模計算及預警訊息發布。本論文主要內容在闡述 *e*BEAR 系統的方法與成效。為了調整此系統，選取 154 個規模 4.0 到 6.5 地震進行離線測試。測試結果顯示，平均地震定位誤差為 4.2 公里，規模誤差為 0.3，系統發佈預警訊息時間為地震發生之後 14.7 秒。另外，實際系統運作情形顯示對於島內及島外地震，平均處理時效分別為地震發生之後 15 秒及 26 秒，比起過去的預警系統平均島內地震快 3.2 秒，島外地震快 5.5 秒。目前 *e*BEAR 系統已經將預警訊息於地震發生之後，即時地傳遞到全國中小學，以爭取在強烈地震波抵達學校前的數秒到數十秒時間發出警報。為持續提升地震監測能力，強化地震預警系統，本研究將 543 個低價位地震儀與中央氣象局地震觀測網整合，建置更高密度地震觀測網。選取 46 個規模 4.5 到 6.5 地震進行離線測試。測試結果顯示，系統發佈預警訊息時間可從地震發生之後 14.7 秒，進步到 13.1 秒。

目前地震預警系統仍存在許多待突破的困難，本文建議如下：對於測站覆蓋的空缺角(GAP)過大時，造成地震定位精確度不良的問題，透過



分析現有測站覆蓋度，建議在台灣東部地區增加測站密度；對於規模大於 7 以上地震可能造成的規模低估情形，建議延長 P 波時間窗，以利完整記錄斷層錯動時所釋放的能量；對於短時間內發生數個地震導致預警系統可能漏報的情形，建議以即時震度分布圖估算地震大略位置與規模。

由於即時地震資料無論是來自不同的地震觀測儀器，或是來自不同的地震觀測機構，都能夠經由 Earthworm 軟體整合至同一個作業平台。因此在 Earthworm 環境下所發展的地震預警系統(eBEAR)能夠有效地在不同的觀測環境下運作。目前 eBEAR 系統已經在印度、韓國及太平洋海嘯警報中心等機構測試。

關鍵字: 地震預警、地震網、P 波預警、Earthworm、Palert

# Abstract



For more than 10 years, the Central Weather Bureau of Taiwan has operated an earthquake early warning (EEW) system and has issued warnings for specific agencies. Since 2012 the Earthworm platform in Taiwan has been used to integrate real-time seismic data streams from different types of seismic stations and to monitor seismicity. Using the Earthworm platform, the Earthworm Based Earthquake Alarm Reporting (*e*BEAR) system is currently in development for shortening reporting times and improving the accuracy of warnings for EEW purposes. The *e*BEAR system consists of new Earthworm modules for managing P-wave phase picking, trigger associations, hypocenter locations, magnitude estimations, and alert filtering prior to broadcasting. Here, we outline the methodology and performance of the *e*BEAR system. To calibrate the *e*BEAR system, an offline test was implemented using 154 earthquakes with magnitudes ranging from  $M_L$  4.0 to 6.5. Comparing between the *e*BEAR and the CWB catalog the results from the offline test show that the epicenter error is about 4.2 km, the standard deviation of magnitude is about 0.3, and the reporting time is about 14.7 s. Additionally, in a comparison of online performance using the current EEW system, the *e*BEAR system reduced reporting times and improved the accuracy of offshore earthquake locations and magnitudes. Online performance of the *e*BEAR system indicated that the average reporting times afforded by the system are approximately 15 and 26 s for inland and offshore earthquakes, respectively. The *e*BEAR system in average can provide more warning time than the current EEW system (3.2 s and 5.5 s for inland and offshore earthquakes, respectively). The *e*BEAR system now delivers warnings to

elementary and junior high schools in Taiwan. For further improving the capabilities of monitoring earthquakes, an EEW system with dense seismic network is constructed by deploying a total of 543 low-cost sensors in Taiwan and incorporating with the official seismic network of Taiwan's Central Weather Bureau (CWB). The experiment results show that the integrated system can have stable results of source parameters and issue alarms faster (from 14.7 s to 13.1s) than the current system run by only the CWB seismic network (CWBSN).

Key Words:

Earthquake Early Warning, Seismic Network, P-wave method, Earthworm, Palert

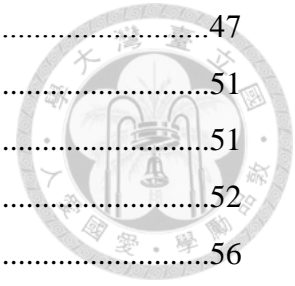
# Contents



Acknowledgements.....	1
Chinese Abstract.....	2
English Abstract.....	4
Contents.....	6
List of Figures.....	8
List of Tables.....	10
1 Introduction.....	11
1.1 Motivation and Research Goal.....	11
1.2 Concept of EEW.....	12
1.3 Worldwide EEW Development.....	14
1.4 Taiwan EEW system.....	15
1.5 Earthworm for EEW system.....	17
1.6 Dissertation Plan.....	18
2 Methods and EEW Modules.....	19
2.1 Earthquake Location Estimation.....	19
2.2 Earthquake Magnitude Estimation.....	21
2.2.1 $\tau_c$ method.....	22
2.2.2 $P_d$ method.....	23
2.3 Earthworm System.....	24
2.4 EEW Modules.....	25
2.4.1 PICK_EEW Module.....	26
2.4.2 TCPD Module.....	27
2.4.3 DCSN Module.....	29
3 <i>e</i> BEAR System in CWB.....	32
3.1 CWB Seismic Network.....	32
3.2 <i>e</i> BEAR System Configuration.....	38
3.3 Offline Test.....	40
3.4 Online Performance.....	43



3.5 EEW Disseminations.....	47
4 Low-cost seismometer for EEW.....	51
4.1 Palert Seismic Network.....	51
4.2 System Configuration.....	52
4.3 Magnitude Estimations Using Palerts.....	56
4.4 Offline Test.....	59
4.5 Summary.....	66
5 A Case Study for Mw7.6 Chi-Chi Earthquake.....	68
5.1 Signal Interruption.....	69
5.2 System Configuration.....	72
5.3 Results.....	73
5.4 Summary.....	76
6 Discussion and Conclusions.....	80
6.1 Station Coverage.....	80
6.2 Magnitude Saturation.....	82
6.3 Multi-Events.....	83
6.4 Application to Earthquake Rapid Reporting System.....	84
6.5 Conclusions.....	85
Reference.....	88
Appendix .....	98
A. Earthworm Software.....	98
A.1 Earthworm Installation.....	98
A.2 Earthworm Features.....	103
B. CWB24 Format.....	109
C. Configure files of EEW modules.....	111
D. Online Display of EEW System.....	115
E. Publications at National Taiwan University.....	117



# List of Figures

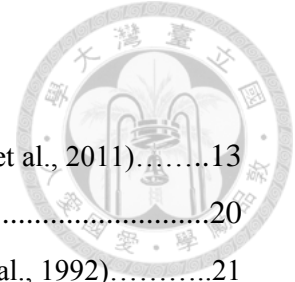
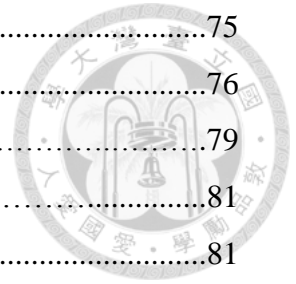


Figure 1-1. Relationship of warning time and epicentral distance. (Satriano et al., 2011).....	13
Figure 2-1. Geometry for velocity given by $v = v(z)$ (Lee et al., 1992).....	20
Figure 2-2. Travel time vs. distance for layer over half-space model (Lee et al., 1992).....	21
Figure 2-3. Two main components in the Earthworm diagram.....	25
Figure 2-4. A flowchart for data processing within the <i>e</i> BEAR system.....	26
Figure 2-5. A flowchart of the algorithms designed for the PICK_EEW module.....	27
Figure 3-1. The station distribution of the CWB Seismic Network.....	33
Figure 3-2. A schematic diagram of the data processing center.....	37
Figure 3-3. A flowchart of the algorithms designed for the PICK_EEW module.....	40
Figure 3-4. A comparison between the offline test and the CWB published catalog.....	42
Figure 3-5. The relationship between reporting time and station coverage gap.....	43
Figure 3-6. Comparisons of location error between the <i>e</i> BEAR and VSN system.....	45
Figure 3-7. Online magnitude error comparison between the <i>e</i> BEAR and VSN system.....	46
Figure 3-8. Online reporting time comparison between the <i>e</i> BEAR and VSN system.....	46
Figure 3-9. Online warning time comparison between the <i>e</i> BEAR and VSN system.....	47
Figure 3-10. Graphical output of the <i>e</i> BEAR system.....	49
Figure 3-11. EEW disseminations of the <i>e</i> BEAR system.....	50
Figure 4-1. Low-cost seismometer.....	51
Figure 4-2. The station distribution of the two seismic networks.....	52
Figure 4-3. A schematic diagram of the data processing of combined seismic network.....	55
Figure 4-4. Relationships between the EEW parameters of combined system.....	55
Figure 4-5. Examples of the automatic P-wave arrival detection.....	58
Figure 4-6. The comparisons of location error between CWBSN and ISN.....	60
Figure 4-7. The comparisons of magnitude error between CWBSN and ISN.....	65
Figure 4-8. The comparisons of reporting time between CWBSN and ISN.....	65
Figure 4-9. The comparisons of blind zone radius between CWBSN and ISN.....	66
Figure 5-1. Distribution of real-time strong-motion stations of CWB.....	70
Figure 5-2. Seismograms recorded in the Chi-Chi Earthquake.....	71

Figure 5-3. System configuration for a case study of Chi-Chi earthquake.....	75
Figure 5-4. Simulation results for six stages after the earthquake occurrence.....	76
Figure 5-5. $P_d$ values of the Chi-Chi earthquake.....	79
Figure 6-1. Station coverage and density.....	81
Figure 6-2. Damage earthquakes in Taiwan (Hsiao et al., 2011).....	81
Figure 6-3. Timeline of the 2015 Hualien earthquake.....	84
Figure 6-4. System architecture of the ERR system and EEW system.....	87



# List of Tables



Table 1. *e*BEAR Picker ( PICK\_EEW ) parameters.....31

Table 2. Data for offline test in integration system.....61

# Chapter 1



## Introduction

### 1.1 Motivation and Research Goal

An EEW system is a practical tool for mitigating earthquake hazards. EEW systems are capable of estimating the occurrence time, location, and magnitude of an earthquake and of issuing warnings before strong ground shaking hits a target area. With timely information, people and manufacturing facilities are able to take the necessary precautions to reduce the seismic hazards caused by large earthquakes.

Taiwan is located on one of the most active seismic zones in the world, in an area where the Philippine Sea plate moves toward the Eurasia plate at approximately 7 cm/yr (Yu et al., 1997). When two tectonic plates collide, stresses accumulate then cause earthquakes. The largest damaging inland earthquake to strike Taiwan in the past 20 years was the 1999  $M_w$  7.6 Chi-Chi earthquake (Shin and Teng, 2001). Because of rapid urbanization in Taiwan, seismic risks have recently increased. For example, the March, 31<sup>st</sup>, 2002  $M_w$  7.1 eastern Taiwan offshore earthquake caused strong ground shaking inside the Taipei basin (Huang et al., 2010). During strong ground shaking, a crane operating on top of the construction area of the Taipei 101, the tallest building in Taiwan (508 m tall), crashed and dropped to the ground. The March, 4<sup>th</sup>, 2010  $M_w$  6.3 Jiasian earthquake brought strong ground motions to southern Taiwan, causing an operating Taiwan High Speed Rail train to run off its tracks (Huang et al., 2011; Wu et al., 2011). Given these types of incidents in Taiwan, a reliable and fast EEW system is urgently

needed to provide early warnings for next large earthquakes.

The purpose of this research is to develop a new EEW system with advanced improvements. Three Earthworm modules were created for managing P-wave phase picking, trigger associations, hypocenter locations, magnitude estimations, and alert filtering prior to broadcasting. Moreover, a low-cost seismic network has been incorporated into the official CWBSN for EEW purpose. Although, some problems existing in the EEW system are not easy to be solved. These problems including earthquakes occurred outside seismic network, magnitude saturation, and multi-event occurred within a short time, were also discussed in this research.

## 1.2 Concept of EEW

EEW systems are designed to provide warnings to people or pre-programmed systems before the intense ground shakings may cause damage to target areas. Because the velocity of seismic waves (about 3.5 km/s for S wave) is slower than the speed of communication, it is possible to obtain several to several tens of seconds for reducing damages. With a timely issuance of earthquake information (location and magnitude) provided by EEW systems after large earthquakes, we can take immediate precautions against seismic hazards. In general, there are two types of EEW systems. One is on-site EEW system in which the seismometers are deployed in the protected area. This kind of system uses the information of P waves, which propagates faster, to predict the later S waves which have larger amplitudes. The other one is regional EEW system in which the seismometers are deployed in some remote sites from the protected area. This kind of system uses information from those seismometers near the epicenter to determine certain

source parameters and then issue warnings to the target area. Figure 1-1 shows the relationship of warning time and epicentral distance. It demonstrates that the onsite system can provide a warning to targets closer to the epicenter.

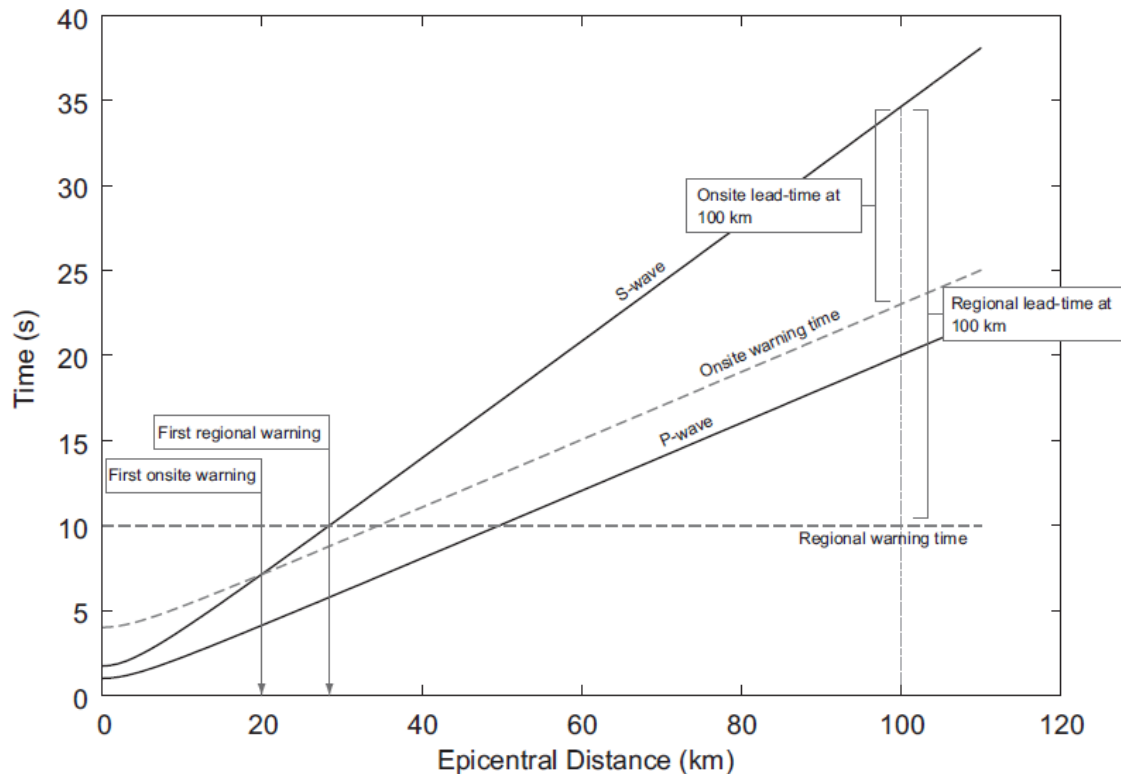
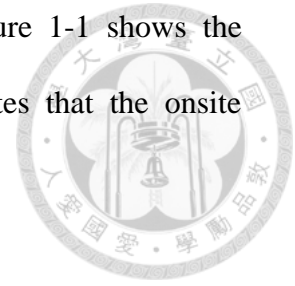


Figure 1-1. Relationship of warning time and epicentral distance. (Satriano et al., 2011)

Currently, the earthquake locations can be well determined by the P-wave arrivals obtained by dense stations around the source area (Rydelek and Pujol 2004; Satriano, 2008). However, the most challenging work in EEW system is to improve the reliability and accuracy of the empirical method for estimating earthquake magnitude since only the initial portion of seismic waves are used. Based on the precise magnitude and hypocenter estimates, the ground motion can be predicted reliably. On the other hand, overestimation and underestimation of earthquake magnitude may lead to releases of false or missed

alarms that would result in additional economic loss and societal impacts.



### 1.3 Worldwide EEW Development

The EEW system is becoming a key practical tool for mitigating loss due to seismic events. Depending on the distance to the earthquake, it provides a few seconds to a few tens of seconds warning for people and automated facilities. Currently, many countries have an online operating or experimental EEW system, such as Japan (Nakamura 1988; Odaka et al., 2003; Horiuchi et al., 2005; Wu and Kanamori 2008b), Taiwan (Wu et al., 1998; Wu et al., 1999; Wu and Teng 2002; Hsiao et al., 2009; Hsiao et al., 2011), Mexico (Espinosa-Aranda et al., 1995; Espinosa-Aranda et al., 2009), the United States (Allen and Kanamori 2003; Wu et al., 2007; Allen et al., 2009; Bose et al., 2009a), Italy (Zollo et al., 2006; Zollo et al., 2009), Turkey (Alicik et al., 2011), Beijing (Peng et al., 2011), and Romania (Bose et al., 2009b).

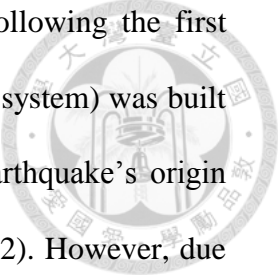
The station coverage gap (GAP), defined as the angle between epicenter and two adjacent stations, can be used as a metric for evaluating the quality of an EEW report (Wu et al., 1997; Wu et al., 2013a). A dense seismic network can provide a sufficient number of triggered stations to reach the good coverage of seismic stations (e.g., a small value of GAP) within a relative short time after an earthquake occurs. Therefore, it can be a potential solution to provide faster and more reliable earthquake early warnings. However, it is expensive to deploy a large number of traditional seismic stations. Fortunately, recent advances in electrical and mechanical technologies have made it possible to build low-cost seismometers for constructing dense seismic networks. Holland (2003) first monitored earthquakes using seismic data streams from low-cost seismometers and



short-period seismic sensors. The concept of home seismometers has been implemented in Japan (Horiuchi et al., 2009). The Quake Catcher Network (QCN) project is able to rapidly expand and increase the density of ground-motion observations with relative low cost (Cochran et al., 2009). The QCN initiated Rapid Aftershock Mobilization Programs (RAMP) following the 2010 M7.2 Darfield, New Zealand, earthquake (Lawrence et al., 2014), respectively. The results demonstrated that the QCN can be used to detect and locate moderate to large earthquakes, and estimate their magnitudes using ground-motion parameters. The Self-organizing Seismic Early Warning Information Network (SOSEWIN) has been tested in Istanbul based on wireless communications (Fleming et al., 2009).

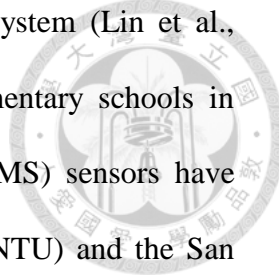
## 1.4 Taiwan EEW Development

Over the years, many studies have been conducted regarding the development of an EEW system in Taiwan. In 1995, an earthquake rapid reporting system began operating on the basis of 16-bit strong-motion seismometers and was a type of early-stage EEW system for Taiwan (Wu et al., 1997). Although the system could not issue warnings prior to large ground shaking, it provided rapid reporting within 102 s for the Chi-Chi earthquake and was the leading technology at that time (Wu et al., 2000). As EEW system necessity demanded, the Central Weather Bureau (CWB) was the first to test an EEW prototype system within the Hualien area in Taiwan. To reduce reporting times and provide early warnings for distant metropolitan regions, a new idea, based on the prototype system, was proposed for applying the subnetwork method to earthquake monitoring (Wu et al., 1999). Using the subnetwork concept and  $M_{L10}$ , a quick magnitude



determination method (Wu et al., 1998) that adopted 10 s records following the first P-wave arrival, the current EEW system (the virtual subnetwork [VSN] system) was built and achieved an average 22 s reporting time (the time between an earthquake's origin time and the time the EEW system issues a report) (Wu and Teng, 2002). However, due to the limits of the  $M_{L10}$  method, the reporting time could not be reduced to within 10 s. To further reduce reporting times, the P-wave method, based on the peak amplitude of displacement records ( $P_d$ ) for the vertical component using a 3 s time window for magnitude determinations (Wu and Zhao, 2006), was tested and operated (Hsiao et al., 2009, 2011). The CWB has recently upgraded seismic facilities within the original seismic network and deployed 30 borehole stations, as well as one cable-based ocean-bottom seismic station. At the same time, to enhance the density and coverage of station distributions, real-time seismic data streams from various seismic networks were integrated using the Earthworm platform, a program originally developed by the U.S. Geological Survey (Johnson et al., 1995). Based on the above, an Earthworm-based EEW prototype system was constructed and has been tested since 2007 (Hsiao et al., 2011; Chen et al., 2012).

In addition, some experimental on-site EEW systems have been tested and operated as well. Wu et al., (2006) determined the relationships between the earthquake magnitude and characteristic parameters from the first three seconds of the P-wave. They demonstrated that single-station approach can be used to estimate earthquake magnitudes well. Wu et al., (2011) demonstrated that the on-site EEW system can provide valuable information to the Taiwan High Speed Railway in the 2010 JiaSian earthquake. The National Center for Research on Earthquake Engineering (NCREE) has developed neural



network method for predicting structural response in on-site EEW system (Lin et al., 2011). The on-site EEW system has been put into practice in elementary schools in Taiwan (Lin, 2011). Some Micro Electro Mechanical Systems (MEMS) sensors have been developed for EEW system. The National Taiwan University (NTU) and the San Lien Corporation, a high-tech oriented company (<http://www.sanlien.com.tw>), have developed an accelerometer, named Palert, based on MEMS technology. The Palert Seismic Network (PSN) has been tested and operated for both on-site and regional EEW systems by NTU since 2010 and is capable of providing high quality and stable data streams for earthquake monitoring (Wu et al., 2013b; Hsieh et al., 2014; Wu, 2014).

## 1.5 Earthworm for EEW system

Earthworm is a popular software for real-time earthquake monitoring. It has been used all over the world. There are five advantages of the Earthworm system. First, Earthworm is free and open source. It makes the system operator easy to modify it and save cost. Second, Earthworm can receive real-time data streams from different kinds of seismic instruments. Even those sensors are made from different companies, Earthworm is able to integrate all data in the same platform. Third, Earthworm was composed by modules. Users can take different set of modules to construct their own Earthworm system. Moreover, because modules are running separately, users can create new modules without disturbing current modules. Forth, in the same computer, Earthworm uses shared memories for communicating message with other modules. Among different computers, Earthworm use TCP/IP protocol to exchange messages. In this way, Earthworm can efficiently exchange message among modules and process data in parallel.

Compared to the former EEW system in Taiwan, Earthworm system provides an excellent opportunity to improve the construction of the EEW system. Instead of using telephone line for real-time data transmitting in old EEW system, for modern system, data are packed as 1-sec length packet and transmitted based on TCP/IP protocol. Earthworm can integrate all data and be a server to provide real-time waveforms to clients as long as the internet is available. In addition, Earthworm can process data in memory. It is more efficient than processing data using text or binary files.

## 1.6 Dissertation Plan

In this dissertation, the fundamental EEW concepts and the review of EEW researches are introduced in chapter 1. Methods of location and magnitude estimations, and EEW modules are described in chapter 2. EEW system in CWB is described in chapter 3. Integrating low-cost seismic network and official seismic network is described in chapter 4. A case study of the  $M_w$  7.6 Chi-Chi earthquake is described in chapter 5. Discussion and Conclusions are described in chapter 6.

# Chapter 2



## Methods and EEW Modules

### 2.1 Earthquake Location Estimation

Consider a one-dimensional continuous velocity model, shown as Figure 2-1. In this case, the ray equation becomes:

$$\frac{1}{v(z)} \frac{dx}{ds} = \text{const}, \quad \frac{d}{ds} \left( \frac{1}{v(z)} \frac{dz}{ds} \right) = -\frac{1}{v^2} \frac{dv}{dz}$$

where the velocity,  $v(z)$ , is a function of depth ( $z$ ),  $ds$  is the differential of ray path. In

Figure 2-1, the direction cosines are:

$$\begin{aligned} \cos \alpha &= \frac{dx}{ds} = \sin \theta \\ \cos \gamma &= \frac{dz}{ds} = \cos \theta \end{aligned}$$

Then, a 'Snell's Law' can be obtained:

$$\frac{\sin \theta}{v(z)} = \text{const.} \equiv p$$

where  $p$  is called the ray parameter. The velocity is given by:

$$v(z) = g_0 + gz$$

Where  $g_0$  and  $gz$  are constants,  $z$  is depth. In Figure 2-1, the center of this arc is given by:

$$x_c = \frac{x_B^2 - 2(g_0/g)z_A - z_A^2}{2x_B}, \quad z_c = \frac{-g_0}{g}$$

The travel time of this linear velocity is:



$$T = \int_{\theta_A}^{\theta_B} \frac{d\theta}{g \sin \theta} = \frac{1}{g} \ln \left[ \frac{\tan(\theta_B/2)}{\tan(\theta_A/2)} \right]$$

$$\theta_A = \tan^{-1} \left( \frac{z_A - z_C}{x_C} \right), \quad \theta_B = \tan^{-1} \left( \frac{-z_C}{x_B - x_C} \right)$$

Finally, the spatial derivatives of travel time,  $T$ , at the source are:

$$\left. \frac{\partial T}{\partial x} \right|_A = \frac{-\sin \theta_A}{(g_0 + g z_A)}$$

$$\left. \frac{\partial T}{\partial z} \right|_A = \frac{-\cos \theta_A}{(g_0 + g z_A)}$$

In the procedure of the Geiger's method (1910, 1912), a half-space model was used to calculate the predicted travel times. Figure 2-2 shows the relationship between the travel time and the distance.

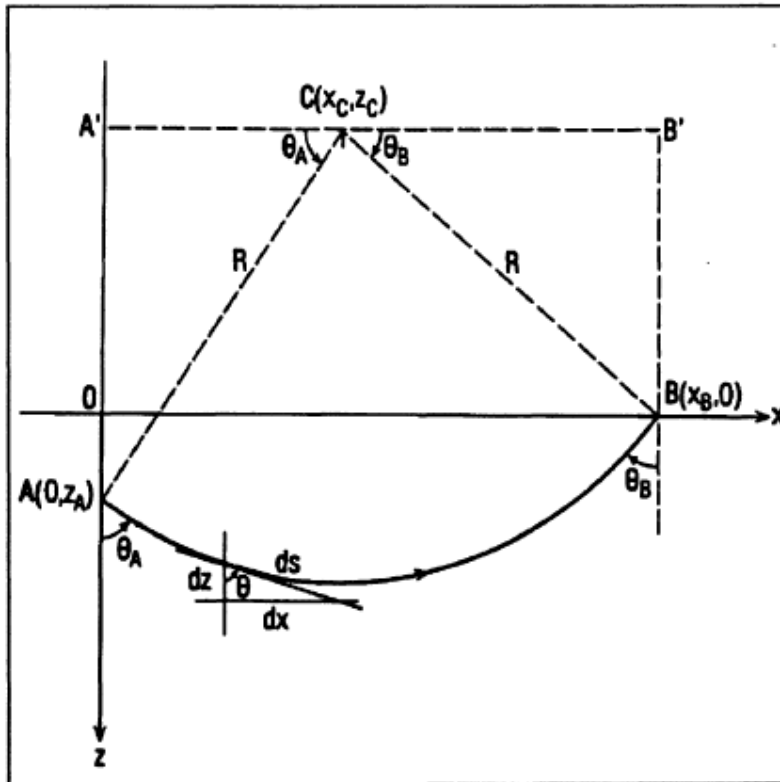


Figure 2-1. Geometry for velocity given by  $v = v(z)$  (Lee et al., 1992).

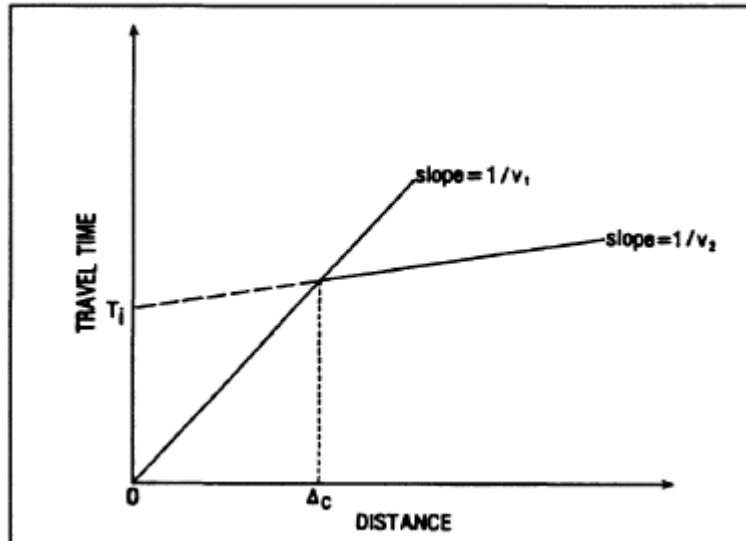


Figure 2-2. Travel time vs. distance for layer over half-space model. (Lee et al., 1992)

## 2.2 Earthquake Magnitude Estimation

To precisely measure the size of an earthquake, we must take a certain length of time window extending after the P-wave arrival until the enough observed waveforms are available. This time window has variant values depending on different EEW algorithms and is one of the components adding a delay to the overall alert time (Behr et al., 2015). For EEW purposes, it is necessary to detect earthquake magnitude in the beginning stage of the earthquake occurrence. Wu and Teng (1998) used an empirical method to correlate local magnitude and the predicted magnitude over 10 seconds after the first P-wave arrival is detected. Recently, P-wave methods has been widely studied and implemented in EEW systems. There are two kinds of the P-wave methods. One is associated with the frequency content of the initial waveforms. Allen and Kanamori (2003) has proposed a method based on the predominant period ( $\tau_p$ ) measured over a varying time window after the P-wave arrival. When 1-, 2-, 3-, and 4-s time window of data are available, the  $\tau_p$

values are measured and the magnitude would be updated. In addition, the average period parameter ( $\tau_c$ ) of the initial 3-s P waves can be used for estimating magnitudes (Wu and Kanamori, 2005). The other kind of P-wave method is associated with the amplitude content of the initial waveforms. Wu and Zhao (2006) take the peak amplitude in vertical displacement ( $P_d$ ) over a 3-s time interval after P-wave arrival. They showed that the upper limit of the magnitude prediction is 6.5 because the time window is too short to contain whole rupture information from larger events. Using the combinations of P and S wave signals, Zollo et al., (2006) demonstrated that the peak displacements measured in 2-s P-wave time window and 2-s S-wave time window can be correlated with magnitude in the ranged from 4.0 to 7.4. Lancieri and Zollo (2008) used peak displacement over 2- and 4-s P-wave time window and 1- to 2-s S-wave time window with Bayesian approach to estimate magnitude at each time step.

### 2.2.1 $\tau_c$ Method

Following the procedure from Wu and Kanamori (2005a), take the ground-motion displacement,  $u(t)$ , and velocity,  $u'(t)$ , from the vertical component record and compute the following ratio  $r$  by

$$r = \frac{\int_0^{\tau_0} \dot{u}^2(t) dt}{\int_0^{\tau_0} u^2(t) dt}$$

where the integration is over the time interval  $(0, \tau_0)$  after the onset of the P wave.

Usually,  $\tau_0$  is set at 3 sec. Using Parseval's theorem,



$$r = \frac{4\pi^2 \int_0^\infty f^2 |\hat{u}(f)|^2 df}{\int_0^\infty |\hat{u}(f)|^2 df} = 4\pi^2 \langle f^2 \rangle$$



where  $\hat{u}(f)$  is the frequency spectrum of  $u(t)$ , and  $\langle f^2 \rangle$  is the average of  $f^2$  weighted by  $|\hat{u}(f)|^2$ . Thus,

$$\tau_c = \frac{1}{\sqrt{\langle f^2 \rangle}} = \frac{2\pi}{\sqrt{r}}$$

can be used as a parameter representing the period of the initial portion of the P wave.

The larger  $\tau_c$  is, the larger the event is. Following Wu et al., (2007), a regression equation can be used for magnitude estimation:

$$M = 4.218 \log \tau_c + 6.166 \pm 0.385$$

### 2.2.2 $P_d$ Method

The peak amplitude of the initial P-wave displacement,  $P_d$ , reflecting the attenuation relationship of the ground motion with distance, can be used as an amplitude parameter to predict sizes of earthquakes. Therefore, if we can determine the attenuation relationship of  $P_d$ , then we can use  $P_d$  to estimate the magnitude when the hypocentral distance is available. Only vertical-component records are used to determine  $P_d$ . The seismograms are integrated once or twice to obtain the displacement and then a 0.075 Hz high-pass recursive Butterworth filter is applied to remove the low-frequency drift after the numerical integration. We assumed a linear relationship among the logarithmic  $P_d$ , the magnitude  $M$  and the logarithmic hypocentral distance  $R$ :

$$\log P_d(R) = A + B \cdot M + C \cdot \log(R)$$

where A, B and C are constants to be determined; R is hypocentral distance; M is magnitude; the units of  $P_d$  and R are cm and km, respectively.



## 2.3 Earthworm System

Earthworm is a software originally developed by the United States Geological Survey (USGS) since 1994. The preliminary purpose was to construct a system which is able to quickly notify earthquake information to the public. Earthworm has been developed and improved continuously by users because Earthworm is a free and open-source software. Currently, Earthworm has become a robust and well tested software. Many earthquake monitoring center use this software to detect earthquakes and archive waveform records. The software has also been successfully extended to volcano observation and is also used in many tsunami centers.

Because of two main components in the earthworm, the system can be enlarged and become more dedicate. Figure 2-3 shows the two main components in the Earthworm (module and shared memory). With shared memories, modules can exchange information directly in the memory. Every Earthworm system can have different compositions of modules and shared memories. Based on this design, the Earthworm system is very flexible and maintainable.

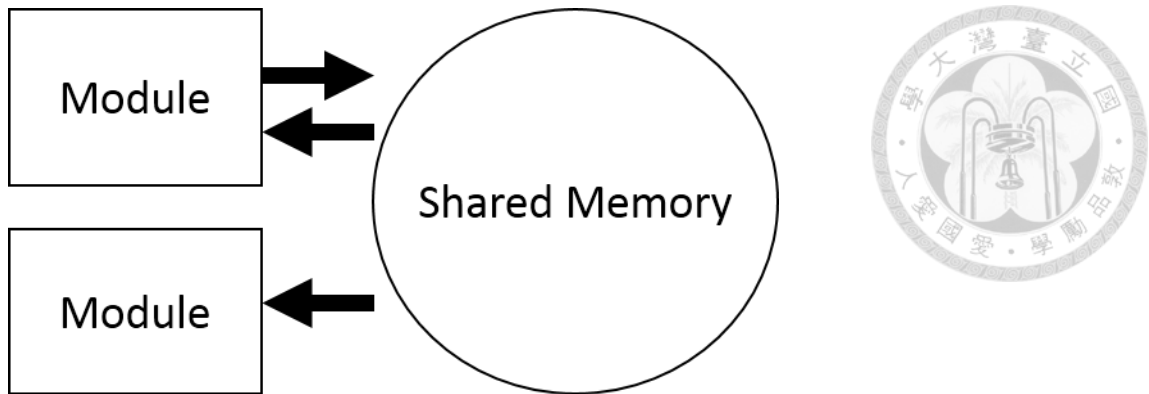


Figure 2-3. Two main components in the Earthworm diagram. The rectangle represents a module; the circle represents a shared memory. Modules can exchange data with shared memories.

Earthworm is a command-line based system. It is not easy to install and be understood.

The procedure of Earthworm installation described in Appendix A.1 is useful for quickly setup Earthworm system. In addition, a summary of the Earthworm features are described in Appendix A.2.

## 2.4 EEW Modules

An Earthworm diagram that describes data flow within the *e*BEAR system is provided in Figure 2-4. For system calibration, we ran the system in offline mode using the TANKPLAYER module. To receive real-time data for online operations, we applied the IMPORT module. The three circles provided in Figure 2-4 represent shared memories within Earthworm. The first shared memory, WAVE\_RING, contains waveform data that can be processed using the PICK\_EEW module to determine P-wave arrivals, as well as the peak amplitudes for P-wave displacement ( $P_d$ ), velocity ( $P_v$ ), and acceleration ( $P_a$ ) within a 3 s time window. The second shared memory, PICK\_RING, not only contains

information from the PICK\_EEW module, but also provides information to the TCPD module for generating earthquake messages, including source parameters. When an earthquake occurs, the TCPD module may update information for the event and create earthquake messages. Updated earthquake messages are stored within the third shared memory, HYPO\_RING. At the end of the process, the DCSN module filters earthquake messages using specific criteria (as discussed later) and generates EEW reports for broadcasting as an XML-formatted file.

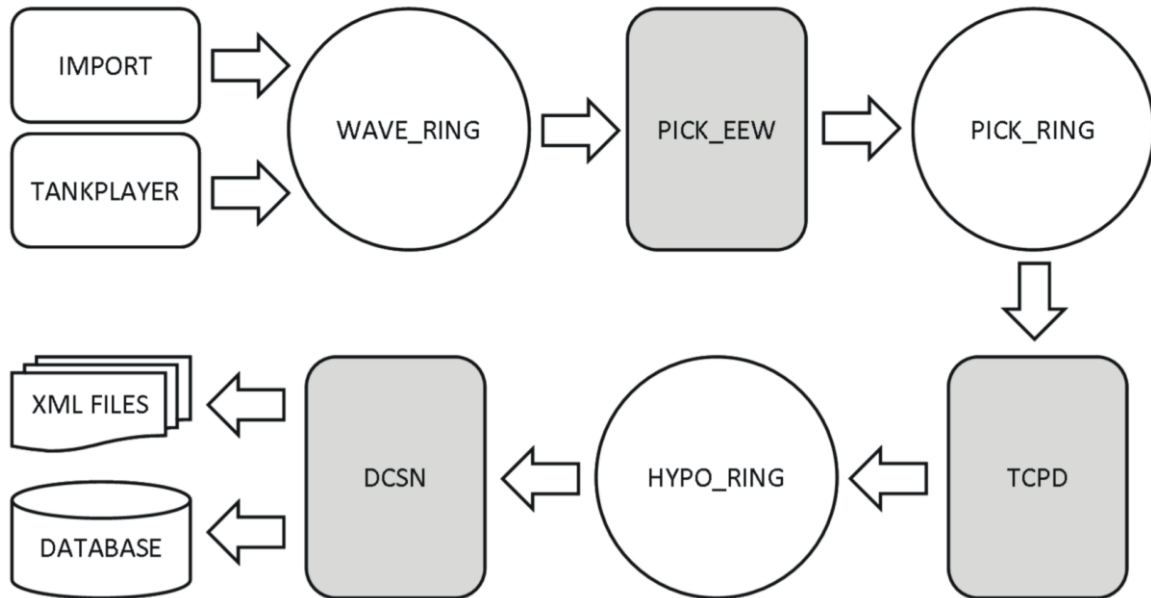


Figure 2-4. A flowchart for data processing within the eBEAR system.

### 2.4.1 PICK\_EEW Module

The original Earthworm module, PICK\_EW, requires time to check the seismic coda term within the auto-picking procedure. The work is time consuming and not suitable for EEW systems. Therefore, we created a new module named PICK\_EEW by revising the module to run without checking the seismic coda term. To avoid false pickings caused by

background noise, we also added two parameters,  $P_a$  and  $P_v$ . Because seismic waveforms from field stations have different noise levels depending on vibrations from the natural environment or artificial activities, these two parameters can be used as thresholds for ignoring spikes caused by noise. Table 1 provides the parameters we used in the PICK\_EEW module of the eBEAR system. The parameters are modified from the Earthworm's module named PICK\_EW. Some parameters related to the coda term are eliminated. Two parameters,  $P_a$  and  $P_v$ , are added.

Figure 2-5 displays the procedure for P-wave autopicking. The PICK\_EEW module declares possible picks based on the short-term average (STA) and long-term average (LTA) algorithm. To become a candidate pick of a seismic trace, the ratio of STA/LTA should be greater than two times a certain threshold. Following a pick based on the threshold, and to distinguish ground noise and the seismic signal, we considered three additional conditions: the number of zero crossings, the signal-to-noise ratio, and the  $P_a$  and  $P_v$ . Using this procedure, the module was able to qualify the candidate pick as a valid seismic pick. In practice, because each seismic station has different background noise, we tested different sets of picking parameters by performing an offline test.

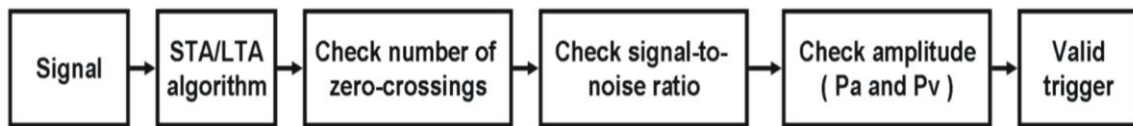
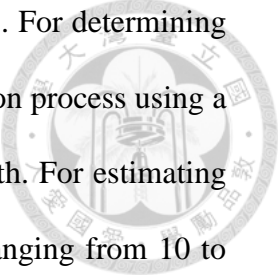


Figure 2-5. A flowchart of the algorithms designed for the PICK\_EEW module.

## 2.4.2 TCPD Module

After the TCPD modules jointly trigger using a space-time window based on



expected travel times, the event hypocenter is estimated using two steps. For determining the event epicenter, the module first adopts Geiger's method, an inversion process using a half-space velocity model in which velocity linearly increases with depth. For estimating event depth, the module then uses a grid search method with depths ranging from 10 to 100 km in steps of 10 km. Theoretical travel times to each station are calculated and compared to those observed at each depth. Finally, the depth with minimum residuals and the epicenter determined by Geiger's method are considered as the event hypocenter. The procedure is performed within the TCPD module via an updating process. At the beginning of the process, after at least six picks of seismic waveforms, the TCPD module begins to locate an event. When the root mean square of travel-time residuals resulting from the inversion process is larger than 0.8, the pick with the largest travel-time residuals is removed and the inversion process is again performed. When additional picks of seismic waveforms participate, the procedure of hypocenter determination is repeated and the estimated hypocenter is updated.

Earthquake magnitudes are predicted using the initial portion of P-wave peak displacement  $P_d$  within the 3 s time window. Following a double-integrated, strong-motion, and integrated broadband, the PICK\_EEW module applies a 0.075 Hz high-pass filter to displacement records. The  $P_d$  value is then used to estimate magnitude ( $M_{Pd}$ ) based on empirical formula. The empirical formula for borehole stations has not yet been established. Earthquake magnitude is estimated by obtaining an average for each  $M_{Pd}$  value from each seismic station. However, the false picking of P-wave arrivals, the directivity effect, and site effects may lead to unreasonable  $M_{Pd}$  values. For obtaining robust estimations of magnitude and to reduce errors, three steps are applied. First, only

$M_{Pd}$  values within one standard deviation of the dataset are used. Next, each record is weighted according to P-wave travel-time residuals. The weighting factor is expressed as

$$W_i = \left( \frac{1}{1 + |R_i|} \right)^2 \quad (1)$$

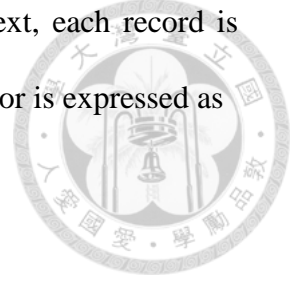
in which  $W_i$  is the weighting factor of each  $M_{Pd}$  value and  $R_i$  (in seconds) is the P-wave travel-time residual for each corresponding  $M_{Pd}$  value. Finally, a weighted average for obtaining earthquake magnitude is expressed as

$$M = \sum \left( \frac{W_i}{\sum W_i} \times X_i \right) \quad (2)$$

in which  $X_i$  is the  $M_{Pd}$  value for each station.

### 2.4.3 DCSN Module

When an earthquake occurs, the number of seismic picks are increased as seismic waves propagate away from the epicenter. As a result, the TCPD module determines the earthquake message and continuously updates that message. We propose that the numbers of updating earthquake messages will increase quickly and will be significant for large and local earthquakes. In contrast, for small earthquakes or for noise, the number of updating earthquake messages will increase slowly and will be small. Therefore, if the EEW system determines a large number of updating earthquake messages for an ongoing earthquake, we consider the EEW information as a reliable warning. To prevent false alarms, the DCSN module always skips the first and second earthquake message generated from the TCPD module. The third earthquake message is the first EEW report



to users. The EEW report is written in an XMLformatted file for broadcasting. The EEW report is updated either when differences in the magnitude or the epicenter are larger than 0.5 or 20 km, respectively, as compared to the last EEW report. A user display pops up automatically when an XML-formatted message is received. The display estimates the seismic intensity, the wave fronts of P- and S-waves, and the remaining warning time (defined as the time between the reporting time and the arrival of the S wave to the target area). If the EEW report is updated, the user display directly changes the location of the epicenter and again re-estimates EEW-related parameters.

The DCSN module takes the EEW report from the HYPO\_RING for other applications such as generating the XML-formatted messages for clients running the EEW display and warning program provided by the CWB (Chen et al., 2015). The DCSN module will also pop up EEW messages on the corresponding CWB staff's computers, insert EEW message into the MySQL database, and archive the triggered seismic waveforms.



Table 1. *e*BEARS Picker ( PICK\_EEW )

Modified from the PICK\_EW



Parameters	Short Description	Default Value
MinSmallZC	Defines the minimum number of zero-crossings for a valid pick within the first second after P-wave arrival.	3 for broadband or 5 for acceleration
MaxMint	The maximum interval (in samples) between zero crossings.	100
RawDataFilt	Sets the filter parameter RawDataFilt applied to the raw trace data.	0.939
CharFuncFilt	Sets the filter parameter CharFuncFilt applied during calculations of the characteristic function of waveform data.	3
StaFilt	Sets the filter parameter (time constant) StaFilt used in the calculation of the short-term average (STA) of the characteristic function of the trace.	0.6
LtaFilt	Sets the filter parameter (time constant) LtaFilt used in the calculation of the long-term average (LTA) of the characteristic function of the trace.	0.15
EventThresh	Sets the STA/LTA event threshold.	5
RmavFilt	The filter parameter (time constant) used to calculate the running mean of the absolute value of the waveform data.	0.9961
DeadSta	Sets the dead station threshold (counts).	1000000
MinPa (new)	Defines the minimum value of peak amplitude for acceleration (unit is cm/sec <sup>2</sup> )	0.01
MinPv (new)	Defines the minimum value of peak amplitude for velocity (unit is cm/sec)	0.0001

# Chapter 3



## *e*BEAR System in CWB

### 3.1 CWB Seismic Network

Currently, two seismic networks are operated within the CWB. The first network, the Real-Time Data stream (RTD) seismic network, consists of 110 stations equipped with one Geotech Smart24A seismometer that transmits real-time, strong-motion data to the CWB via 4800-baud leased telephone lines. Each telemetered signal is digitized at 50 samples per second using a 16-bit resolution. The current EEW system, VSN, operates within this seismic network. The second, the Central Weather Bureau Seismic Network (CWBSN), is an upgraded and integrated network that improves data quality, station coverage, and density by integrating various types of seismic stations and seismic networks from other institutes. The *e*BEAR system is operated under the CWBSN. The station distribution of the CWBSN, which integrates different types of seismic stations operated by the CWB and the Institute of Earth Sciences (IES) of Academia Sinica (which provides waveforms for 23 stations from the Broadband Array in Taiwan for Seismology), is shown in Figure 3-1. In addition, using a connection to buffer uniform data of the Incorporated Research Institutions of Seismology (IRIS), one Japanese station (YOJ) has been merged into the monitoring network and has improved station coverage within the eastern offshore region of Taiwan. Each real-time seismic signal, digitized at 24-bit resolution and obtained using time stamps from a Global Positioning System, is packed and transmitted to CWB headquarters in Taipei via Ethernet or Internet. With the

exception of IRIS data at 20 samples per second, digital signals are digitized at 100 samples per second.

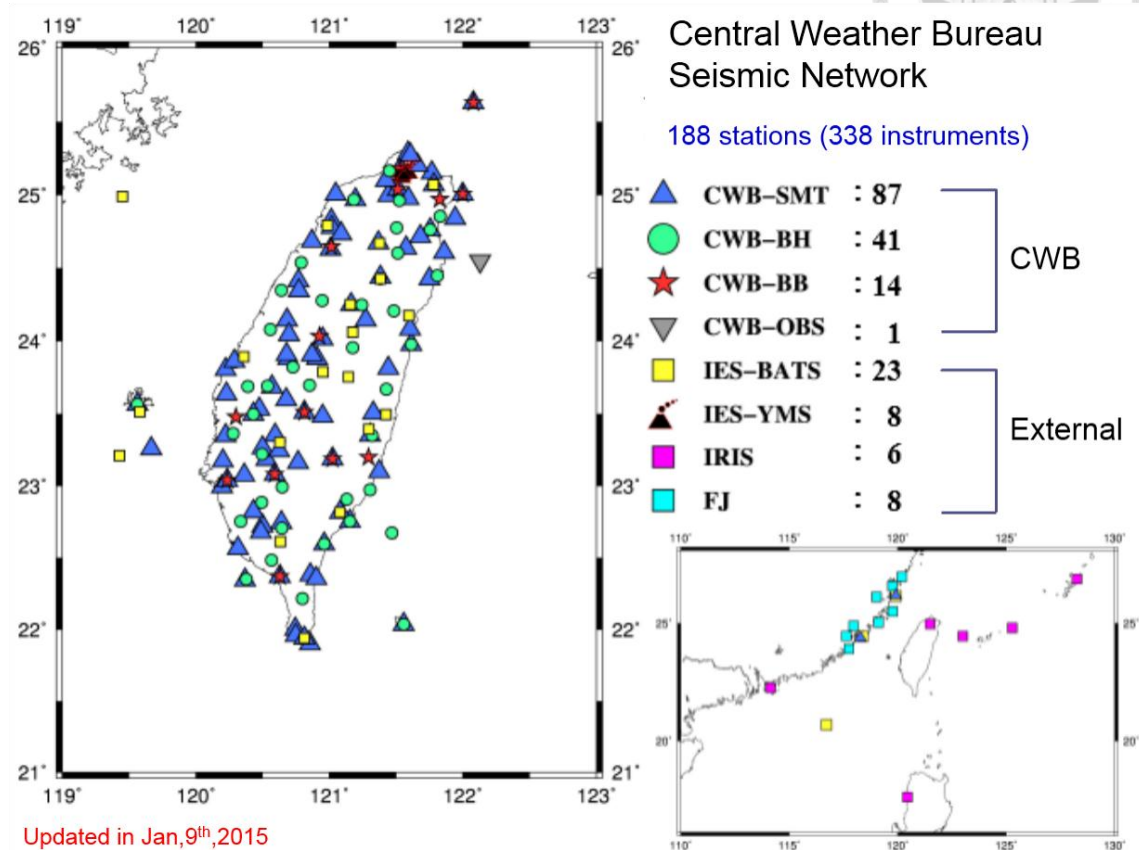
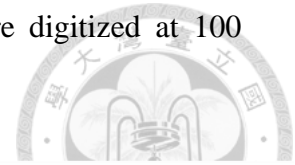


Figure 3-1. The station distribution of the CWB Seismic Network.

The CWBSN consists of four types of seismic stations including six-channel seismic stations, broadband seismic stations, borehole seismic stations, and one cable-based ocean-bottom seismic station. Among seismic stations, some have been upgraded from older types, while others have been newly added. Six-channel seismic stations were upgraded and combined from original short-period and strong-motion instruments, digitized at 12- and 16-bit resolutions, respectively (Teng et al., 1997). Prior to station upgrades, two types of instruments were operated separately and transmitted data through telephone lines; signal time was stamped by the central station (Chang et al., 2012). Since

2007, using Geotech Smart24A accelerometers to replace the original instruments (Geotech A900A) and to connect Teledyne Geotech S13 short-period sensors, the CWB has combined these two types of seismic signals. As a result, 70 upgraded six-component stations have been constructed, each hosting three-component short-period velocity sensors and one three-component strong-motion sensor.

For EEW purposes, the data loggers located at broadband seismic stations were replaced using modern equipment capable of sending seismic waveforms with a 1 s packet length. The system consists of 23 stations that use one three component broadband seismograph. To prevent clipped waveforms caused by near-field strong shakings, most stations are equipped with an additional three-component strong-motion sensor. Such high-quality waveforms are also used to obtain centroid moment tensor (CMT) solutions (Shin et al., 2013).

In addition, 30 borehole seismic stations are operational. Each hosts a three-component strong-motion seismograph on the surface and a three-component strong-motion seismograph, as well as a broadband seismograph within boreholes at a depth of approximately 300 m from the surface. Seismic signals from borehole seismometers provide waveforms with a high signal-to-noise ratio, useful for improving the accuracy of phase picking. Since 2008, the number of borehole seismic stations has increased by approximately five stations each year. In the near future, the total number of borehole stations will increase to 70.

In November 2011, the first cable-based ocean bottom seismometer, the Marine Cable Hosted Observatory (MACHO), began operating in Taiwan. The MACHO has one seismic station located within the northeastern offshore area of Taiwan, with a cable line

length of 45 km, and hosts a three-component strong-motion accelerometer and a three component broadband seismograph (Hsiao et al., 2013). The MACHO is very expensive, and only one station is currently in operation. However, because the Philippine Sea plate subducts beneath the Eurasia plate of northeastern Taiwan and since many large earthquakes have occurred in this area in the past, the MACHO system is critical to the EEW system. The MACHO is capable of detecting seismic waves faster than inland stations.

All CWBSN waveforms are archived in CWB24 Format, shown in Appendix B. The CWB continuously records all seismic waveforms and archives into file every four minutes. Every day the CWB staff manually scan the continuous files and cut individual earthquake as a file. These files can be used for adjusting auto-picking parameters.

Figure 3-2 provides the system configuration of the CWBSN for a three-layer structure within the data-processing center used for the acquisition, integration, and application of real-time seismic signals. In the first layer, real-time seismic data streams are packaged and transmitted from field stations or external seismic networks then received by commercial software or Earthworm via various Internet Protocol (IP)-based networks. SMARTGeoHub and Scream software packages are used to receive real-time seismic waveforms from instruments made by Geotech and Güralp, respectively. Seismic waveforms from external seismic networks provided by IES and IRIS are received using the Earthworm modules IMPORT\_ACK and SLINK2EW, respectively. In the second layer, an Earthworm cluster integrates seismic data streams from different seismic instruments and provides two types of seismic waveforms. One waveform type, WAVE\_SERVERV, can store and provide seismic waveforms over a period of time and

is used for data displays and archives. The second waveform type, EXPORT\_ACK, can provide data streams much faster than the previous one and is used for real-time data processing. For system backup, two computers running WAVE\_SERVERV and three computers running EXPORT\_ACK are operated in parallel. In the third layer, also called the application layer, several tasks are performed. These include EEW operation, the generation of products obtained from the earthquake catalog and the CMT, the maintenance of the seismic waveform data archive, and the display.

Via its modules and shared memory regions, the Earthworm system is designed for automatic seismic data processing (Johnson et al., 1995). Each module has specific tasks such as data acquisition, processing, and archiving. Adopting shared memory regions makes it convenient for each module to easily receive or broadcast messages such as waveform data, P-wave arrivals, hypocenter, and magnitude. Earthworm prepares seismic-related modules and is open source. Therefore, users can use existing modules or create new modules for specific purposes.

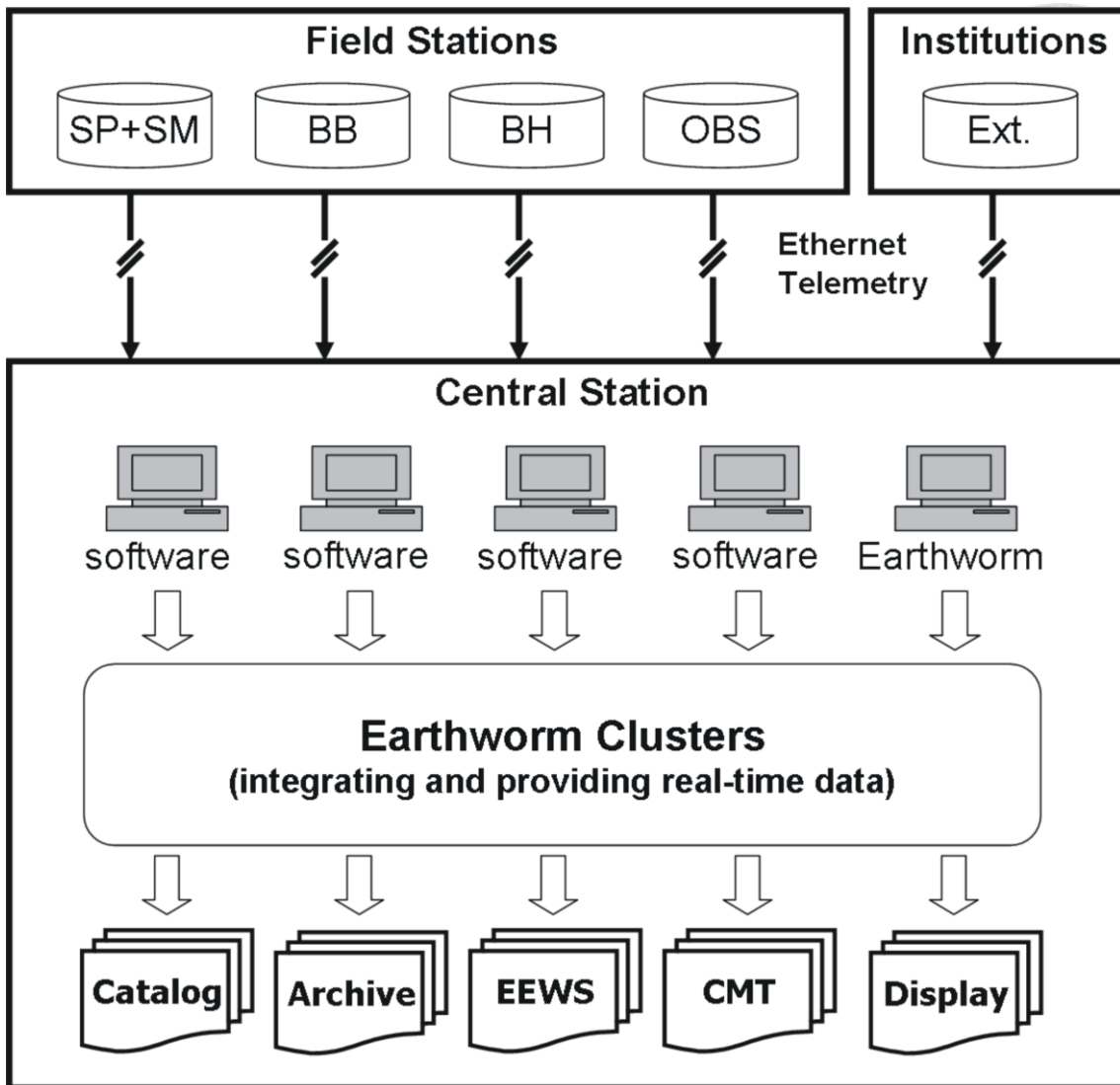



Figure 3-2. A schematic diagram of the data processing center. SP indicates short-period stations; SM indicates strong-motion stations; BH indicates borehole stations; and OBS indicates cable-based ocean bottom seismic stations. “Ext” indicates stations operated by external institutions.

### 3.2 *e*BEAR System Configuration



Real-time data streams retrieved from seismic stations are integrated in Earthworm system. In order to process data effectively, three Earthworm modules (PICK\_EEW, TCPD, and DCSN) were developed in this study. Appendix A. shows the configured files of the three modules. The configured files describe names of shared memories for data in and out. They also defined specific parameters and provide some detail information for the three modules. First, the PICK\_EEW module is in charge of detecting onsets of P-wave arrival and estimating  $P_d$  and  $\tau_c$  values. Thus, the configured file of PICK\_EEW provides station information including location, gain factor and specific auto-picking parameters for each channel. Second, the TCPD module is in charge of locating earthquake and estimating magnitude. Thus, the configured file of TCPD provides parameters for associating P-wave arrivals, P-wave velocity model, and other related parameters. Third, the DCSN module is in charge of decision making and delivering EEW information. Thus, the configured file of DCSN provides criteria for alarm release, information of MySQL database, directories for storing XML-formatted file.

The velocity model used in the TCPD module is a one-dimension continuous velocity model. The equation can be shown by:

$$V(D) = G_0 + G \times D$$

where  $V$  represented velocity is a function of depth  $D$ ,  $G_0$  and  $G$  are constants. The unit of  $V$  and  $D$  are km/s and km, respectively. In this study, an averaged one-dimension velocity model was obtained from averaging three-dimension velocity model (Wu et al., 2009).

For depth shallower than 40 km:

$$V(D) = 5.103 + 0.067 \times D$$



For depth deeper than 40 km:

$$V(D) = 7.805 + 0.005 \times D$$

For magnitude estimation, the regression equations are represented as follows:

For BroadBand Sensor:

$$M_{pd} = 5.000 + 1.102 \times \log_{10}(P_d) + 1.737 \times \log_{10}(R)$$

For Acceleration Sensor:

$$M_{pd} = 5.067 + 1.281 \times \log_{10}(P_d) + 1.760 \times \log_{10}(R)$$

For Short-Period Sensor:

$$M_{pd} = 4.811 + 1.089 \times \log_{10}(P_d) + 1.738 \times \log_{10}(R)$$

Earthquake magnitude is estimated by obtaining an average for each  $M_{Pd}$  value from each seismic station, following section 2.4.2 in this dissertation. Figure 3-3 provides the hardware configuration of the *e*BEAR system. For system backup, we designed two parallel EEW units, EEW1 and EEW2 that run the same procedure and data for generating earthquake messages. When an earthquake occurs, both EEW1 and EEW2 send earthquake messages to the system running the DCSN module. Only the first system sending the earthquake message is activated within the DCSN module. After receiving an earthquake message, the DCSN module writes an XML-formatted file onto the EEW server used to broadcast EEW reports to end users; then, to warn the end user, a display program pops up on the computer screen.



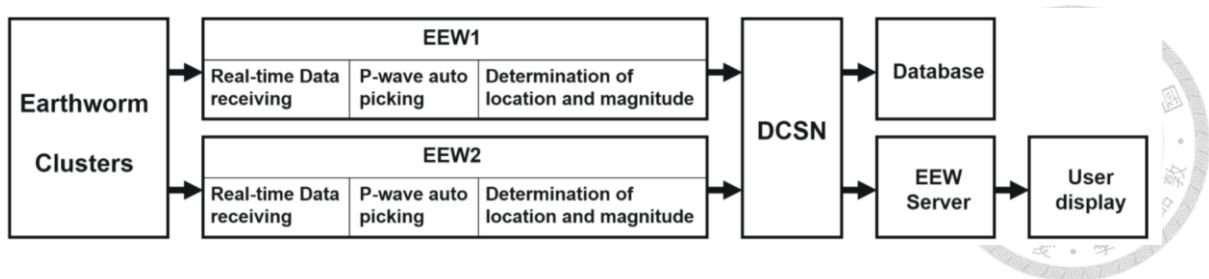
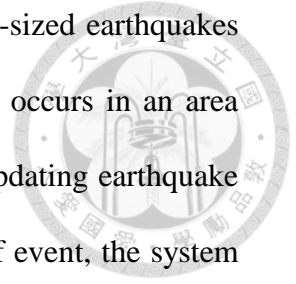


Figure 3-3. A flowchart of the algorithms designed for the PICK\_EEW module. The rectangle represents different computers.

### 3.3 Offline Test

To calibrate the *e*BEAR system, an offline test was implemented in this study. From 2012 to 2013, we collected recorded seismic waveforms with magnitudes greater than 4.0, depths less than 40 km, and epicenters within 40 km of the coastline of Taiwan based on the upgraded CWBSN. A total of 154 seismic events, including four events with magnitudes between 6.0 and 6.5, were used in the test. The results, including earthquake locations and magnitudes, were compared to the CWB earthquake catalog. The reporting time of the offline test (defined as the time the EEW report is issued following the event origin time) does not include a telemetry delay of within 2 s. Figure 3-4 provides the offline performance of the *e*BEAR system in comparison with the results from the CWB catalog. The average errors for epicenter and focal depth locations are 4.2 and 5.3 km, respectively. The standard deviation of the local magnitude is 0.3 units. The average reporting time is 14.7 s. Some events located in southwestern Taiwan with relatively higher station density and coverage may be reported within 10 s. The offline results are acceptable for EEW purposes and suggest three points. First, the two-step method for determination of the epicenter and focal depth is suitable for a complicated tectonic environment such as Taiwan. Second, using a  $P_d$  value within a 3 s time window

following P-wave arrival is useful for measuring the size of moderate-sized earthquakes with magnitudes ranging from 4.0 to 6.5. Third, when an earthquake occurs in an area with a relatively higher station density and coverage, the number of updating earthquake messages quickly increases within the *e*BEAR system. For this type of event, the system is able to obtain a third earthquake message (an EEW report) within a short period of time. For further discussion of the reporting time, Figure 3-5 provides the relationship between the reporting time and the station coverage gap. For most inland events with a station coverage gap generally less than 150°, reporting can occur within 15 s. On the other hand, for offshore events the reporting times may take more than 20 s when the station coverage gap is greater than 200°. The results indicate that currently the station coverage gap is a key factor for controlling the reporting time of the *e*BEAR system.



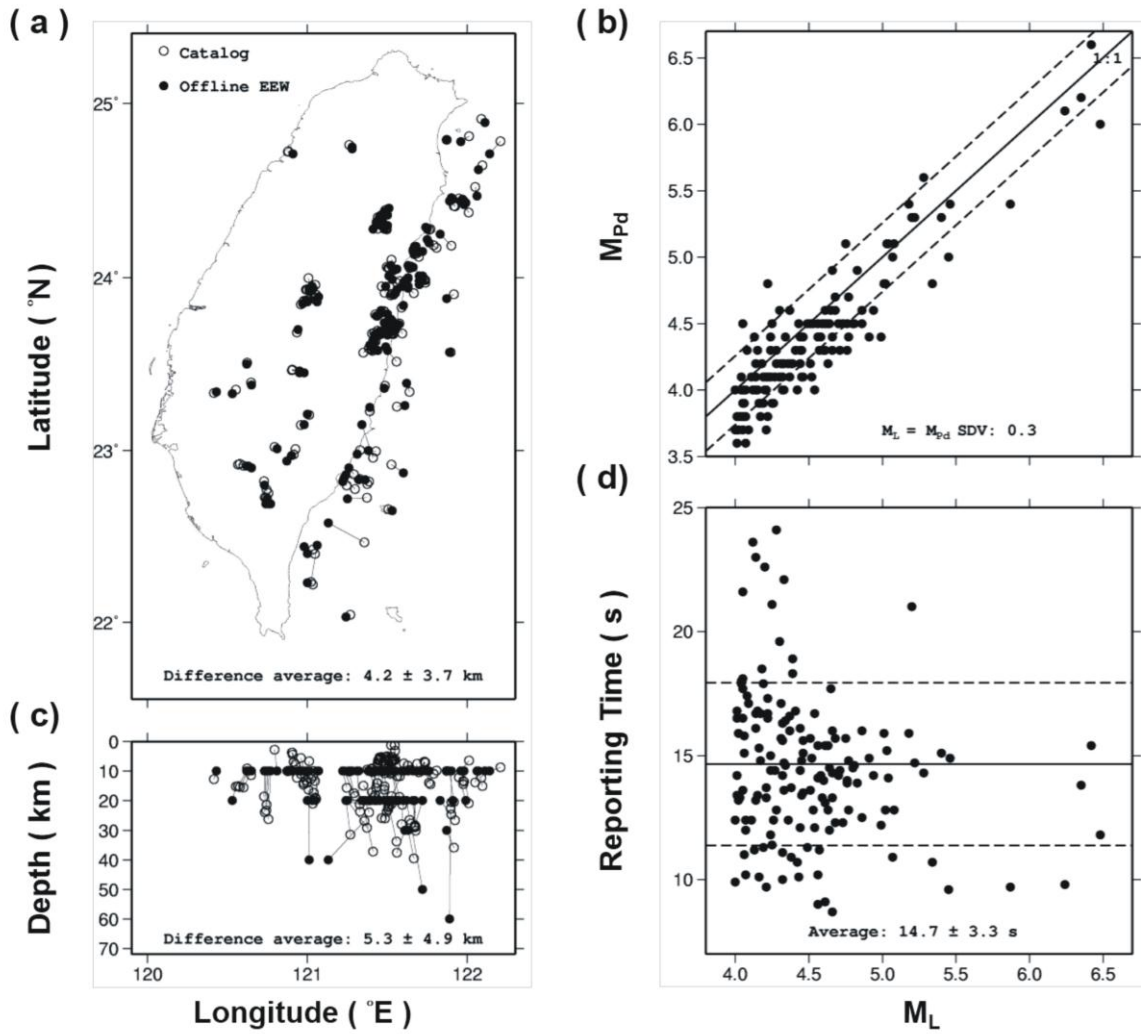


Figure 3-4. A comparison between the offline test and the CWB published catalog, as follows: (a) the epicenters, (b) the magnitudes, (c) the focal depths, and (d) the reporting time of the offline test. Open circles represent earthquake locations obtained from the published CWB catalog. Solid circles represent earthquake locations from the *e*BEAR system.

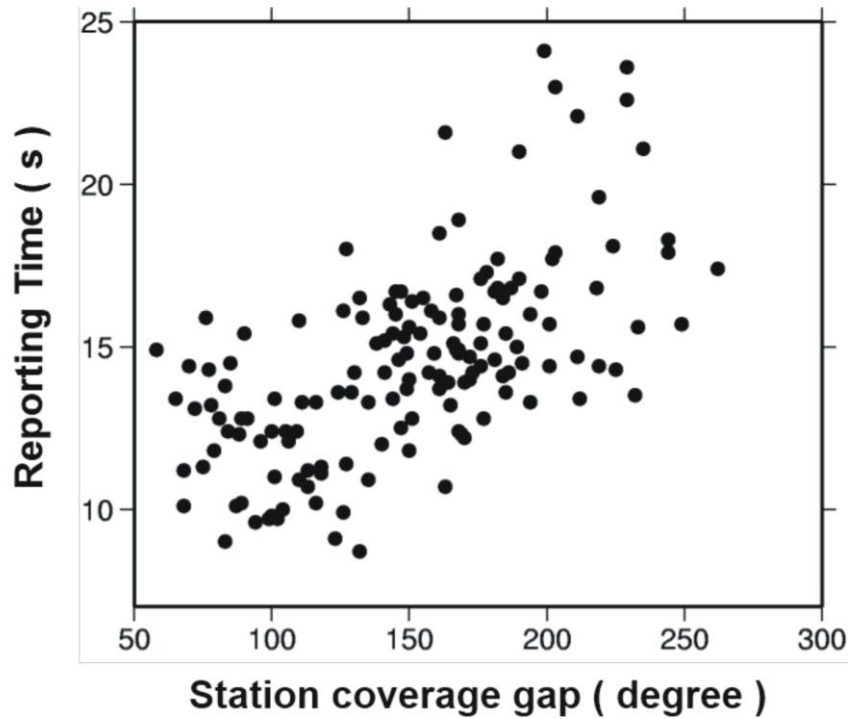
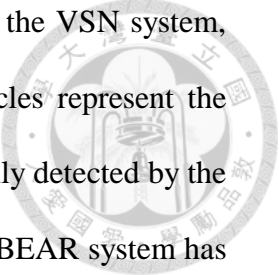


Figure 3-5. The relationship between reporting time and station coverage gap.

### 3.4 Online Performance

For an online system comparison between the VSN and *e*BEAR systems, we collected online operating performance data from January to March of 2014. Figure 3-6 indicates that the *e*BEAR system had no missed events and that determinations of location were better than for the VSN system. For inland earthquakes, both systems had location errors less than 10 km. On the other hand, for offshore earthquakes, the VSN system missed two events and displayed larger location errors of approximately 50–100 km. On average, the epicenter errors of the *e*BEAR and VSN systems are 10.0 and 16.2 km, respectively. When considering depth determinations, the VSN displayed better results than the *e*BEAR system because the VSN system used both P- and S-wave arrivals, whereas the *e*BEAR system only used P-wave arrivals. For magnitude determinations, the



*e*BEAR system yielded a smaller standard deviation (0.2) compared to the VSN system, with a standard deviation of 0.5, shown in Figure 3-7. The solid circles represent the events detected by both systems; the open circles represent the events only detected by the *e*BEAR system. If we only compare the solid circles, it also shows the *e*BEAR system has better magnitude estimations than the VSN system. In the comparison of reporting times, Figure 3-8 indicates that almost every earthquake processed by the *e*BEAR system displayed an earlier reporting time. On average, the *e*BEAR system shortens reporting times by 3.2 and 5.5 s, compared to the VSN system for inland and offshore earthquakes, respectively. Because the *e*BEAR system contains 149 seismic stations distributed in a smaller station coverage gap and because station locations are denser than the VSN system based on 110 stations, the *e*BEAR system can obtain an EEW report more efficiently than the VSN system. Moreover, for an earthquake that occurred in the southern Taiwan offshore area, the station distributions of the *e*BEAR system and the VSN system are similar, but the difference of the reporting time is about 9 s. This indicates the *e*BEAR system can be operated more efficiently than the VSN system without considering the influence of the station distribution. Figure 3-9 provides warning times to target areas in metropolitan Taipei. Warning time is defined as the time between the reporting time and the arrival of the S wave. The *e*BEAR system provides a longer warning time than the VSN system. For the eastern offshore area of Taiwan, the *e*BEAR system can provide a warning time that is 5 s longer, on average, than the VSN system. The major reason is that by adding the MACHO system and the YOJ station into the seismic network, the *e*BEAR system has a smaller station coverage gap. In addition, for events with the approximate locations of the 1999 Mw 7.6 Chi-Chi earthquake and the

2002 Mw 7.1 eastern Taiwan offshore earthquake, the Taipei metropolitan area would have had a warning time of 26 and 15 s, respectively.

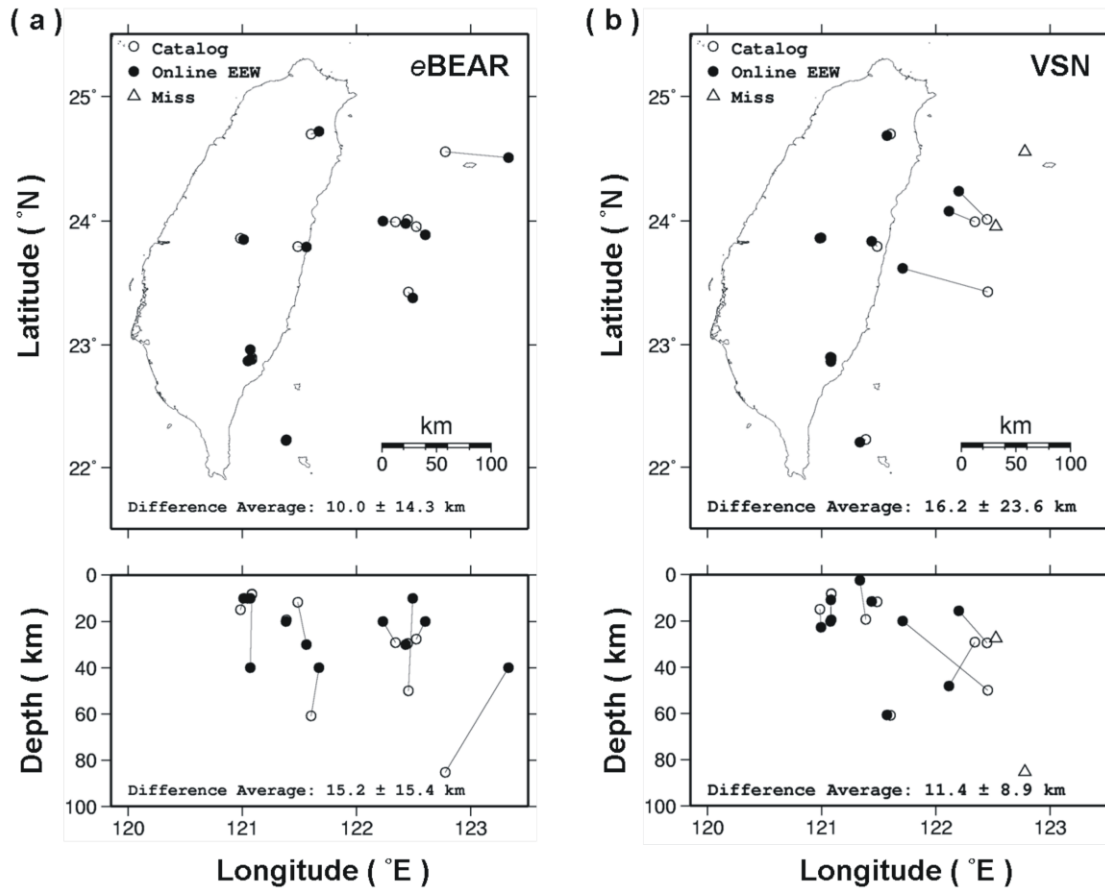
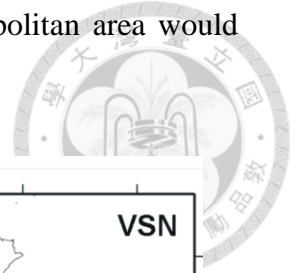


Figure 3-6. Location estimations as compared to online performance between the *e*BEAR and VSN systems, as follows: (a) the epicenter distribution of the CWB catalog and events of the EEW alarms & missed alarms from the *e*BEAR system, and (b) the epicenter distribution of the CWB catalog and events of the EEW alarms & missed alarms from the VSN system. Open circles represent earthquake locations from the published CWB catalog. Solid circles represent earthquake locations from the EEW system. Open triangles represent missing reports from the EEW system.

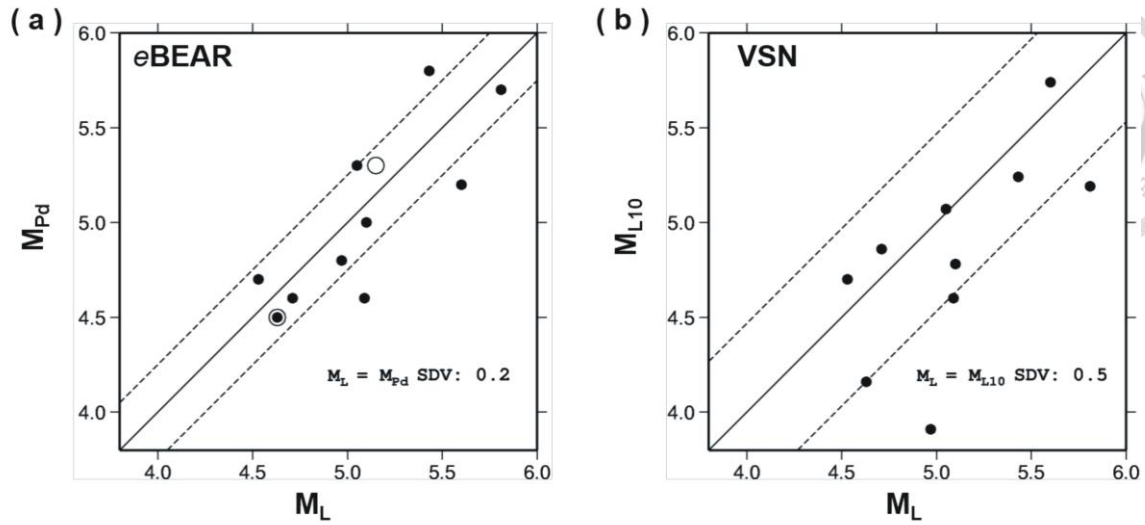


Figure 3-7. Magnitude estimations as compared to online performance between the *e*BEAR and VSN systems, as follows: (a) results from the *e*BEAR system and (b) results from the VSN system. The solid circle represents the events detected by the *e*BEAR and VSN systems. The open circle represents the events only detected by the *e*BEAR system. The solid line represents the 1:1 line. Dashed lines represent one standard deviation.

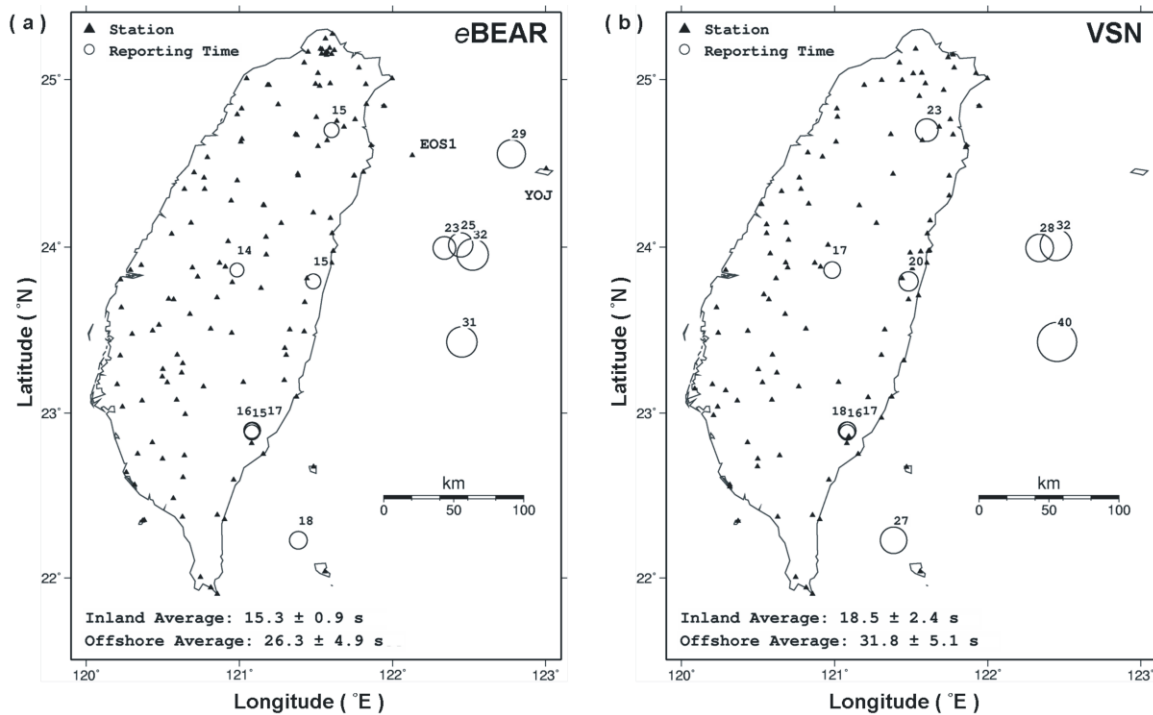


Figure 3-8. The reporting time comparison for online performance between the *e*BEAR and VSN systems, as follows: (a) results from the *e*BEAR system using 149 stations within the CWBSN, and (b) results from the VSN system using 109 RTD stations.



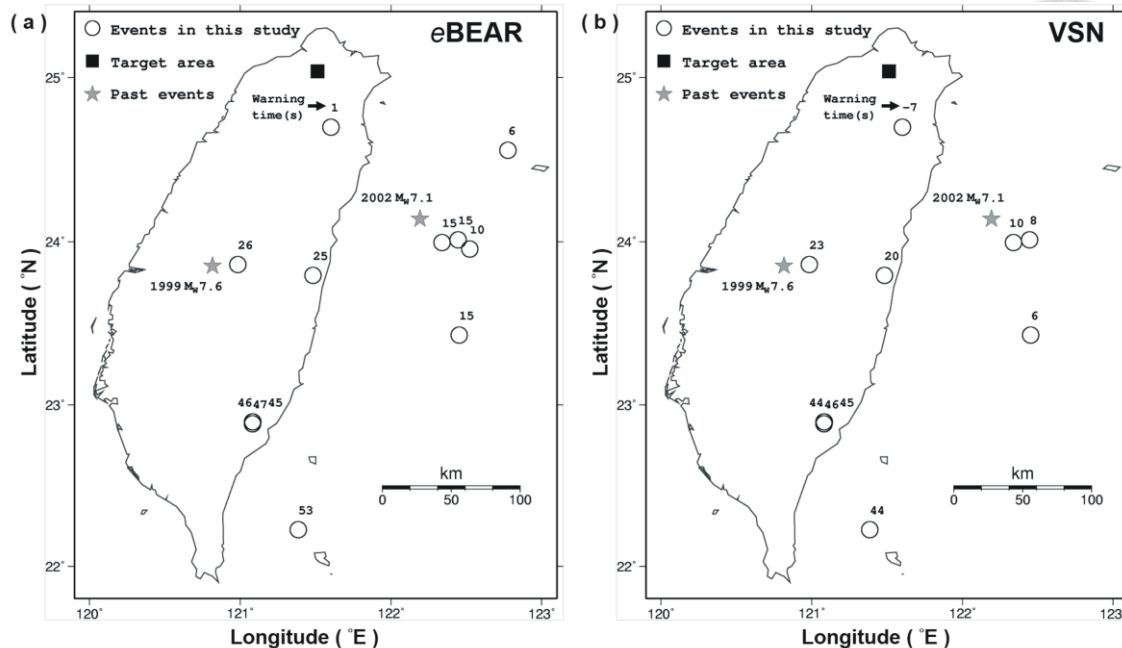


Figure 3-9. Warning time comparisons for online performance between the *e*BEAR and VSN systems, as follows: (a) results from the *e*BEAR system using 149 stations, and (b) results from the VSN system using 109 RTD stations. The solid square represents the target area for obtaining warnings. Open circles represent epicenters. The number over the open circle is the warning time, defined as the time between the reporting time and the arrival of the S-wave. If the warning time value is negative, the target area has no warning time.

### 3.5 EEW Disseminations

The *e*BEAR system has issued EEW warnings to about 3600 junior and senior high schools in Taiwan since January 2014. Those schools receive warnings from the CWB and transfer messages to their broadcast system using a user display software, shown in Figure 3-10. From January 2014 to September 2014, there are 28 earthquakes with magnitude greater than 4.5 and depth less than 40 km reported by the CWB. The *e*BEAR system has reported 20 events and missed 8 events. Figure 3-11 shows the epicenters distribution of the reported and missed events, as well as the reporting times of the

*e*BEAR system. All of the missed events are located on the offshore area. For the reported events, the average location error is  $4.7 \pm 2.9$  km and the average magnitude error is  $0.2 \pm 0.1$ . The 21 May 2014 Hualien earthquake with local magnitude 6.0 is the largest event during this period. The *e*BEAR system issued the alert 15.4 s after the earthquake occurrence. It can provide about 25 s leading time for the Taipei area.

Since January 2014, there have been two false alerts issued by the system. Neither false alert was caused by false triggers. Instead, improper operation caused the false alerts to be generated and sent to the schools. The first false alarm was caused by performing an offline test; because the offline and the online systems run on the same computer, the result of the offline test was sent to the online reporting system and caused a false alert. To avoid this kind of false alarm, we separated the offline and online systems. The second false alarm was caused by the Earthworm communication modules that provide a rapid message exchange facility between two Earthworm processing systems. When the earthquake occurred, the EEW1 determined the source parameters and sent them to the DCSN using the communication modules. However, the EEW message could not be sent (and instead was stored in the memory) because the connection between the communication modules was broken. When the system operator found the connection problem and restarted them several hours later, they were reconnected again. As a result, the source parameters were received by the DCSN. The alert was then sent to the schools, but it was delayed for several hours after the earthquake occurred. To solve the connection problem, we started to monitor heartbeat debug messages, which is a hand-shaking procedure between the communication modules. The system operator can figure out the connection problems and fix them before the system is triggered by

earthquakes.



Figure 3-10. Graphical output of the eBEAR system during a simulation of the  $M_L$  6.5 earthquake in central Taiwan. (top-left) The origin event time and the name of the target city. (center) The rectangle represents the target area. The black line represents the wave front of the P wave. The white line represents the wave front of the S wave. (center-right) The countdown timer for S-wave arrival. (top-right) The predicted intensity of the target area.

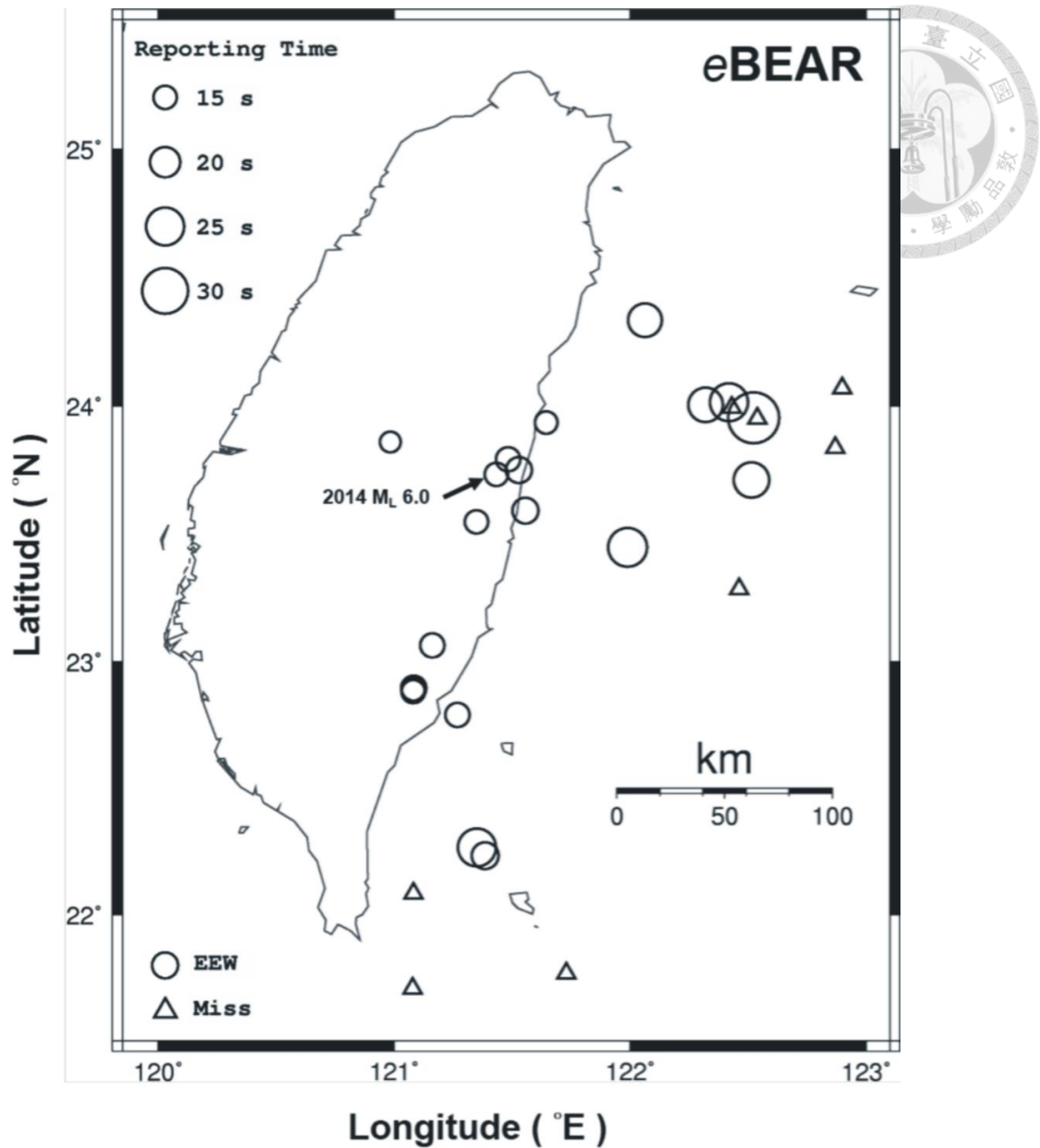


Figure 3-11. EEW disseminations of the *e*BEAR system. There are 28 events with magnitude greater than 4.5 and depth less than 40 km from January 2014 to September 2014. The *e*BEAR system reported 20 events of them indicated as open circles. The size of circles corresponds to the reporting time. Eight events did not reported by the *e*BEAR system (open triangles). During this period the largest event occurred in the Hualien area with local magnitude 6.0 and reported at 15.4 seconds after the earthquake occurrence.

# Chapter 4



## Low-cost Seismometer for EEW

### 4.1 Palert Seismic Network

The PSN, which consists of 543 low-cost accelerometers, transmits three-component real-time data streams, i.e., the x, y, and z axis data streams, back to the data processing center for regional EEW. The Palert device, shown in Figure 4-1, can sample earthquake shaking at a frequency of 100Hz. Sampled data are digitized with 16-bit resolution between -2g and +2g dynamic range, and time stamped by the Network Time Protocol (NTP) server through the Internet. Figure 4-2 shows the station distribution of the PSN. Most of the devices are installed on the wall or pillar at elementary schools. Real-time data are packed by each one-second duration and transmitted via Internet. Each Palert accelerometer can transmit data to two servers located at the NTU and the Academia Sinica Grid Computing (ASGC) Centre.

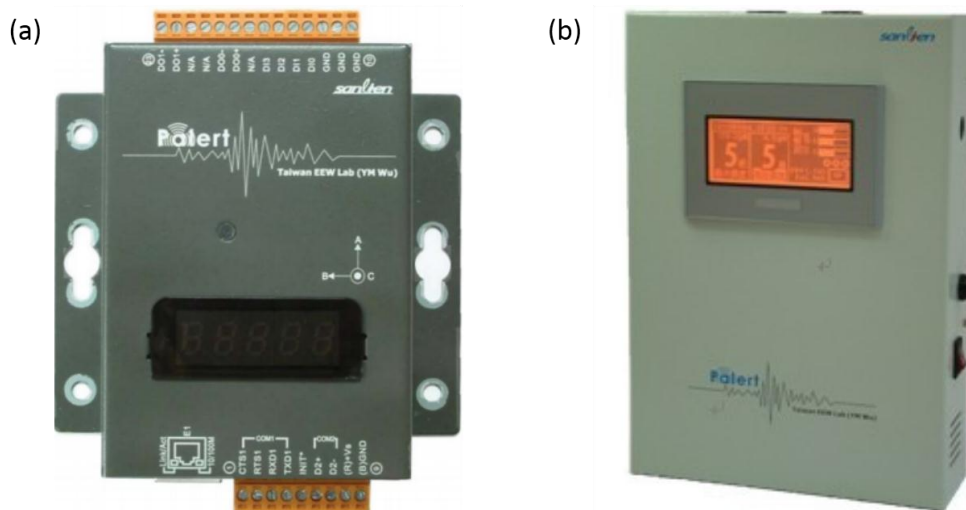


Figure 4-1. Low-cost seismometer. (a)The Palert device. (b) The i-touch device.

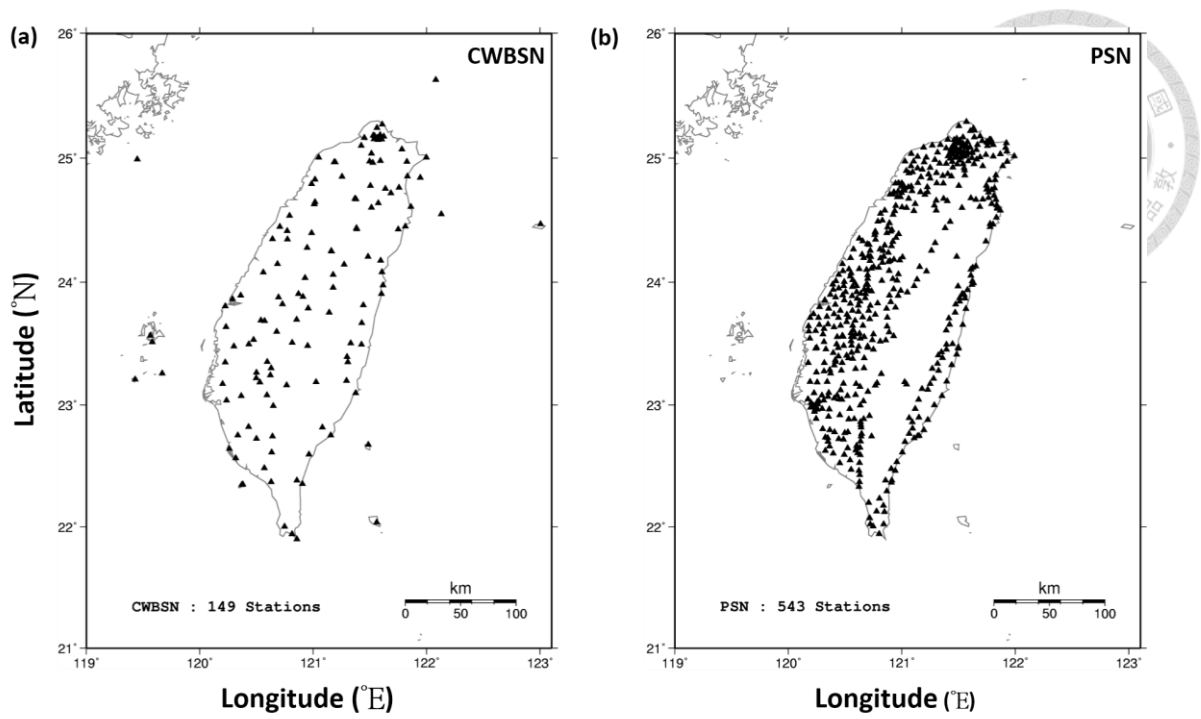
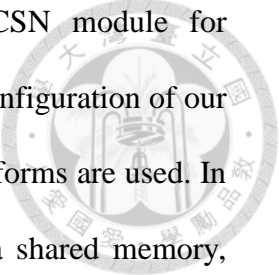


Figure 4-2. The station distribution of the two seismic networks. (a)The station distribution of the Central Weather Bureau Seismic Network (CWBSN), (b) The station distribution of the Palert Seismic Network (PSN).

## 4.2 System Configuration

Figure 4-3 shows that the PSN and the CWBSN are integrated by the Earthworm platform. Although the seismic sensors of the CWBN are made by different manufacturers, corresponding modules can be found in the Earthworm for receiving data streams from the filed seismic stations or other data centers.

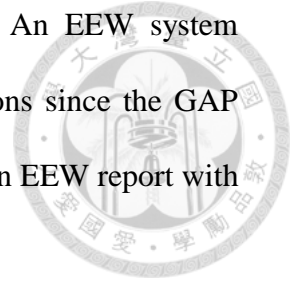
EEW systems aims to process real-time seismic data in order to determine the onset of the P-wave arrival, the amplitude of the triggered waveforms and then calculate the location and magnitude of the earthquake. Consequently, through a decision making procedure, warnings are issued to the target areas. In our EEW system, three Earthworm modules, including the PICK\_EEW module for P-wave auto-picking, the TCPD module



for earthquake magnitude and location determination, and the DCSN module for warnings reporting are used (Chen et al., 2015). Figure 4-4 shows the configuration of our EEW system in which only the vertical component of the seismic waveforms are used. In Earthworm platform, each waveform packet is temporally stored in a shared memory, called WAVE\_RINGs, which has a limited size and only keeps the latest data. The PICK\_EEW module detects P-wave arrivals and obtains the peak amplitude in displacement ( $P_d$ ) of the initial P waves within three-second time window. Then, the detected parameters are sent into another shared memory, called PICK\_RING, in which the TCPD module uses the stored parameters for generating the EEW report including the earthquake origin time, location and magnitude. Finally, the DCSN module takes the EEW report from the EEW\_RING for other applications such as generating the XML-formatted messages for clients running the EEW display and warning program provided by the CWB (Chen et al., 2015). The DCSN module will also pop up EEW messages on the corresponding CWB staff's computers, insert EEW message into the MySQL database, and archive the triggered seismic waveforms.

When a large earthquake occurs and the seismic wave propagates away from the epicenter, the number of triggered seismic stations will increase with time. The EEW system will update the EEW report along the triggered seismic stations. However, in the early stage, the EEW report of the system may contain large uncertainties in location because only few stations are triggered. Thus, other metric should be used to ensure that the EEW report is reliable. The GAP is one of the key factors to determine if the earthquake location report is good enough when the earthquake is inside a seismic network (Wu et al., 1997, 1999, 2013). In the earthquake localization process, the

localization error can be reduced with a small value of the GAP. An EEW system normally updates its report along with the increase of triggered stations since the GAP value decreases. It is necessary to find a suitable criteria for obtaining an EEW report with relatively low GAP and low reporting time.



We analyzed the data set from the online CWBSN-EEW (Hsiao et al., 2011; Chen et al., 2012; Chen et al., 2015). There are 117 earthquakes detected by the system from January, 2014 to August, 2014. Figure 4-4(a) shows the relation between the order of the EEW reports and the number of triggered stations; Figure 4-4(b) shows the relation between the order of the EEW reports and the reporting time and the GAP. Generally, the GAP decreases along with the EEW reports but the reporting time increases. We found an intercept in Figure 4-4(b), which shows the fifth EEW report could be a good point for determining decent source parameters. Moreover, in order to obtain a specific proxy of the criteria, Figure 4-4(a) shows that the fifth report needs at least 13 triggered stations in average. Therefore, in this study, the CWBSN-EEW will issue reports when the number of triggered station is at least 13. In addition, for generating more stable results of the ISN-EEW, we chose EEW reports with GAP equal or less than the reports generated by the CWBSN-EEW.



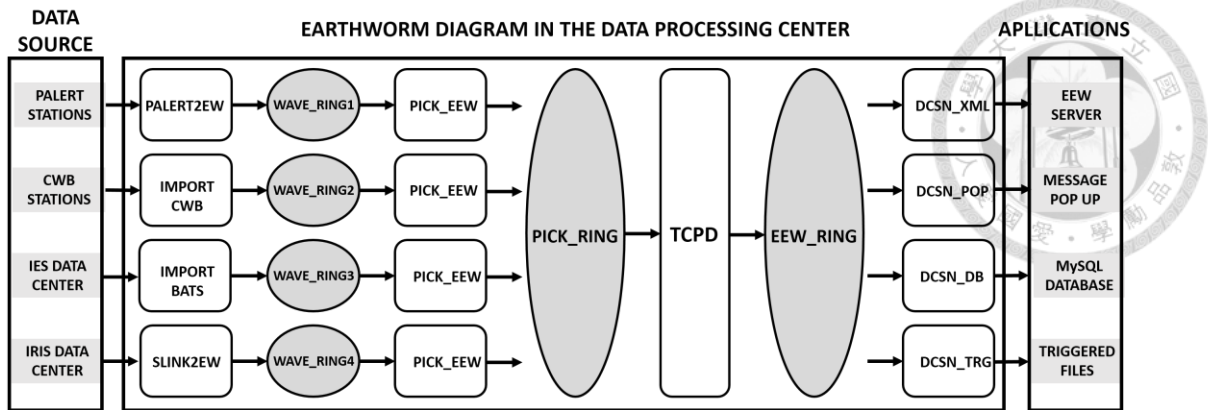


Figure 4-3. A schematic diagram of the data processing of combined seismic network. The first part is the data source which provides real-time seismic data streams from different kind of seismic sensors and other institutions. The middle part is the procedure of data processing in the Earthworm system at the data center. The last part is the applications which receive information from the middle part and use the information.

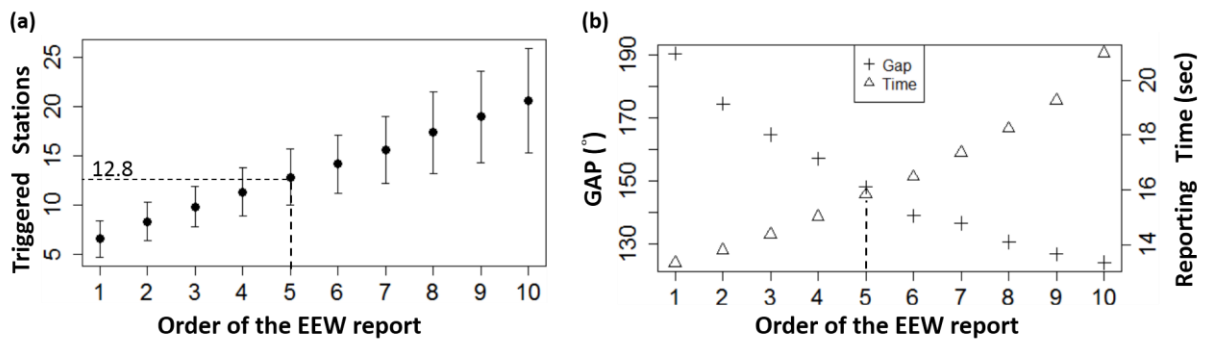
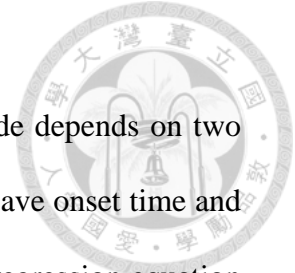


Figure 4-4. Relationships between the EEW parameters of combined system. (a) Relationships between the order of the EEW report and the triggered stations; (b) Relationships between the order of the EEW report, and the reporting time, and the GAP.

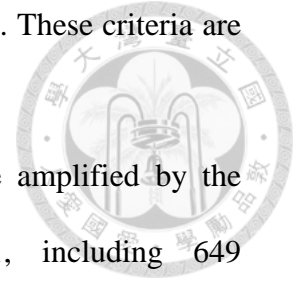
### 4.3 Magnitude Estimation Using Palerts



For the EEW system, a reliable estimation of earthquake magnitude depends on two primary factors. One of them is a robust picker for precisely detect P wave onset time and intelligently avoiding the noise. The other is a statistically significant regression equation for predicting earthquake magnitudes using only the initial portion of P waves. Palerts installed in the buildings of elementary schools may be affected by human activities and may be amplified the amplitude by building responses. Therefore, we adopted the Earthworm's picker (Chen et al., 2015) and followed by new picking constraints for better determine the P wave onset time and preventing from false picks caused by noise. We also constructed a new regression equation to correct for the building response and aim to get better predictions of the earthquake magnitudes.

To ensure every P-wave picks from Palerts with high quality is crucial for the EEW system. We applied the P-wave picking algorithms from the Earthworm module, PICK\_EEW, (Chen et al., 2015), and followed by new picking constraints with three parameters, XON, XP0 and XP1, for evaluating qualities of picks. XON is the first deference of filtered data at pick time; XP0 is the first maximum filtered data of the preceding half cycle; XP1 is the second maximum filtered data of the preceding half cycle. All of them are normalized by the 1.6 times of the running mean absolved value of filtered data. Each valid picks generated from Palerts should be satisfied by one of the following two criteria. One is that either XP0 or XP1 should larger than 13.0 and the XON should larger than 3.0. Another is that either XP0 or XP1 should larger than 20.0 and the XON should larger than 0.8. Figure 4-5(a) shows examples illustrating that picks corresponding to the criteria were considered as high quality; in contrast, Figure 4-5(b)

shows examples illustrating that picks were considered as poor quality. These criteria are quite useful to evaluate qualities of picks detected by the Palerts.



To correct that the seismograms recorded by the Palerts were amplified by the building response, we used 46 events, shown in Table 1, including 649 vertical-component records to determine  $P_d$ , which is the peak amplitude of the initial P-wave displacement, in 3-second time window. The seismograms recorded by the Palerts were integrated twice to obtain the displacement and then a 0.075 Hz high-pass recursive Butterworth filter was applied to remove the low-frequency drift after the numerical integration. Each P-wave arrivals was verified manually to ensure the quality is good for constructing an empirical formula between the  $P_d$  values and the earthquake magnitudes. We assume a linear relationship among the logarithmic  $P_d$ , the magnitude  $M$ , and the logarithmic hypocentral distance  $R$ :

$$\text{Log } P_d = A + B \times M + C \times \log_{10}(R) \quad (1)$$

where  $A$ ,  $B$  and  $C$  are constants to be determined from the regression analysis using the P waves from the 46 events. In the regression analysis, we used R software (R Development Core Team, 2006) to detect and remove outliers within the data, and then fit the model to the data. The best-fitting attenuation relationship for  $\log P_d$  is found to be

$$\text{Log } P_d = -2.797 + 0.404 \times M - 0.539 \times \log_{10}(R) \pm 0.33 \quad (2)$$

The equation (2) was used for estimating earthquake magnitudes using vertical-component P waves recorded by the Palerts.

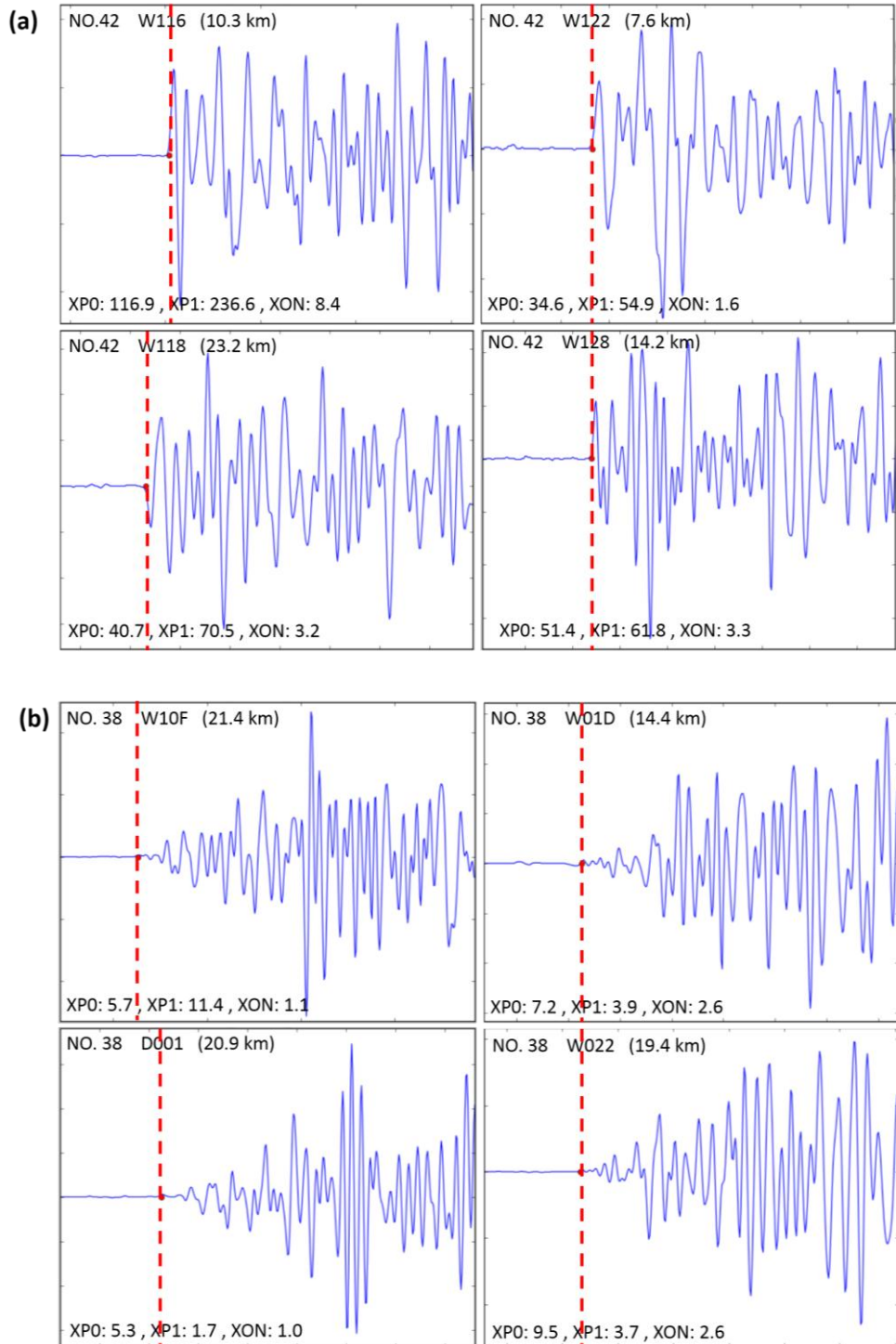
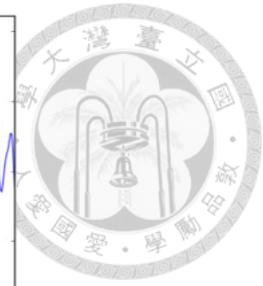


Figure 4-5. Examples of the automatic P-wave arrival detection. (a) High quality picks. The parameters XPO, XP1 and XON are over the criteria; (b) Poor quality picks. The parameters XPO, XP1 and XON are under than the criteria

## 4.4 Offline Test

To test the integrated system, ISN-EEW, in off-line mode, we collected seismic waveforms with magnitudes greater than 4.5, depths less than 40 km, and epicenters within 40 km of the coastline of Taiwan from 2013 to January 2015. Table 1 shows the dataset which consists of 46 events including three events with magnitudes between 6.0 and 6.5. The results of the off-line simulations are compared with those generated by the CWBSN-EEW.

In the off-line test, the ISN-EEW use the same Earthworm's picker but different criteria to detect P wave arrivals for the P waves recorded by the CWBSN and the ISN. Figure 4-6 shows the comparison of the source location errors between the CWBSN-EEW and the ISN-EEW. The difference of epicenter error of CWB-EEW and ISN-EEW are 0.3 km. For the depth error, the ISN-EEW is a little better than the CWB-EEW. It means the ISN-EEW can have stable results in earthquake location. The  $P_d$  values from the CWBSN are used to estimate earthquake magnitudes ( $M_{Pd}$ ) based on the empirical formula of Hsiao et al., (2011). However, for the  $P_d$  values from the PSN, the equation (2) was used for estimated earthquake magnitudes. Figure 4-7 shows the comparison for the estimated magnitudes. The estimated magnitudes from CWBSN-EEW and ISN-EEW are compared to the CWB catalog created by manual phase picking and locating. The CWBSN-EEW and the ISN-EEW have error of 0.28 and 0.25 unit, respectively. The ISN-EEW is able to provide robust estimations of earthquake magnitudes. The results implies that the amplified P waves caused by the building effects are correcting by the equation (2). Comparing Figure 4-8, the reporting time are 14.7 and 13.1 seconds for the CWBSN-EEW and ISN-EEW, respectively. Figure 4-9 shows the

comparisons of blind-zone areas distribution of each event. Some events located in the region with dense seismic stations may be reduced the blind zone area to 30 km.

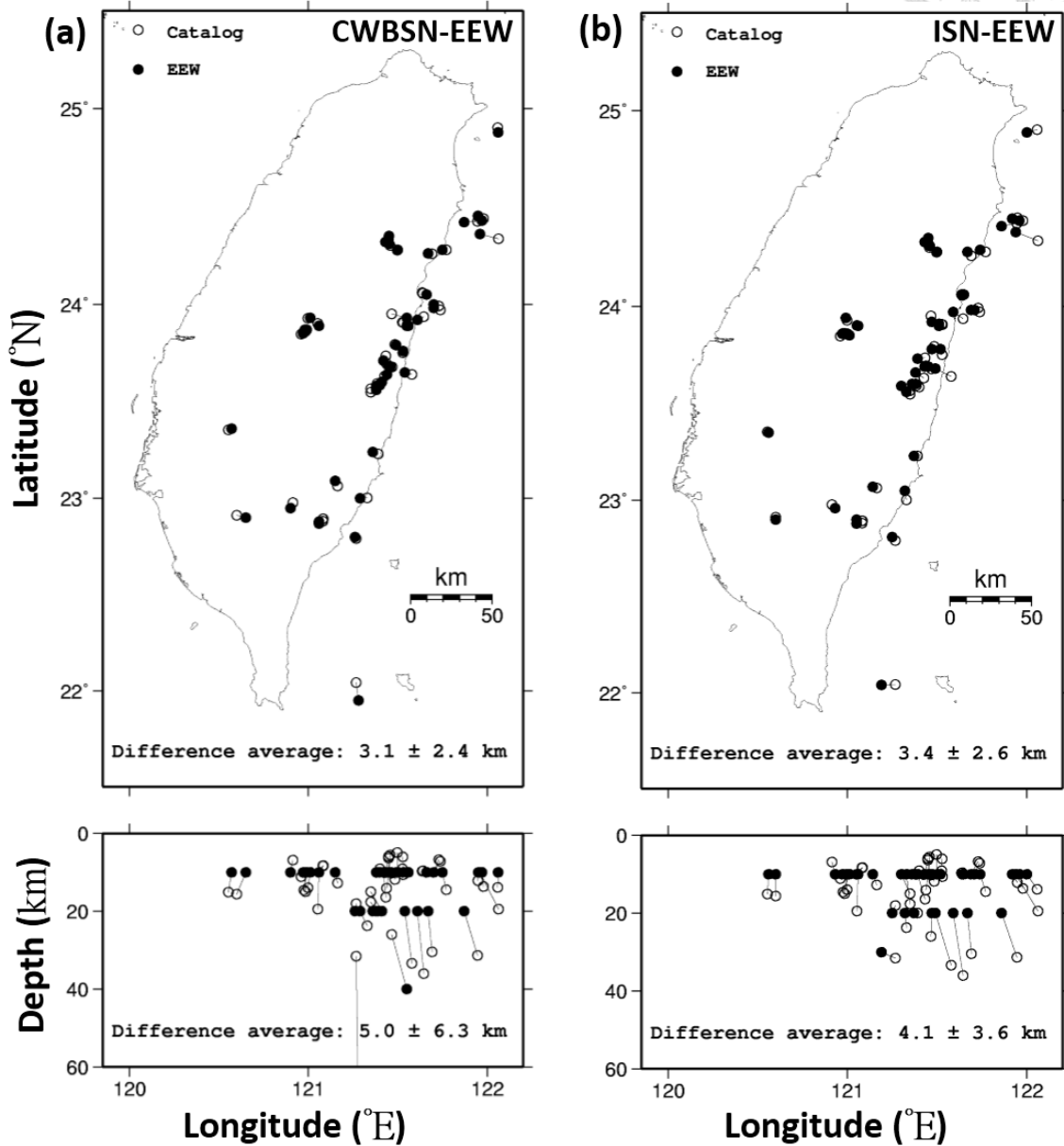
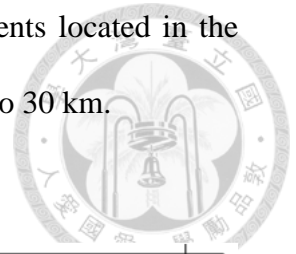
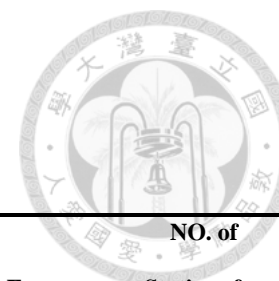


Figure 4-6. The location error comparisons between CWBSN and ISN. (a) Comparison between the CWBSN-EEW and the CWB catalog analyzed by manual phase picking; (b) Comparison between the ISN-EEW and the CWB catalog analyzed by manual phase picking.

1  
2

Table 2. Data for offline test in integration system



Event NO.	Date (mm/dd/yy)	Latitude (°)	Longitude (°)	Depth (km)	ML	Time		Gap		Epicenter Error		NO. of Stations for ISN-EEW	
						CWBSN-EEW (sec)	ISN-EEW (sec)	CWBSN-EEW (°)	ISN-EEW (°)	CWBSN- EEW (km)	ISN-EEW (km)	Total	Palert
1	01/02/13	121.74	23.97	7	4.7	17.8	18	204	197	4.0	3.0	26	1
2	01/03/13	121.73	23.99	7	4.7	14.5	14.5	219	219	3.2	4.3	18	2
3	01/17/13	121.98	24.44	14	5.1	13.2	12.2	181	177	1.3	1.9	18	8
4	02/17/13	121.45	24.32	6	4.6	11.8	12.5	143	108	1.9	2.4	11	3
5	02/19/13	120.55	23.35	15	4.6	18.2	12.1	65	40	1.9	0.8	37	21
6	02/19/13	120.60	22.91	16	4.7	14.1	9.8	158	82	5.3	1.4	13	11
7	02/20/13	121.39	23.23	20	4.5	15.2	15.4	156	148	3.4	2.1	16	3
8	03/04/13	121.33	23.00	24	4.6	14.8	11.1	177	173	4.0	5.4	16	4
9	03/07/13	121.46	24.30	6	5.9	14.1	12.1	69	69	1.3	1.1	16	4
10	03/07/13	121.45	24.34	6	4.6	13.7	13.6	69	69	1.6	1.6	20	3
11	03/20/13	121.95	24.45	12	4.6	18.9	19.4	149	145	0.5	2.9	60	15

12	03/27/13	121.05	23.90	19	6.2	9.8	9.8	102	82	1.5	0.8	21	16
13	03/27/13	121.00	23.93	14	4.5	11.8	7.4	96	67	1.3	1.5	11	6
14	05/21/13	121.77	24.28	14	4.9	12.3	12.2	199	188	2.1	3.3	19	6
15	06/01/13	121.27	22.04	32	5.0	23.2	25.4	271	251	10.3	8.0	22	1
16	06/02/13	120.97	23.86	15	6.5	12	15.7	75	52	1.9	3.9	49	16
17	07/14/13	120.91	22.98	7	4.6	16.1	16.1	54	45	3.3	2.5	19	4
18	07/16/13	121.50	24.28	5	5.5	14.3	14	77	76	0.4	0.4	33	15
19	07/24/13	121.53	23.91	9	4.8	14.4	9.5	170	107	3.2	1.7	18	14
20	07/24/13	121.53	23.91	11	5.0	15.2	10.1	175	98	3.6	2.0	15	9
21	09/30/13	120.96	23.85	11	4.7	15	9.4	75	74	1.2	1.9	20	15
22	10/31/13	121.35	23.57	15	6.4	15.4	10.5	140	129	7.3	5.6	25	19
23	10/31/13	121.40	23.58	9	4.6	13.9	14.5	121	121	2.2	2.7	12	3
24	10/31/13	121.38	23.59	10	4.6	12.9	12.9	134	108	1.7	2.5	13	4
25	10/31/13	121.43	23.63	10	5.1	16.5	11.1	155	90	1.8	5.6	20	10
26	10/31/13	121.44	23.69	14	4.8	14	14.7	169	169	2.0	1.3	16	1
27	11/03/13	121.47	23.68	10	4.6	20	10.4	156	73	1.0	4.2	21	14
28	11/03/13	121.47	23.95	26	4.9	15.1	10	84	67	8.9	3.4	19	15
29	11/07/13	121.64	24.06	10	4.6	14.2	14.6	179	176	2.8	0.5	15	4
18	11/07/13	121.64	24.06	10	4.5	24.1	13.7	182	175	2.1	1.1	26	4
19	01/14/14	120.98	23.86	15	5.0	12.2	12.1	72	71	1.1	1.6	37	9





20	01/14/14	121.08	22.89	8	5.1	12.1	11.4	60	51	2.6	3.5	29	14
21	01/14/14	121.08	22.88	8	5.1	14.4	14.9	60	51	2.5	3.2	22	13
22	01/14/14	121.08	22.89	8	4.5	11.7	11.6	60	52	2.8	3.4	28	12
23	01/25/14	121.48	23.79	12	4.7	13.8	13.1	147	106	0.8	2.1	23	10
24	04/25/14	121.35	23.55	18	4.7	14.3	11	115	76	3.5	2.3	18	10
25	05/04/14	121.65	23.94	36	5.2	12.4	11.9	188	146	4.0	6.8	21	9
26	05/21/14	121.43	23.74	16	6.0	10.9	11.2	133	81	3.0	4.4	21	11
27	05/25/14	121.16	23.06	13	5.0	16.8	12.4	92	90	3.2	2.4	15	5
28	06/14/14	121.53	23.75	6	4.6	16	16	177	174	1.0	3.3	26	6
29	09/10/14	122.06	24.34	20	4.7	13.4	17.6	222	218	10.8	13.4	23	1
30	09/25/14	121.27	22.79	18	5.3	16.3	16.2	102	109	1.2	2.7	26	5
31	10/07/14	121.58	23.64	33	5.2	18.8	14.5	183	161	4.3	10.2	26	8
32	11/19/14	122.06	24.90	14	5.2	13.1	12.4	241	235	2.6	6.0	16	6
33	01/07/15	121.69	24.26	30	5.5	11	11.1	161	151	2.2	3.1	23	6
34	01/16/15	121.95	24.43	31	4.9	12.8	12.6	212	205	7.7	8.9	18	1
35	01/02/13	121.74	23.97	7	4.7	17.8	18	204	197	4.0	3.0	26	1
36	01/03/13	121.73	23.99	7	4.7	14.5	14.5	219	219	3.2	4.3	18	2
37	01/17/13	121.98	24.44	14	5.1	13.2	12.2	181	177	1.3	1.9	18	8
38	02/17/13	121.45	24.32	6	4.6	11.8	12.5	143	108	1.9	2.4	11	3
39	02/19/13	120.55	23.35	15	4.6	18.2	12.1	65	40	1.9	0.8	37	21



40	02/19/13	120.60	22.91	16	4.7	14.1	9.8	158	82	5.3	1.4	13	11
41	02/20/13	121.39	23.23	20	4.5	15.2	15.4	156	148	3.4	2.1	16	3
42	03/04/13	121.33	23.00	24	4.6	14.8	11.1	177	173	4.0	5.4	16	4
43	03/07/13	121.46	24.30	6	5.9	14.1	12.1	69	69	1.3	1.1	16	4
44	03/07/13	121.45	24.34	6	4.6	13.7	13.6	69	69	1.6	1.6	20	3
45	03/20/13	121.95	24.45	12	4.6	18.9	19.4	149	145	0.5	2.9	60	15
46	03/27/13	121.05	23.90	19	6.2	9.8	9.8	102	82	1.5	0.8	21	16
Average						14.7	13.1	139.8	120.7	3.1	3.4	22.1	8.2



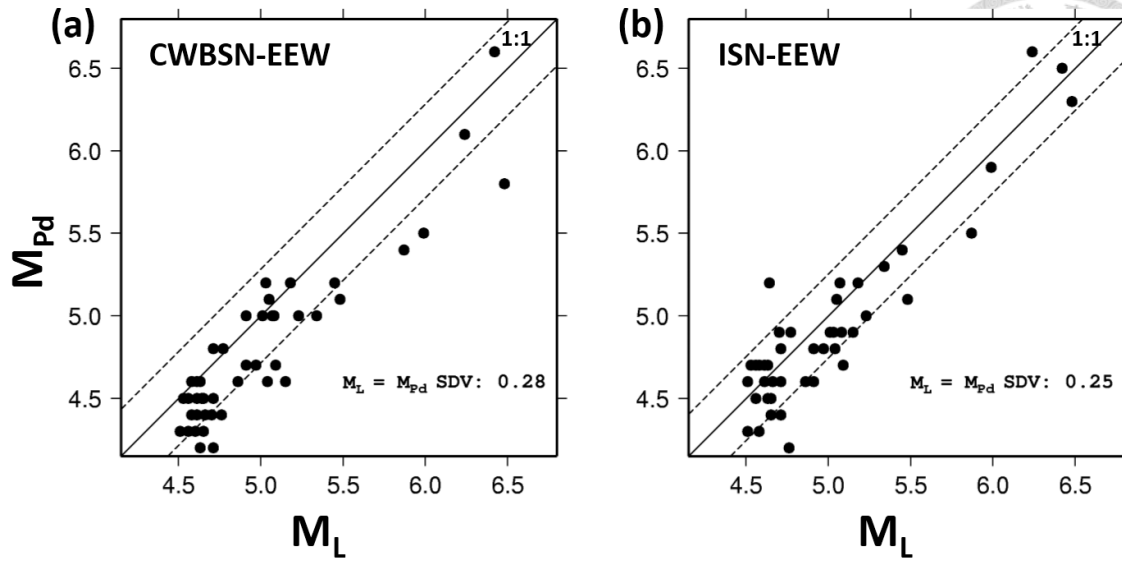


Figure 4-7. The magnitude error comparisons between CWBSN and ISN. (a) Comparison between the CWBSN-EEW and the he CWB catalog analyzed by manual phase picking; (b) Comparison between the ISN-EEW and the he CWB catalog analyzed by manual phase picking.

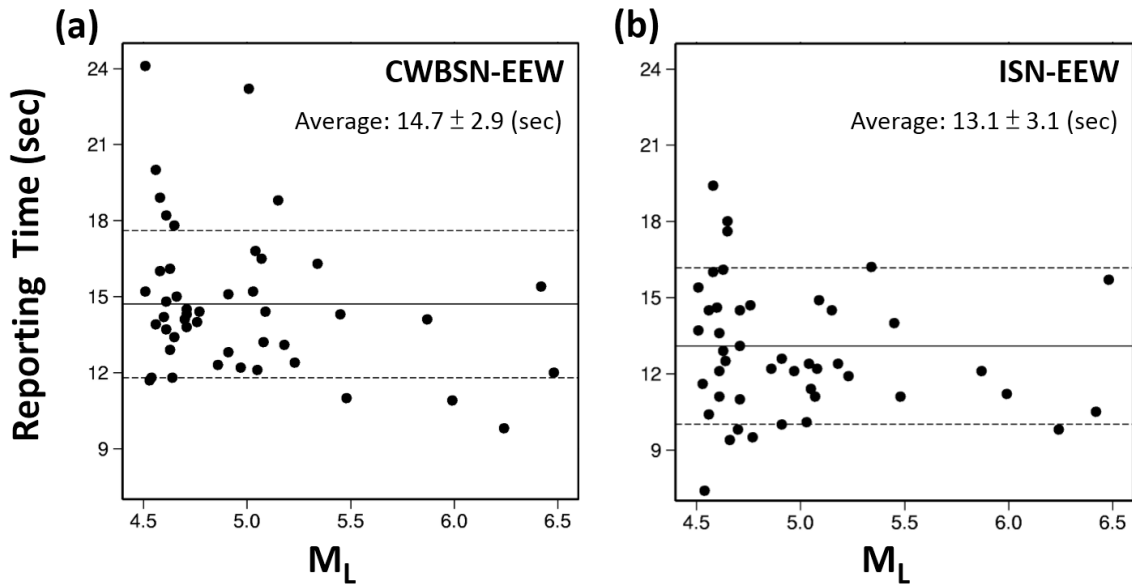


Figure 4-8. The reporting time comparisons between CWBSN and ISN. (a) Reporting time of the CWBSN-EEW; (b) Reporting time of the ISN-EEW. In average, the ISN-EEW has smaller reporting time than the CWBSN-EEW.

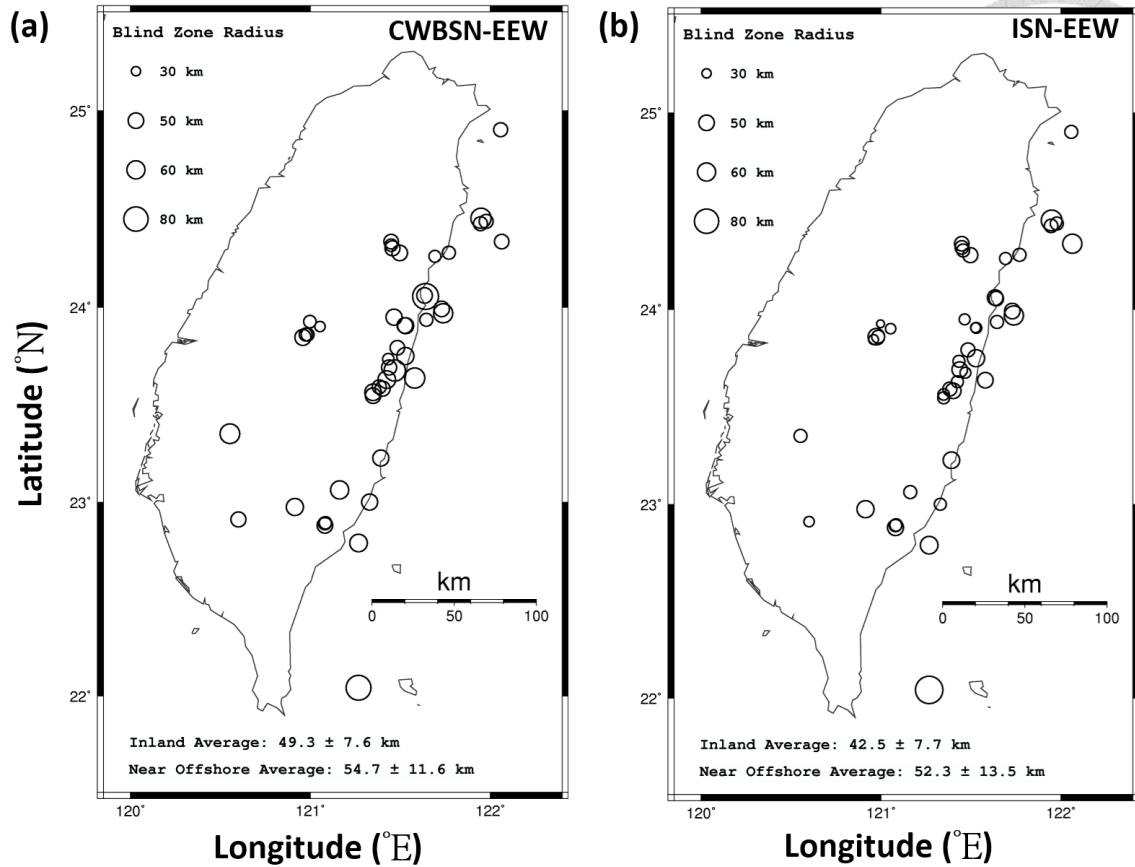


Figure 4-9. Blind zone radius comparisons between CWBSN and ISN. (a) Blind zone radius of the CWBSN-EEW; (b) Blind zone radius of the ISN-EEW.

## 4.5 Summary

Using low-cost seismometers to construct a regional seismic network is an attractive solution for EEW systems. In spite of the relative low signal-to-noise ratio and the impact of building responses on the amplitude of the seismic waveforms, the P-wave arrival time, detected by the Earthworm's picker (Chen et al., 2015) and followed by the new picking constraints, is precise for large earthquake and the amplitude can be corrected by removing the building responses. Wu et al., (2013b) demonstrated that the regional seismic network based on the Palerts is good enough for determining earthquake location,

magnitude and intensity. We further integrate the PSN and the CWBSN to make a regional seismic network, ISN, with higher density in Taiwan. This is the first time to integrate a traditional seismic network with a low-cost seismic network. Because of the dense station coverage of the ISN, when inland earthquakes occurred, the EEW system based on the ISN is able to gather P-wave arrivals faster than that based on the CWBSN. The results of the off-line test implies that the EEW system based on the ISN can reduce reporting time and estimate decent earthquake location and magnitude for the purpose of earthquake early warning.

EEW system updates the earthquake information along with the arrival of new data in the system. It is a challenge to decide when the accuracy of the updated result will be good enough. One possible metric is to use GAP. For earthquakes occurred inside the seismic network the lower the GAP, the higher the accuracy may be reachable for the estimated earthquake location as well as the magnitude. However, lower GAP usually needs more stations. For earthquake localization, it means that the calculation should wait until more stations are triggered and the reporting time of the system is increased. By studying the relationship between the GAP and the number of triggered stations, a specific criteria of 13 triggered stations is found for the specific condition in Taiwan to compromise the tradeoff between the speed and the accuracy in the EEW system.

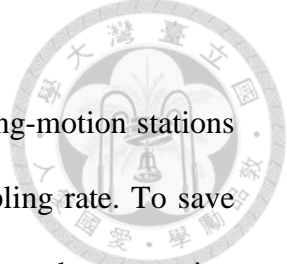
# Chapter 5

## A Case Study for Mw7.6 Chi-Chi Earthquake



As a result of the large ground shaking of the 1999 Chi-Chi earthquake, several electrical power towers collapsed, which resulted in real-time data interruption. If the 1999 Chi-Chi earthquake were to happen again with limited workable stations and signal recording length, we wonder if the proposed EEW system would provide precise and reliable event information. It is a big challenge to the current EEW methods in magnitude and intensity estimations, because the data streams might be broken within the initial 10 seconds after the first P-wave arrival, as happened in the 1999 Chi-Chi earthquake. The purpose of this study is to offline test the new proposed EEW system (Hsiao et al. 2011) by feeding the raw records of the 1999 Chi-Chi earthquake into the system. Both  $\tau_c$  and  $P_d$  were used to estimate the magnitude. The results indicate that the first warning is available in about 12 seconds after the earthquake origin time and the magnitude estimated by the  $\tau_c$  method ( $M_{\tau_c} = 7.4$ ) is better than that from using the  $P_d$  method ( $M_{P_d} = 6.3$ ). Even with limited stations and data interruptions such as occurred during the 1999 Chi-Chi earthquake, the proposed EEW system still can provide quick and satisfying event information.

## 5.1 Signal Interruption



Before the 1999 Chi-Chi earthquake, there were 61 real-time strong-motion stations operated by the CWB with a 16-bit dynamic range and a 50-Hz sampling rate. To save communication expenses, some of the stations directly transmitted data to the processing center via 4.8-K phone line, while others first transmitted data to sub-centers, which are multiplex all data streams, and then transmitted them to the data processing center via a broadband dedicated line, named the T1 line. Unexpectedly, the Hualien T1 line, consisting of six stations, was interrupted five seconds before the Chi-Chi earthquake due to a mechanical problem. In addition, during the strong ground-shaking period the electrical power tower collapsed, also causing serious signal communication problems. Many real-time data streams lacked later S waves or were filled with non-seismic spikes. Therefore, the current  $M_{L10}$  method for estimating magnitude was difficult or impossible to implement. We divided the station operating conditions into A, B, and C types, indicating signals are normal (A), capable of being used by the P-wave method (B), or unacceptable for analysis (C). Figure 5-1 shows the distribution of stations according to the station health. Only nine out of 61 stations recorded complete waveforms. However, if we consider the initial part of P waves, an additional 20 stations of type B, including the nearest stations, become able to be used by the  $\tau_c$  and  $P_d$  methods. Figure 5-2 shows the seismograms of the three nearest stations of type B. Despite the fact that the data streams of type B were spoiled by serious spikes or discontinuities, the initial portion of P waves are still usable, even at the nearest stations, which provides valuable records.

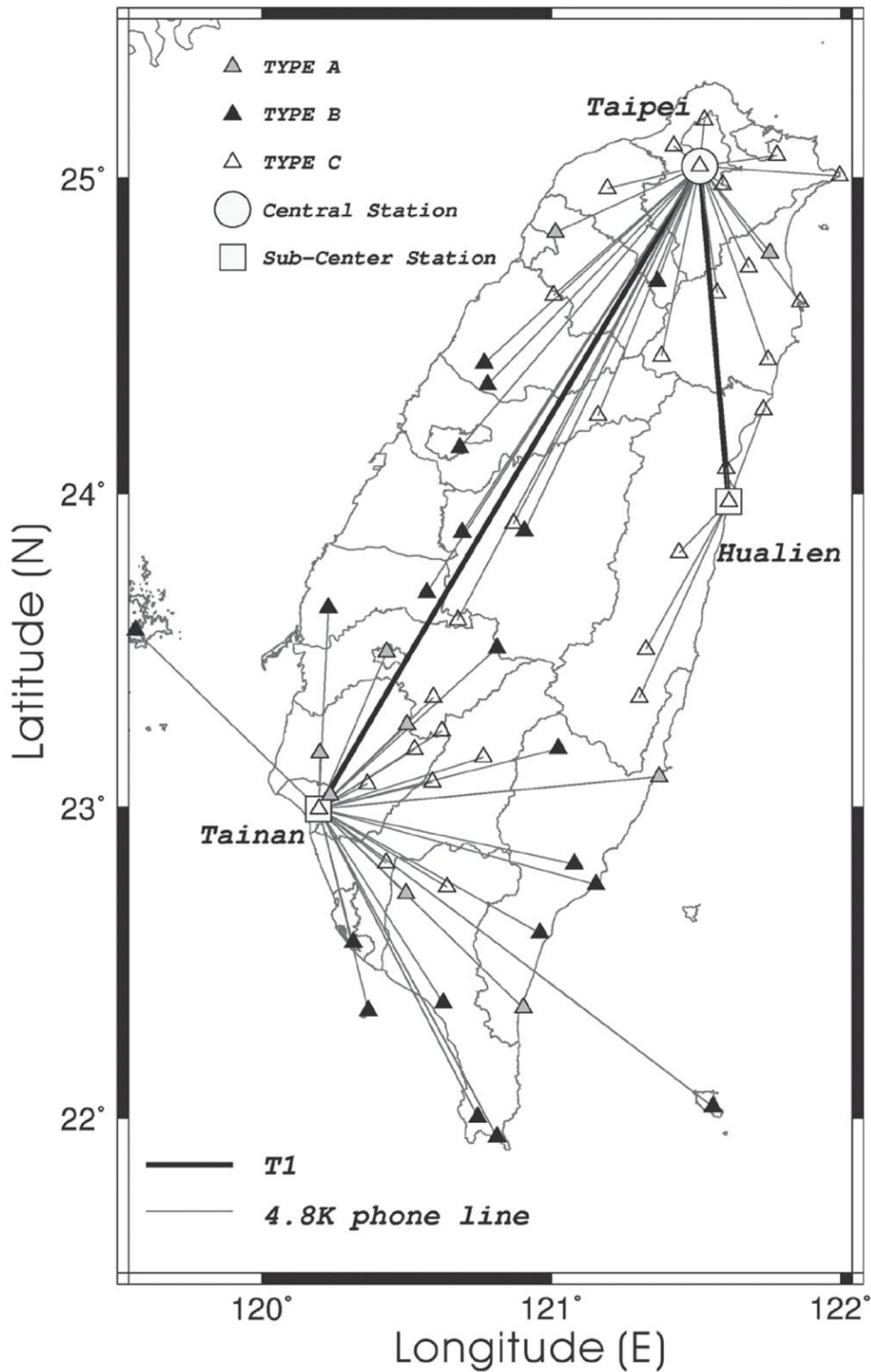


Figure 5-1. Distribution of real-time strong-motion stations of CWB. Station signals during the Chi-Chi earthquake occurrence are classified A, B, or C for normal; capable to be used by the P-wave method; and unacceptable for analysis, respectively.



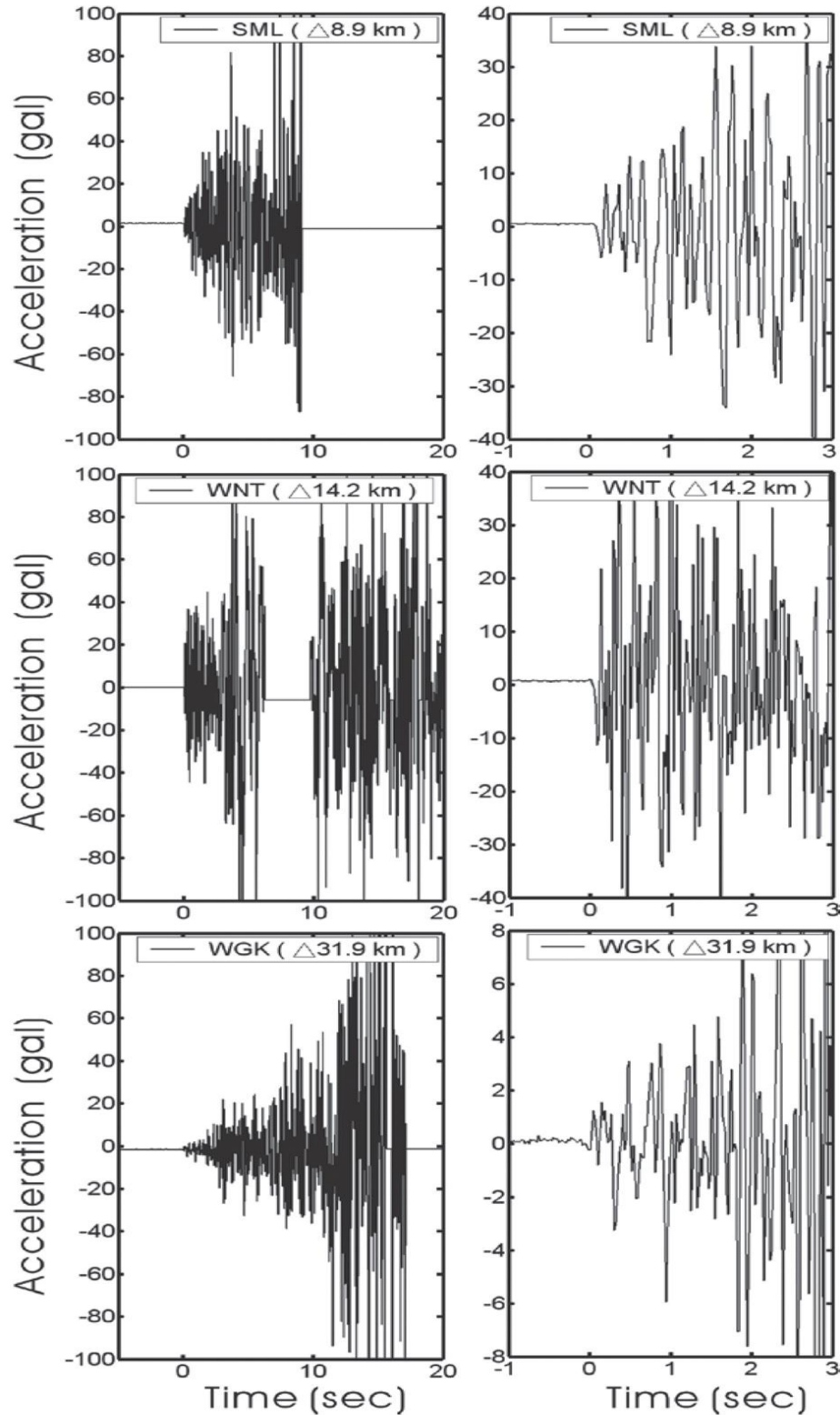
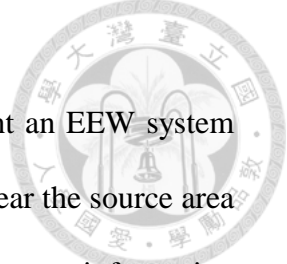
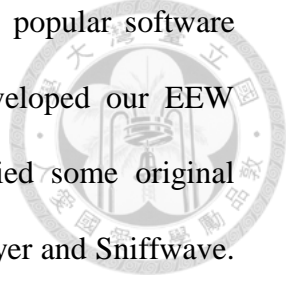


Figure 5-2. Seismograms recorded in the Chi-Chi Earthquake. The seismograms on the left show the type B real-time strong-motion signals of the 1999 Chi-Chi earthquake. The plots on the right show the initial three seconds of signals after the P arrival.

## 5.2 System Configuration



Either a regional or onsite method is a possible way to implement an EEW system (Kanamori 2005). The regional method uses a group of seismometers near the source area to determine earthquake location and magnitude and then transmits the event information to target areas farther away from the earthquake. On the other hand, the onsite method uses only one station or a small array to predict the ground motion at the same site. It takes advantage of the initial portion of the P wave, which is faster than S waves and contains the information about earthquake source. Using the  $P_d$  attenuation relationship with hypocentral distance,  $M_{Pd}$  is more oriented to the regional method.  $M_{\tau_c}$ , which can be obtained by only one station and does not need earthquake location, is computed by averaging all the available single  $M_{\tau_c}$  among the stations for the sake of minimizing the effect of abnormal values. Each method has advantages and disadvantages. The regional method may be more reliable but it takes much more time than the onsite method. Thus, it cannot offer early warning for regions closer to the epicenter. However, it is possible to offer more warning time than the on-site approach for regions further away from epicenter. On the other hand, an onsite system can provide timely warning to regions closer to the epicenter (Satriano et al. 2010). The general tendency nowadays is to integrate these two approaches (Zollo et al. 2010). Figure 5-3(A) shows the configuration of the proposed EEW system (Hsiao et al. 2011) in the CWB. Field stations transmit real-time data streams via modem. Some of them are directly connected to the data center; others are first connected to the sub-centers and later to the data center. Then the data center integrates all data in a serial port server. The program, named RTDREC, continuously generates the waveform files with a length of three seconds. These files are



the data source for the EEW system. Earthworm is one of the most popular software platforms for real-time seismic data integration processing. We developed our EEW system in the Earthworm environment (Figure 5-3(B)). We modified some original modules from Earthworm to meet our requirements, including Tankplayer and Sniffwave. In order to feed the continuous data files into Earthworm, we created a new module, named Rtd2ew, modified from Tankplayer. Data streams are continuously stored in a temporal memory space, named WAVE RING, which contains a volume of 1,024 kb. Then Sniffwave4eew, modified from the Earthworm program called Sniffwave, automatically detects earthquakes and applies a 0.075-Hz recursive high-pass filter to double integrated accelerograms. Then  $P_d$  and  $\tau_c$  are calculated within three seconds after P arrival. Each Sniffwave4eew can only handle one trace. Because only the vertical component is used, 61 Sniffwave4eew programs must be operated at the same time. Once the Sniffwave4eew detects a P-arrival triggering, parameters including station location, P arrival time,  $P_d$ , and  $\tau_c$  are sent to the shared memory. In the final stage, the Tcpcd program fetches the event parameters stored in the shared memory and computes earthquake early warning information. Once the warning threshold ( $M > 6.0$ ) is reached, a shaking map is generated. Once the predicted peak ground acceleration (PGA) of populated regions is larger than 80 gal, the early warning message will be delivered.

### 5.3 Results

The raw records of the Chi-Chi earthquake were replayed in the proposed EEW system (Hsiao et al. 2011). The P arrival times of each station were used for locating the earthquake. The parameters  $P_d$  and  $\tau_c$  of each station were used to estimate magnitude by

the empirical formulas of  $M_{Pd}$  (Hsiao et al. 2011) and  $M_{\tau_c}$  (Wu et al. 2007). Figure 5-4 shows six progressive EEW reports. The first event report is available 11.7 seconds after the earthquake origin time. The reporting time is significantly reduced compared to the present average EEW reporting time of 20 seconds. Therefore, the radius of the warning blind zone is shortened from 70 km to about 40 km. The estimated earthquake location is quite satisfactory even in the first report. In each report,  $M_{Pd}$  are all smaller than 7.0, implying that  $P_d$  may saturate for large earthquakes. On the other hand, the estimated  $M_{\tau_c}$  between 7.2 and 7.5 is rather close to the reported  $M_w$  of 7.6.

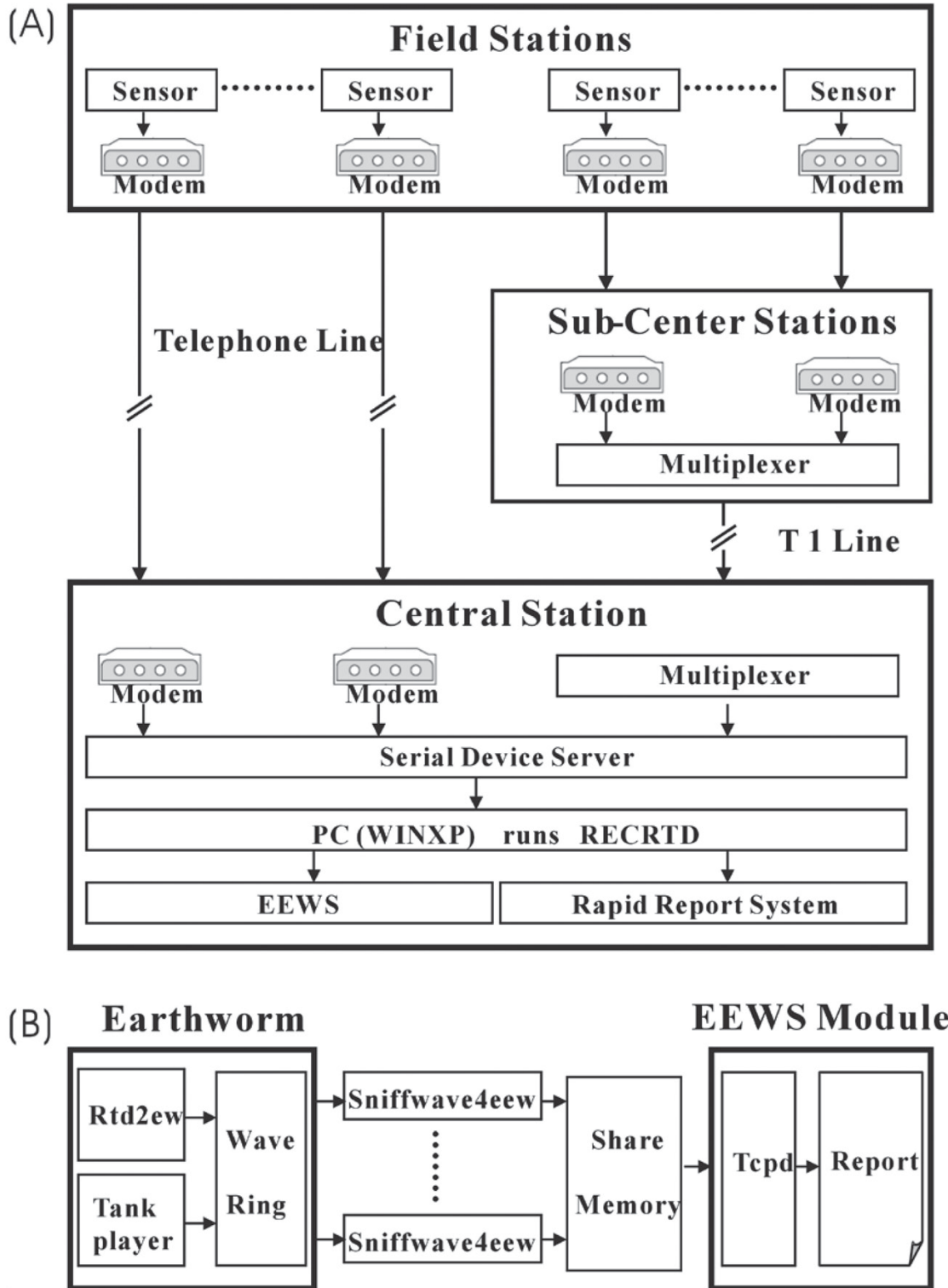


Figure 5-3. System configuration for a case study of Chi-Chi earthquake. (A) Hardware and (B) software configurations of the CWB P-wave earthquake early warning system.

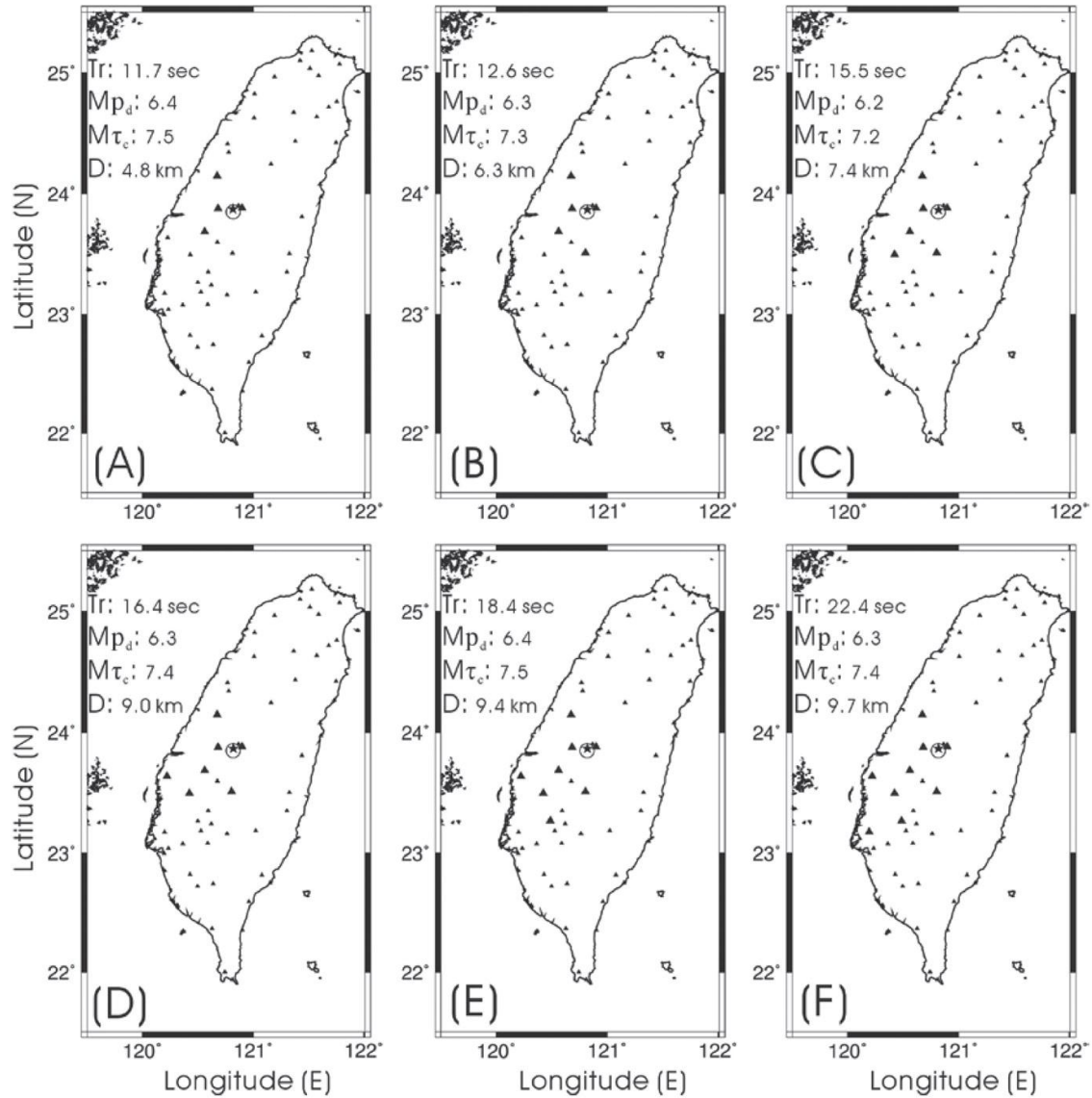
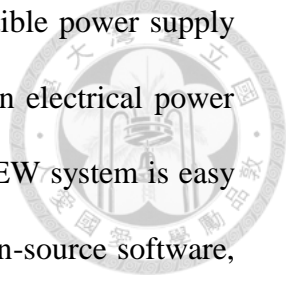


Figure 5-4. Simulation results for six stages after the earthquake occurrence. Open circles and stars indicate the epicenter of the Chi-Chi earthquake from the CWB catalog and simulations, respectively. Large triangles indicate the stations (types A and B) used in simulations.  $T_r$  is the reporting time after the earthquake occurrence, and  $D$  is the focal depth from simulations.  $M_{p_d}$  and  $M_{\tau_c}$  represent the  $P_d$  magnitude and  $\tau_c$  magnitude, respectively.

## 5.4 Summary

After learning the lesson of the 1999 Chi-Chi earthquake, Taiwan has improved the hardware of its seismic networks. The station density and the recording devices have been



gradually improved. Each station now is equipped with an uninterruptible power supply to provide steady electrical power in case of a power failure due to an electrical power tower collapse or a disconnected communication line. The real-time EEW system is easy to implement based on the Earthworm environment. Thanks to its open-source software, users can construct a user designed real-time seismic network and also can easily modify the Earthworm modules for their own data processing tasks. P-wave methods are an effective tool for EEW because only a few seconds of the initial portion of P-wave are needed. In the case of the Chi-Chi earthquake, the first report was generated in only about 12 seconds by the proposed EEW system. The use of the initial P-wave turns out to be a robust system even in those cases in which large ground-shaking may provoke data interruption. Wu and Kanamori (2005b) found the empirical relationship between the peak ground velocity (PGV) and  $P_d$ . By taking advantage of the PGV versus  $P_d$  relationship, the EEW system can also immediately produce a shaking map in PGV, which is useful in emergent resource dispatch management and for quick damage assessment. The size of a large earthquake is more difficult to estimate than that of a small one due to the source dimension and the rupture complexity. In the Chi-Chi earthquake, the fault plane ruptured from south to north and there were two seismic asperities. One is near the hypocenter; the other is about 30 to 65 km north of the hypocentral area. The average slips of these two asperities are about 3 m and 9 m, respectively (Ma et al. 2001). Figure 5-5 plots the spatial distribution of  $P_d$  with the surface trace of the rupturing fault for the Chi-Chi earthquake.  $P_d$  values are larger in the northern part of the fault plane, which is consistent with the rupture directivity of the earthquake. The results in Figure 5-4 suggest that  $P_d$  is not as sensitive as  $\sigma_c$  for the

large-magnitude earthquakes because of the saturation problem. The suggested upper limit of the  $P_d$  methods is about 6.5  $M_W$  (Wu et al. 2006; Wu and Zhao 2006). Estimated by the relationship of  $P_d$  and PGV (Wu and Kanamori 2005b, 2008a), the PGV of the Chi-Chi earthquake are underestimated again, suggesting the  $P_d$  saturation. The study of Lancieri and Zollo (2008) shows that extending the P-wave window to four seconds or more drastically reduces the saturation effect. We also tested the P-wave window at four seconds. We obtained an  $M_{Pd}$  of 6.9, suggesting that the saturation problem really is reduced. Nevertheless,  $M_{Pd}$  can build more magnitude redundancy into the EEW system for earthquakes with magnitudes less than 6.5 or 7.0 (it depends on the P-wave window). In real-time operation, when  $M_{Pd}$  is determined to be larger than 6.5,  $M_{\tau_c}$  will be used for early warning purposes.



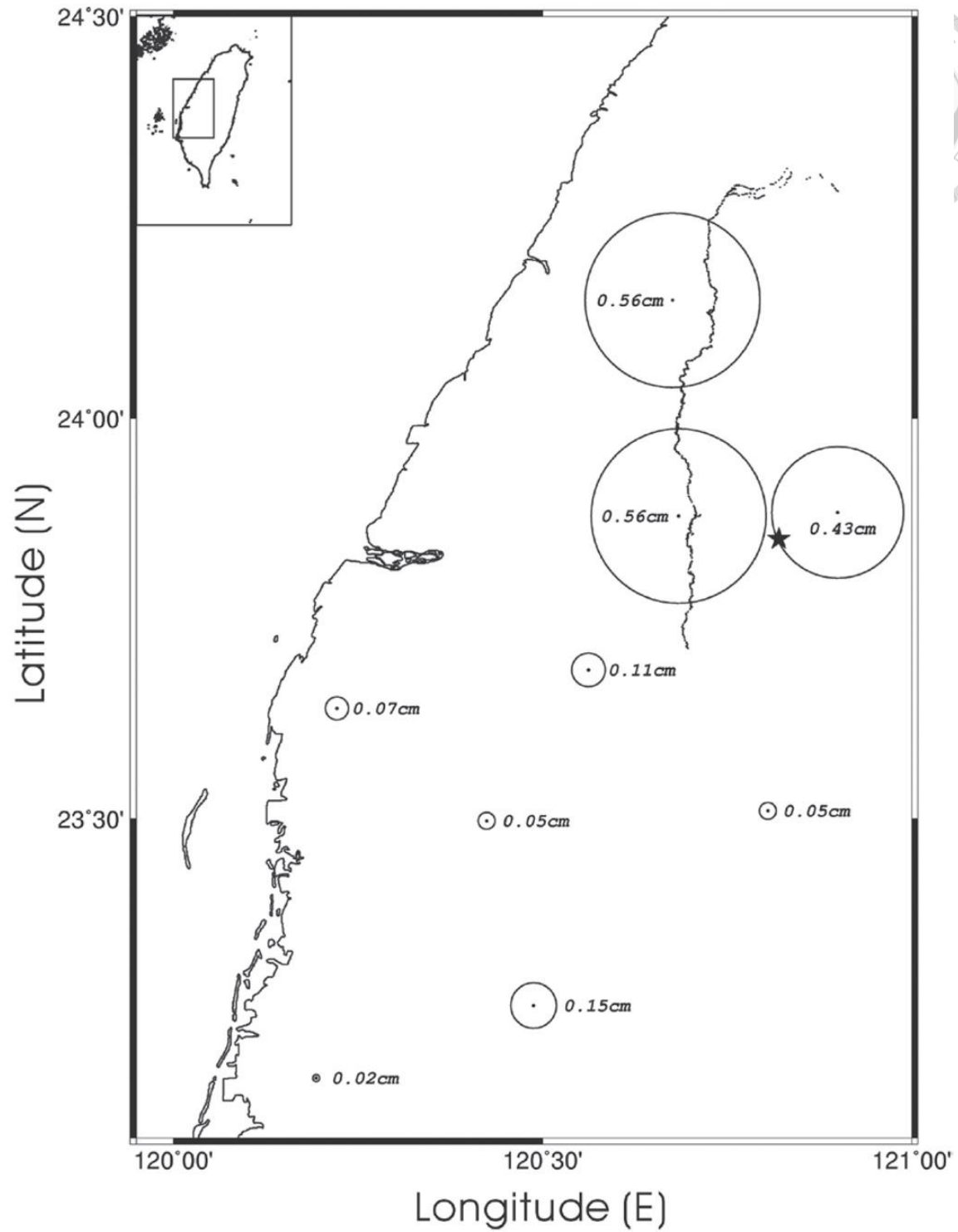


Figure 5-5.  $P_d$  values of the Chi-Chi earthquake.

# Chapter 6



## Discussion and Conclusions

### 6.1 Station Coverage

The station coverage gap (GAP), defined as the angle between epicenter and two adjacent stations, can be used as an indicator to evaluate the quality of earthquake location. Since the precision of earthquake location are involved in the estimation of earthquake magnitude, GAP is a critical value for EEW systems. With good station coverage (e.g., a small value of GAP) the EEW system can provide faster and more reliable earthquake early warnings. On the other hand, with poor station coverage the uncertainty of earthquake location is large. For example, the offshore earthquakes in Taiwan usually have large location error in the initial stage of the EEW updated procedure. Here we discuss the station coverage of the CWBSN.

Figure 6-1(a) shows the distance variations with six stations. The areas with red color means that within 25 km there at least six stations. These areas also represent the areas that the P-wave arrivals can reach at least six stations about 4 seconds. Figure 6-1(b) shows the GAP variations with six stations. Because the offshore areas have poor station coverage, the EEW system may take longer time to locate offshore events. This figure illustrates the weakness of our EEW system. Comparing Figure 6-1 to the Figure 6-2, it is clear that the areas with high potential of damage earthquake should be deployed more stations.

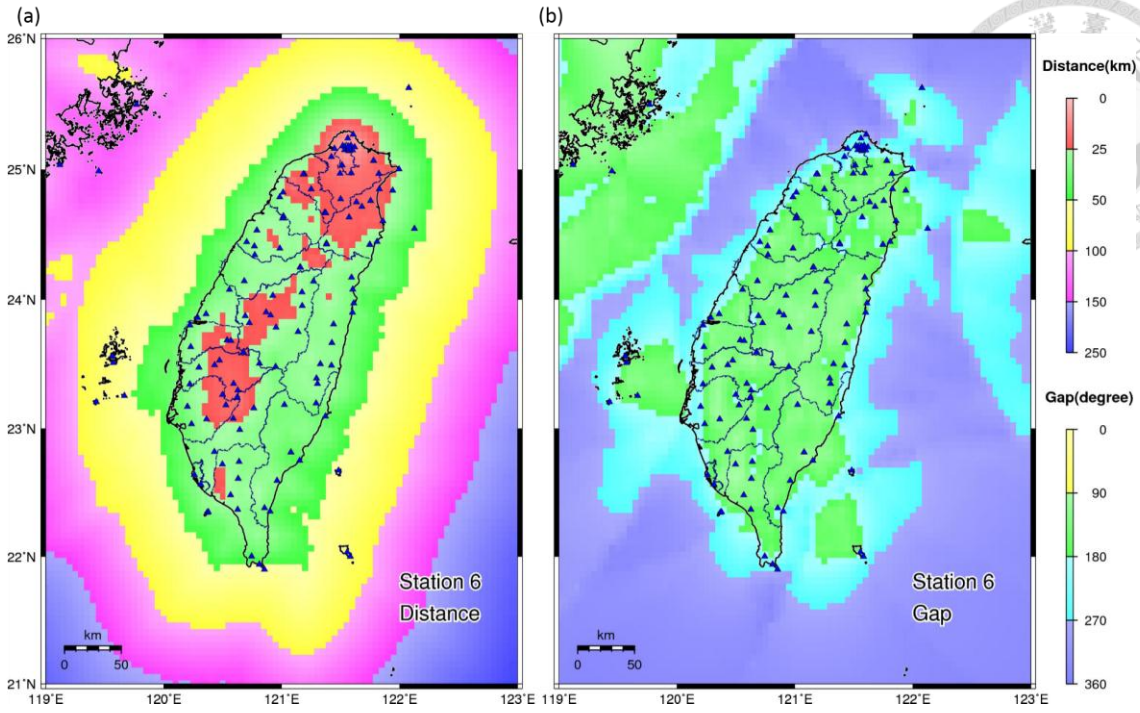


Figure 6-1. Station coverage and density. (a) Distance variations with six stations. (b) GAP variations with six stations.

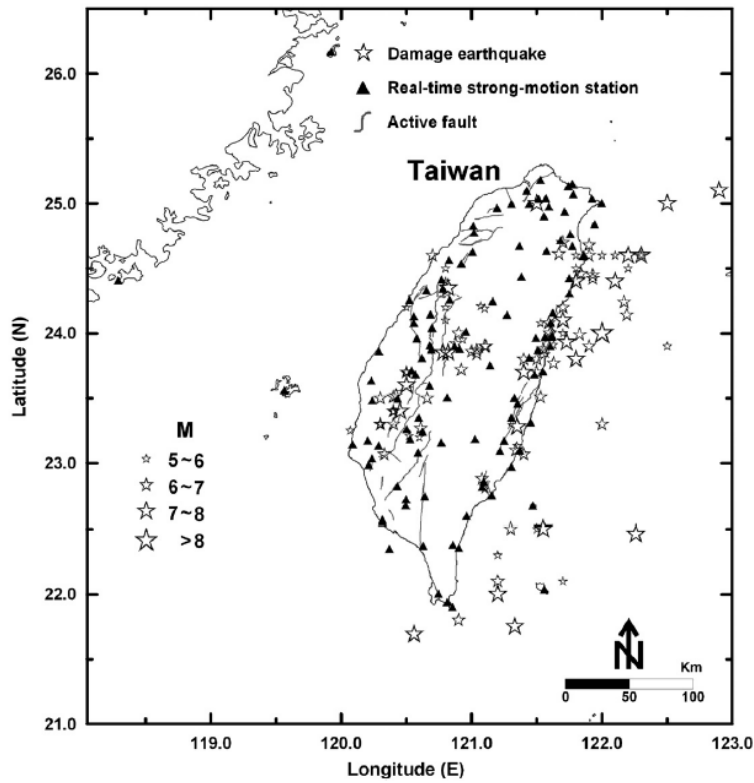


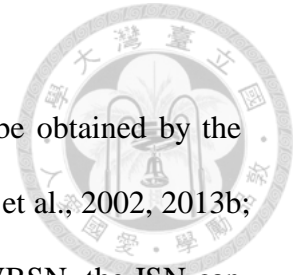
Figure 6-2. Damage earthquakes in Taiwan (Hsiao et al., 2011).

## 6.2 Magnitude Saturation

Earthquake Early Warning (EEW) systems provide warnings to people or pre-programmed systems before the intense ground shakings may cause damage to target areas. With a timely issuance of earthquake information (location and magnitude) provided by EEW systems after large earthquakes, we can take immediate precautions against seismic hazards. Currently, the earthquake locations can be well determined by the P-wave arrivals obtained by dense stations around the source area (Rydelek and Pujol 2004; Satriano, 2008). However, the most challenging work in EEW system is to improve the reliability and accuracy of the empirical method for estimating earthquake magnitude since only the initial portion of seismic waves are used. Based on the precise magnitude and hypocenter estimates, the ground motion can be predicted reliably. On the other hand, overestimation or underestimation of earthquake magnitude may lead to releases of false or missed alarms, respectively, that would result in additional economic loss and societal impacts. For EEW purposes, it is necessary to detect earthquake magnitude in the beginning stage of the earthquake occurrence. However, the 2011,  $M_w$  9.0 Tohoku earthquake demonstrated that for a large earthquake the magnitude cannot be determined by the signals of only the initial several seconds (Hoshihara and Iwakiri, 2011; Colombelli et al., 2012). The on-scale magnitude determination approaches such as W-phase fast source inversion (Kanamori and Rivera 2008; Duputel et al., 2012) and quick  $M_w$  determination using total effective shakings (Wu and Teng 2004; Lin and Wu 2012) could be considered in the future system. It is recommended that the eastern Taiwan area need more stations for faster gathering more P-wave arrivals.

### 6.3 Multi-Events

The near real-time Peak Ground Acceleration (PGA) map can be obtained by the PSN within one minute from the occurrence of a large earthquake (Wu et al., 2002, 2013b; Hsieh et al., 2014; Wu, 2014). By incorporating the PSN into the CWBSN, the ISN can generate a PGA map with more details. The PGA map can be used as an indicator for the most damaged areas, the rupture direction of the fault, and the potential aftershock distribution (Hsieh et al., 2014; Wu, 2014). Moreover, a dense seismic network provides another solution for earthquake magnitude determination. Using the distribution area of the PGA or the  $P_d$  is a quick and robust method for estimating earthquake magnitude (Lin and Wu, 2010; Lin et al., 2011). The EEW system can implement this approach without locating earthquakes. It means the source location error will not be included in the magnitude estimation procedure. In addition, this method is also quite useful for detecting consequent earthquakes and provide warnings, especially for two consecutive earthquakes occurred in a very short time. In this case it is difficult to detect clear P-wave onset time of each event because one event's P-wave phase may be involved in the surface wave of other events. The CWBSN-EEW or ISN-EEW may failed to detect each earthquake due to phase picking problems. However, the distribution area of the PGA or the  $P_d$  can reveal the location and the size of the damage. With a real-time dense seismic network, these observable information will become readily available for the purpose of emergency response after the occurrence of a large earthquake.



## 6.4 Application to Earthquake Rapid Reporting System

Figure 6-3 shows the timeline of the 2015 Hualien earthquake. The first information was issued at 13.4 s after the earthquake occurrence. This is an early warning message that provide warnings to target areas at 50 km away from the epicenter. The following information were created by the Earthquake Rapid Report (ERR) system. The ERR system applied P- and S-wave auto-picking and used those arrivals for locating the earthquake. Meanwhile, the entire waveform records were used for estimating magnitude. This Auto-Report was given in 51 seconds. People on duty in CWB manually checked the quality of waveforms and make sure the intensity of records are not affected by noise or spike. After this procedure, an official earthquake report was released in 3 minute and 17 seconds. Finally, the contour of intensity was given in about 8 minute.

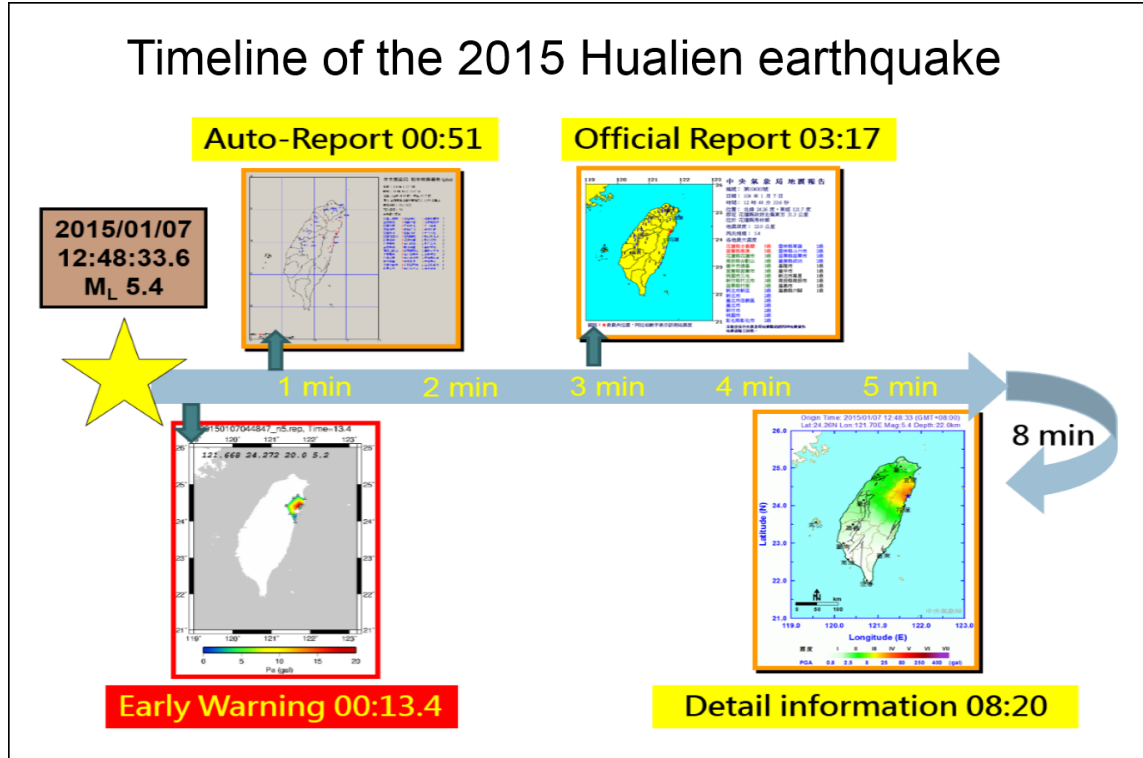
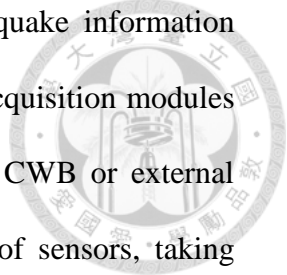


Figure 6-3. Timeline of the 2015 Hualien earthquake.



The EEW system is the initial point in the procedure of earthquake information issuance, shown in Figure 6-4. In the data processing center the data acquisition modules receives real-time data streams from seismic stations maintained by CWB or external institutes. Although those data streams coming from different kind of sensors, taking advantage of the Earthworm software can integrate all of them in the same platform. Meanwhile, the Earthworm software provides two types for serving data streams, WaveServer and WaveRing. The WaveServer stores data for a period of time. Thus, it is usually used for archiving event file. The WaveRing only stores latest data. Thus, it is usually used for real-time data processing.

The EEW system process real-time data from the WaveRing. If an earthquake was detected by the system, there are two procedures will be triggered. One is the EEW procedure. The EEW message will be sent by email, APP and user display. The other is the ERRS procedure. When the EEW message was sent to the ERRS, the ERRS will archive an event and process the file to obtain an auto-report like Figure 6-3. Then, the CWB staff will manually check the report and modify some unreasonable records. Finally, an official report will be released by Website, Fax, and TV.

## 6.5 Conclusions

In this study, the new Earthworm modules, pick\_eev, tcpd and dcsn were created for EEW purposes. The pick\_eev is able to detect P-wave arrival and estimated  $P_d$  value in the 3-s time window after P arrival. A set of parameters are used for automatically detecting the onset of P wave. It is necessary to have a series of offline test to determine those parameters for each station because the background noise and the instrument

sensitivity are different involved in each station. The tcpd module is able to determine location and magnitude of earthquakes using the P-wave arrivals and  $P_d$  values. The dcsn module receives earthquake information from the shared memory in the Earthworm system and creates XML formatted file for EEW issuance. Although the whole system is very simple, it indeed work very well for providing timely earthquake in formation after events occurrences. The online results from EEW system are display in web site, shown in Appendix D.

The Palert sensor is a low-cost accelerometer which can be installed and maintained easily. In this study an Earthworm module, named eew\_svr, was created for receiving real-time data streams from all Palerts and transferring all of them into the Earthworm's shared memory. In this way, it is possible to incorporate Palert Seismic Network into the Central Weather Bureau Seismic Network. Based on the integrated seismic network, EEW system can be implemented faster and more robust.

There are two reasons that the *e*BEAR system is able to be distributed to any seismic network all over the world. One is that the Earthworm is good at integrating different kinds of seismic sensors. The other is that the *e*BEAR system is based on Earthworm software. Currently, the *e*BEAR system has been distributed and tested in India, Korea and Pacific Tsunami Warning Center.



# Configuration of ERRS and EEWS

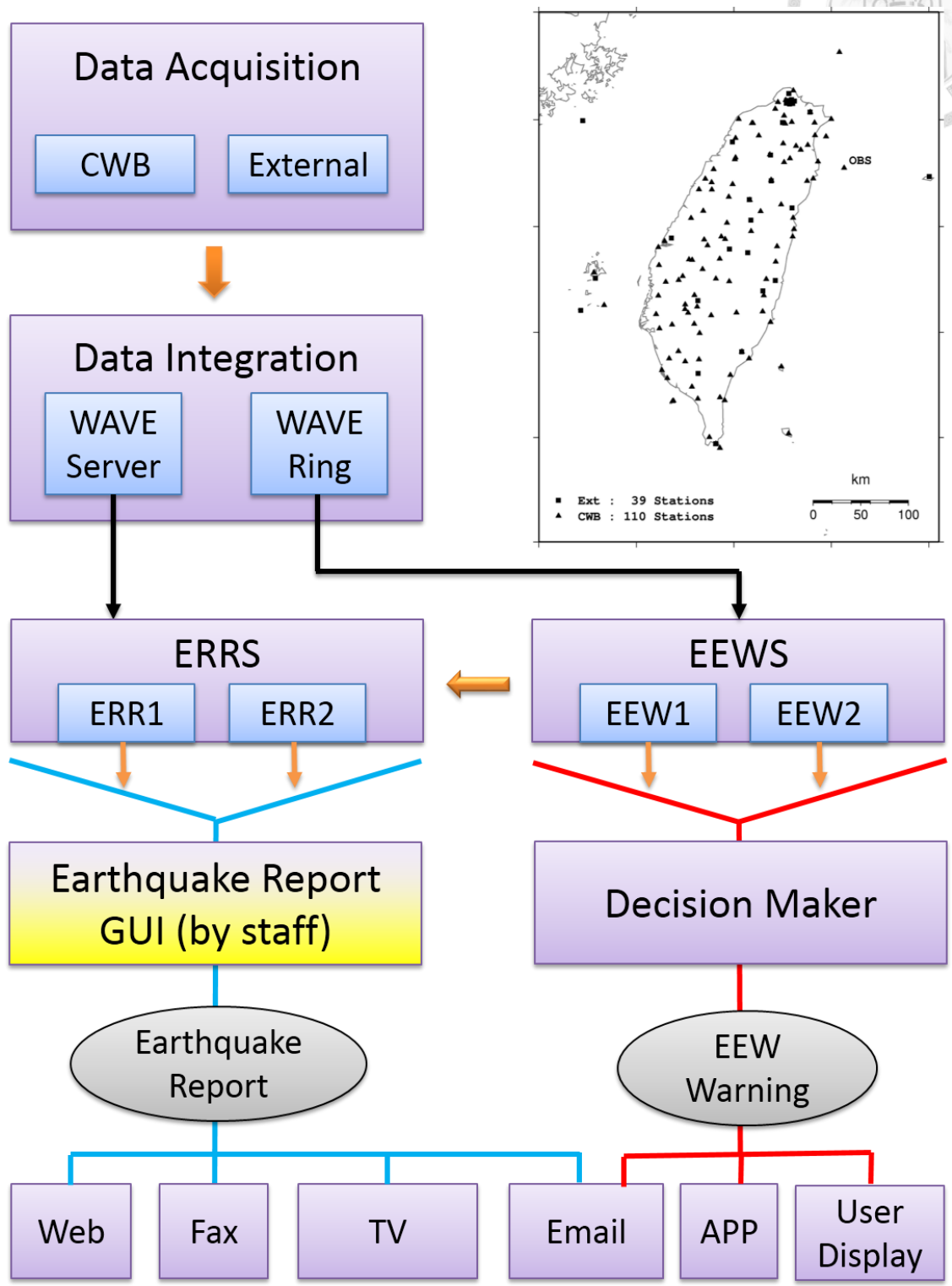
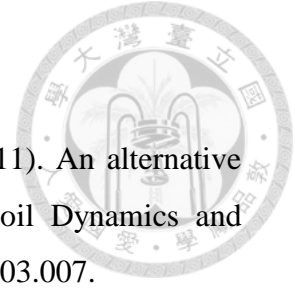


Figure 6-4. System architecture of the ERR system and EEW system.

# References



Alcik, H., O. Brown, Y.-M. Wu, O. M. Nurcan, and E. Mustafa (2011). An alternative approach for the Istanbul earthquake early warning system. *Soil Dynamics and Earthquake Engineering* 31, 181–187; doi:10.1016/j.soildyn.2010.03.007.

Allen, R. M., and H. Kanamori (2003). The potential for earthquake early warning in southern California. *Science* 300, 786–789.

Allen, R. M., H. Brown, M. Hellweg, O. Khainovski, P. Lombard, and D. Neuhauser (2009). Real-time earthquake detection and hazard assessment by ElarmS across California. *Geophysical Research Letters* 36, L00B08; doi:10.1029/2008GL036766.

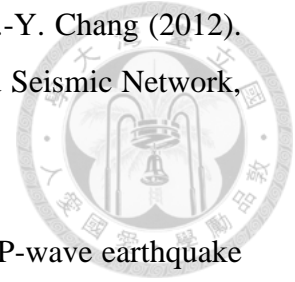
Behr, Y., Clinton, J., Kästli, P., Cauzzi, C., Racine, R., & Meier, M. A. (2015). Anatomy of an Earthquake Early Warning (EEW) Alert: Predicting Time Delays for an End-to-End EEW System. *Seismological Research Letters*.

Beyreuther, M., Barsch, R., Krischer, L., Megies, T., Behr, Y., & Wassermann, J. (2010). ObsPy: A Python toolbox for seismology. *Seismological Research Letters*, 81(3), 530-533.

Bose, M., E. Hauksson, K. Solanki, H. Kanamori, and T. H. Heaton (2009a). Real-time testing of the on-site warning algorithm in southern California and its performance during the July 29 2008 Mw5.4 Chino Hills earthquake. *Geophysical Research Letters* 36, L00B03; doi:10.1029/2008GL036366.

Bose, M., V. Sokolov, and F. Wenzel (2009b). Shake map methodology for intermediate-depth Vrancea (Romania) earthquakes. *Earthquake Spectra* 25, 497–514; doi:10.1193/1.3148882.

Chang, C. H., Y.-M. Wu, D.-Y. Chen, T.-C. Shin, T.-L. Chin, and W.-Y. Chang (2012). An examination of telemetry delay in the Central Weather Bureau Seismic Network, *Terr. Atmos. Ocean. Sci.* 23, 261-268.



Chen, D.-Y., T. L. Lin, Y.-M. Wu, and N.-C. Hsiao (2012). Testing a P-wave earthquake early warning system by simulating the 1999 Chi-Chi, Taiwan, Mw 7.6 earthquake, *Seismol. Res. Lett.* 83, 103-108, doi 10.1785/gssrl.83.1.103.

Chen, D. Y., N. C. Hsiao, and Y. M. Wu, 2015: The Earthworm based earthquake alarm reporting system in Taiwan. *Bull. Seismol. Soc. Am.*, 105 ,doi:10.1785/0120140147

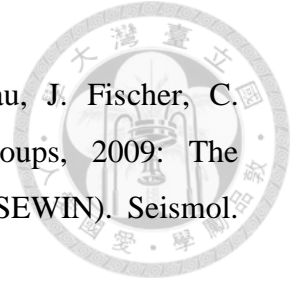
Cochran, E. S., J. F. Lawrence, C. Christensen, and R. S. Jakka, 2009: The quake-catcher network: Citizen science expanding seismic horizons. *Seismol. Res. Lett.*, 80, 26-30, doi:10.1785/gssrl.80.1.26.

Colombelli, S., Zollo, A., Festa, G., and H. Kanamori, 2012: Early magnitude and potential damage zone estimates for the great Mw 9 Tohoku- Oki earthquake. *Geophys. Res. Lett.*, 39, 22-28, doi: 10.1029/2012GL053923.

Duputel, Z., L. Rivera, H. Kanamori, and G. Hayes, 2012: W-phase fast source inversion for moderate to large earthquakes (1990 - 2010), *Geophysical Journal International*, **189**, 1125-1147.

Espinosa-Aranda, J. M., A. Jimenez, G. Ibarrola, F. Alcantar, A. Aguilar, M. Inostroza, and S. Maldonado (1995). Mexico City Seismic Alert System. *Seismological Research Letters* 66, 42–53.

Espinosa-Aranda, J. M., A. Cuellar, A. Garcia, G. Ibarrola, R. Islas, S. Maldonado, and F. H. Rodriguez (2009). Evolution of the Mexican Seismic Alert System (SASMEX). *Seismological Research Letters* 80, 694–706; doi:10.1785/gssrl.83.1.694.



Fleming, K., M. Picozzi, C. Milkereit, F. Kühnlenz, B. Lichtblau, J. Fischer, C. Zulfikar, O. Özcel, and the SAFER and EDIM working groups, 2009: The self-organizing seismic early warning information network (SOSEWIN). *Seismol. Res. Lett.*, 80, 755-771, doi: 10.1785/gssrl.80.5.755.

Geiger, L. (1910). *Herbststimmung bei Erdbeben aus den Ankunftszeiten*, K. Gessell. *Wiss. Goett.* 4, 331-349

Geiger, L. (1912). Probability method for the determination of earthquake epicenters from the arrival time only, *Bull. St. Louis Univ.* 8, 60-71.

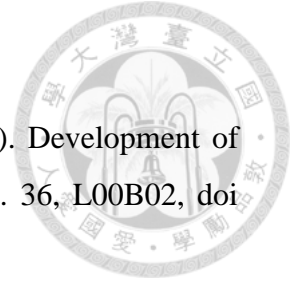
Holland, A, 2003: Earthquake data recorded by the MEMS accelerometer: Field testing in Idaho. *Seismol. Res. Lett.*, 74, 20-26, doi: 10.1785/gssrl.74.1.20.

Horiuchi, S., Y. Horiuchi, S. Yamamoto, H. Nakamura, C. Wu, P. A. Rydelek, and M. Kachi, 2009: Home seismometer for earthquake early warning. *Geophys. Res. Lett.*, 36, L00B04, doi: 10.1029/2008GL036572.

Horiuchi, S., H. Negishi, K. Abe, A. Kamimura, and Y. Fujinawa (2005). An automatic processing system for broadcasting earthquake alarms. *Bulletin of the Seismological Society of America* 95, 708–718; doi:10.1785/0120030133.

Hoshiba, M., and K. Iwakiri, 2011: Initial 30 seconds of the 2011 off the Pacific coast of Tohoku Earthquake (M (w) 9.0)-amplitude and tau(c) for magnitude estimation for Earthquake Early Warning. *Earth, planets and space.* 63, 553-557,

doi:10.5047/eps.2011.06.015.



Hsiao, N.-C., Y.-M. Wu, T.-C. Shin, L. Zhao, and T.-L. Teng (2009). Development of earthquake early warning system in Taiwan, *Geophys. Res. Lett.* 36, L00B02, doi: 10.1029/2008gl036596.

Hsiao, N.-C., Y.-M. Wu, L. Zhao, D.-Y. Chen, W.-T. Huang, K.-H. Kuo, T.-C. Shin, and P.-L. Leu (2011). A new prototype system for earthquake early warning in Taiwan, *Soil Dyn. Earthquake Eng.* 31, 201-208, doi 10.1016/j.soildyn.2010.01.008.

Hsiao, N.-C., T.-W. Lin, S.-K. Hsu, K.-W. Kuo, T.-C. Shin, and P.-L. Leu (2013). Improvement of earthquake locations with the Marine Cable Hosted Observatory (MACHO) offshore NE Taiwan, *Mar. Geophys. Res.*, Online published, DOI:10.1007/s11001-013-9207-3.

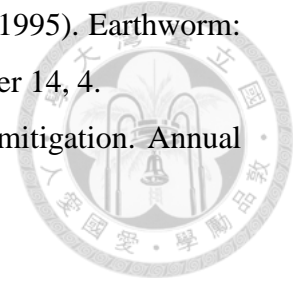
Hsieh, C. Y., Y. M. Wu, T. L. Chin, K. H. Kuo, D. Y. Chen, K. S. Wang, Y. T. Chan, W. Y. Chang, W. S. Li, and S. H. Ker, 2014: Low Cost Seismic Network Practical Applications for Producing Quick Shaking Maps in Taiwan. *Terr. Atmos. Ocean. Sci.* in press, doi: 10.3319/TAO.2014.03.27.01(T).

Huang, H. H., Y. M. Wu, T. L. Lin, W. A. Chao, J. B. H. Shyu, C. H. Chan, and C. H. Chang (2011). The Preliminary Study of the 4 March 2010 Mw6.3 Jiasian, Taiwan, Earthquake Sequence, *Terr. Atmos. Ocean. Sci.* 22, 283-290, doi: 10.3319/TAO.2010.12.13.01(T).

Huang, Y. L., B. S. Huang, K. L. Wen, Y. C. Lai, and Y. R. Chen (2010). Investigation for strong ground shaking across the Taipei basin during the MW 7.0 eastern Taiwan offshore earthquake of 31 March 2002, *Terr. Atmos. Ocean. Sci.* 21, 485-493, doi: 10.3319/TAO.2009.12.11.01(TH).

Johnson, C. E., A. Bittenbinder, B. Bogaert, L. Dietz, and W. Kohler (1995). Earthworm: A flexible approach to seismic network processing, *IRIS Newsletter* 14, 4.

Kanamori, H. (2005). Real-time seismology and earthquake damage mitigation. *Annual Review of Earth and Planetary Sciences* 33, 195–214



Kanamori, H., and Rivera, L. (2008). Source inversion of W phase: speeding up seismic tsunami warning. *Geophysical Journal International*, 175(1), 222-238.

Lancieri, M., and A. Zollo (2008). A Bayesian approach to the realtime estimation of magnitude from the early P and S wave displacement peaks. *Journal of Geophysical Research* 113, B12302; doi:10.1029/2007JB005386.

Lawrence, J. F., E. S. Cochran, A. Chung, A. Kaiser, C.M. Christensen, R. M. Allen, J.W. Baker, B. Fry, T. Heaton, D. Kilb, M. D. Kohler, and M. Taufer, 2014: Rapid Earthquake Characterization Using MEMS Accelerometers and Volunteer Hosts Following the M 7.2 Darfield, New Zealand, Earthquake. *Bull. Seism. Soc. Am.*, 104, 184-192, doi:10.1785/0120120196.

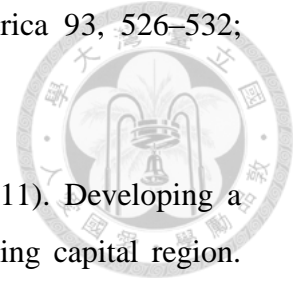
Lee, W. H. K., and D. A. Dodge, (Editors), (1992). "A Course on: PC-Based Seismic Networks", U.S. Geol. Surv. Open-file Report 92 -441, 535 pp.

Ma, K.-F., J. Mori, S.-J. Lee, and S.-B. Yu (2001). Spatial and temporal distribution of slip for the 1999 Chi-Chi, Taiwan earthquake. *Bulletin of the Seismological Society of America* 91, 1,069–1,087; doi:10.1785/0120000728.

Nakamura, Y. (1988). On the urgent earthquake detection and alarm system (UrEDAS). *Proceedings of the Ninth World Conference on Earthquake Engineering* 7, 673–678.

Odaka, T., K. Ashiya, S. Tsukada, S. Sato, K. Ohtake, and D. Nozaka (2003). A new method of quickly estimating epicentral distance and magnitude from a single

seismic record. *Bulletin of the Seismological Society of America* 93, 526–532; doi:10.1785/0120020008.



Peng, H., Z. Wu, Y.-M. Wu, S. Yu, D. Zhang, and W. Huang (2011). Developing a prototype earthquake early warning system (EEWS) in the Beijing capital region. *Seismol. Res. Lett.*, 82, 394–403; doi:10.1785/gssrl.83.1.394.

Lin, C. C. J., Z. P. Shen, and S. K. Huang, 2011: Predicting Structural Response with On-Site Earthquake Early Warning System Using Neural Networks. In: *Proceedings of the Ninth Pacific Conference on Earthquake Engineering Building an Earthquake-Resilient Society*. 2011. p. 14-16.

Lin, P. Y., 2011: Earthquake early warning systems. *International Journal of Automation and Smart Technology*, 1: 27-34, doi:10.5875/ausmt.v1i2.123.

Lin T. L. and Y. M. Wu, 2010: Magnitude estimation using the covered areas of strong ground motion in earthquake early warning. *Geophys. Res. Lett.*, **37**, L09301, doi: 10.1029/2010GL042797.

Lin, T. L., Y. M. Wu, and D. Y. Chen, 2011: Magnitude estimation using initial P-wave amplitude and its spatial distribution in earthquake early warning in Taiwan. *Geophys. Res. Lett.*, **38**, L09303, doi: 10.1029/2011GL047461.

Lin, T. L. and Y. M. Wu, 2012: A fast magnitude estimation for the M 9.0 2011 Great Tohoku Earthquake, *Seismo. Res. Lett.*, **83**, 667-671, doi: 10.1785/0220110119.

R Development Core Team (2006). *R: A language and environment for statistical computing*, R Foundation for Statistical Computing, Vienna, Austria, ISBN 3-900051-07-0, available from <http://www.r-project.org/> (last accessed September 2010).



Rydelek, P. and J. Pujol (2004). Real-time seismic warning with a two-station subarray, Bull. Seism. Soc. Am 94, 1546-1550.

Satriano, C., Lomax, A., & Zollo, A. (2008). Real-time evolutionary earthquake location for seismic early warning. Bulletin of the Seismological Society of America, 98(3), 1482-1494.

Satriano, C., Y.-M. Wu, A. Zollo, and H. Kanamori (2011). Earthquake early warning: Concepts, methods and physical grounds. Soil Dynamics and Earthquake Engineering 31, 106–118; doi:10.1016/j. soildyn.2010.07.007.

Shin, T.-C., and T.-l. Teng (2001). An overview of the 1999 Chi-Chi, Taiwan, earthquake, Bull. Seismol. Soc. Am. 91, 895-913, doi 10.1785/0120000738.

Shin, T.-C., C.-H. Chang, H.-C. Pu, H.-W. Lin, and P.-L. Leu (2013). The geophysical database management system in Taiwan, Terr. Atmos. Ocean. Sci. 24, 11-18.

Teng, T. L., Y. M. Wu, T. C. Shin, Y. B. Tsai and W. H. K. Lee, 1997, One minute after: strong-motion map, effective epicenter, and effective magnitude, Bull. Seism. Soc. Am., 87, 1209-1219.

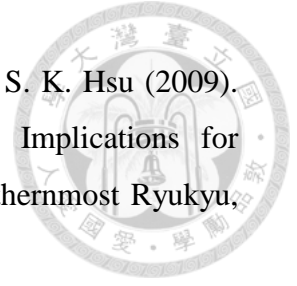
Wu, Y. M., T. C. Shin, C. C. Chen, W. H. K. Lee, and T. L. Teng, 1997: Taiwan rapid earthquake information release system. Seismol. Res. Lett., 68, 931-943.

Wu, Y. M., T. C. Shin, and Y. B. Tsai (1998). Quick and reliable determination of magnitude for seismic early warning, Bull. Seismol. Soc. Am. 88, 1254-1259.

Wu, Y.-M., J.-K. Chung, T.-C. Shin, N.-C. Hsiao, Y.-B. Tsai, W. H. K. Lee, and T.-l. Teng (1999). Development of an integrated earthquake early warning system in



- Taiwan – case for Hualien area earthquakes, *Terr. Atmos. Ocean. Sci.* 10, 719-736.
- Wu, Y. M., W. H. K. Lee, C. C. Chen, T. C. Shin, T. L. Teng, and Y. B. Tsai (2000). Performance of the Taiwan Rapid Earthquake Information Release System (RTD) during the 1999 Chi-Chi (Taiwan) earthquake, *Seismol. Res. Lett.* 71, 338-343.
- Wu, Y.-M., and T.-L. Teng (2002). A virtual subnetwork approach to earthquake early warning, *Bull. Seismol. Soc. Am.* 92, 2008-2018.
- Wu, Y.-M., and H. Kanamori (2005a). Experiment on an onsite early warning method for the Taiwan early warning system. *Bulletin of the Seismological Society of America* 95, 347–353; doi:10.1785/0120040097.
- Wu, Y.-M., and H. Kanamori (2005b). Rapid assessment of damage potential of earthquakes in Taiwan from the beginning of P waves. *Bulletin of the Seismological Society of America* 95, 1,181–1,185; doi:10.1785/0120040193.
- Wu, Y.-M., and L. Zhao (2006). Magnitude estimation using the first three seconds P-wave amplitude in earthquake early warning, *Geophys. Res. Lett.* 33, doi 10.1029/2006gl026871.
- Wu, Y.-M., H. Kanamori, R. Allen, and E. Hauksson (2007). Determination of earthquake early warning parameters,  $\tau_c$  and  $P_d$ , for southern California. *Geophysical Journal International* 170, 711–717; doi:10.1111/j.1365-246X.2007.03430.x.
- Wu, Y.-M., and H. Kanamori (2008a). Development of an earthquake early warning system using real time strong motion signals. *Sensors* 8, 1–9.
- Wu, Y.-M., and H. Kanamori (2008b). Exploring the feasibility of onsite earthquake early warning using close-in records of the 2007 Noto Hanto earthquake. *Earth, Planets, Space* 60, 155–160.



Wu, Y. M., J. B. H. Shyu, C. H. Chang, L. Zhao, M. Nakamura, and S. K. Hsu (2009).

Improved seismic tomography offshore northeastern Taiwan: Implications for subduction and collision processes between Taiwan and the southernmost Ryukyu, *Geophys. J. Int.* 178, 1042–1054

Wu, Y. M., T. L. Lin, W. A. Chao, H. H. Huang, N. C. Hsiao, and C. H. Chang, 2011,

Faster short-distance earthquake early warning using continued monitoring of filtered vertical displacement — a case study for the 2010 Jiasian earthquake, Taiwan, *Bull. Seism. Soc. Am.*, 101, 701–709, doi:10.1785/0120100153.

Wu, Y. M., C. H. Chang, H. Kuo-Chen, H. H. Hunag, and C. Y. Wang, 2013a: On the

use of explosion records for examining earthquake location uncertainty in Taiwan. *Terr. Atmos. Ocean. Sci.*, 24, 685-694, doi: 10.3319/TAO.2013.01.31.01(T).

Wu, Y. M., D. Y. Chen, T. L. Lin, C. Y. Hsieh, T. L. Chin, W. Y. Chang, W. S. Li, and S.

H. Ker, 2013b: A high density seismic network for earthquake early warning in Taiwan based on low cost sensors. *Seismol. Res. Lett.*, 84, 1048-1054, doi: 10.1785/0220130085.

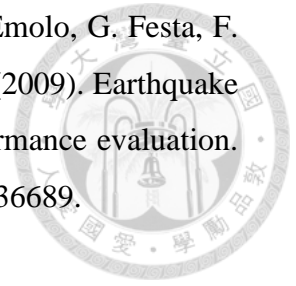
Wu, Y. M., 2014: Progress on development of an earthquake early warning system using

low cost sensors, *Pure and Applied Geophys.* Published online, doi: 10.1007/s00024-014-0933-5.

Yu, S. B., H. Y. Chen, L. C. Kuo, S. E. Lallemand, and H. H. Tsien (1997). Velocity field

of GPS stations in the Taiwan area, *Tectonophysics* 274, 41–59.

Zollo, A., G. Iannaccone, M. Lancieri, L. Cantore, V. Convertito, A. Emolo, G. Festa, F. Gallovic, M. Vassallo, C. Martino, C. Satriano, and P. Gasparini (2009). Earthquake early warning system in southern Italy: Methodologies and performance evaluation. *Geophysical Research Letters* 36, L00B07; doi:10.1029/2008GL036689.



Zollo, A., M. Lancieri, and S. Nielsen (2006). Earthquake magnitude estimation from peak amplitudes of very early seismic signals on strong motion records. *Geophysical Research Letters* 33, L23312; doi:10.1029/2006GL027795.

# Appendix A.



## Earthworm Software

### A.1 Earthworm Installation

For the Earthworm installation, here we demonstrated two examples. First, we illustrated how to construct an empty Earthworm. The empty Earthworm do nothing, but we can add more modules in this Earthworm system. This is the easiest example for us to understand the basics of the Earthworm. To install an empty Earthworm, first we download the Earthworm program, named v7.2, from the Earthworm website (<http://folkworm.ceri.memphis.edu/ew-doc/>). Second, we construct directories including the home directory and running directory, shown as Figure A-1. Third, we put the program, v7.2, into the Earthworm directory, shown as Figure A-2. Fourth, we modify the environment file, shown as Figure A-3. Fifth, we put relative parameters into the run directory shown as Figure A-2. Sixth, we copy startstop\_nt.d into the run directory. Seventh we clear all modules listing in the startstop\_nt.d. Then we open a command line and type “ew\_nt.bat” for setting up Earthworm environment. Finally, we type “startstop” for starting the Earthworm. For normally installing Earthworm system, we can refer to Figure A-4.

Figure A-5 shows Earthworm naming system. There are four kinds of naming schema using in the Earthworm system. According to these names, the Earthworm system is able to identify the source of data. Figure A-6 shows four kind of definition files in the Earthworm system. Earthworm.d defines the module and RING IDs in the system. Before

running Earthworm, make sure the modules we used in the 'startstop\_nt.d' has been defined in this file. For earthworm\_global.d file, we usually do not modify it. Here, we can understand the Installation ID and Message Type ID. For startstop\_nt.d file, we define how many RINGs, what kind of Rings, what kind of modules we used in the Earthworm.

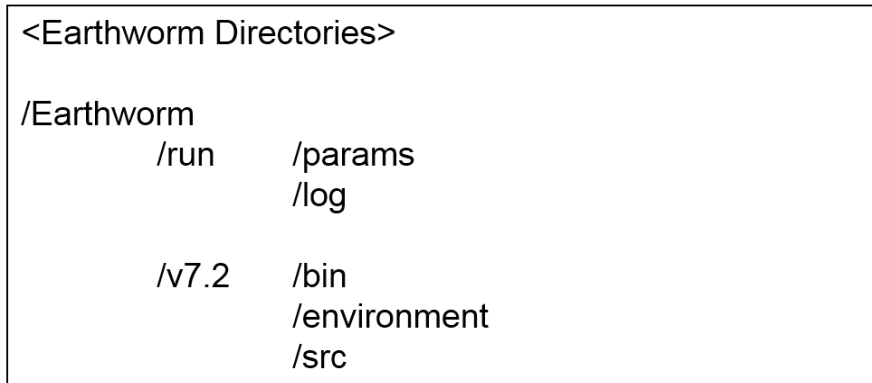


Figure A-1. Earthworm directory structure

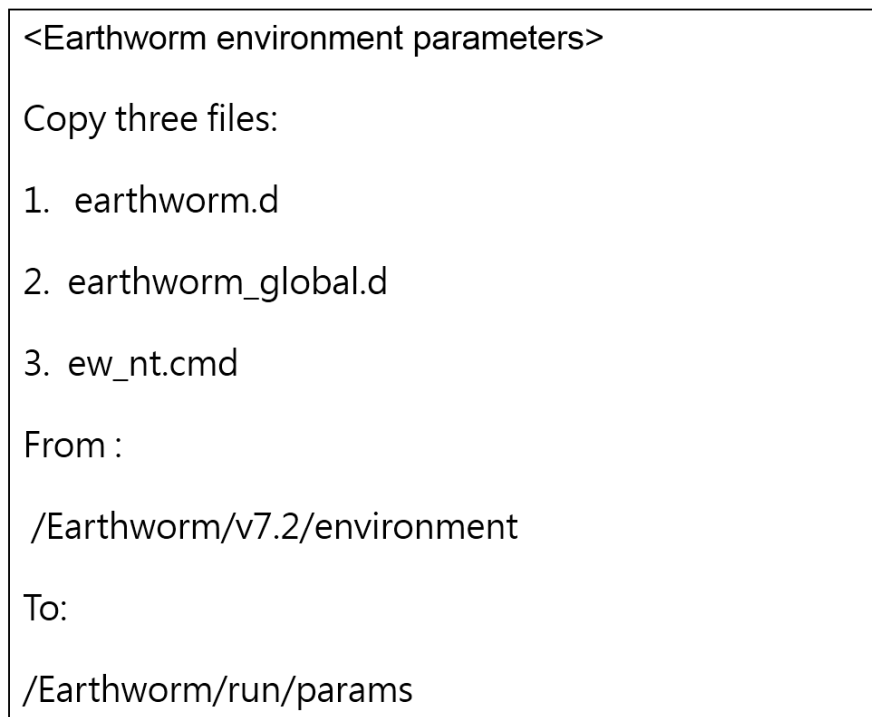


Figure A-2. Earthworm environment parameters

<ew\_nt.cmd>

@rem Set environment variables used by earthworm  
modules at run-time

@rem -----

set EW\_INSTALLATION=INST\_UNKNOWN

set EW\_HOME=D:\earthworm

set EW\_VERSION=earthworm\_7.2

set EW\_PARAMS=%EW\_HOME%\run\params

set EW\_LOG=%EW\_HOME%\run\log\

set SYS\_NAME=%COMPUTERNAME%

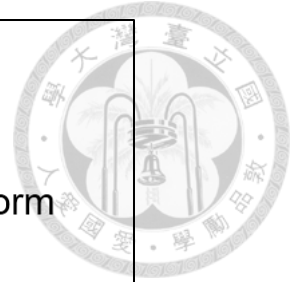


Figure A-3. Earthworm environmental file

#### Earthworm Installation:

STEP 1. Choosing Earthworm modules

STEP 2. Estimating hardware

STEP 3. Drawing Earthworm diagram

STEP 4. Downloading Earthworm software

STEP 5. Constructing Earthworm directories

STEP 6. Setting up Earthworm environment parameters

STEP 7. Setting up Earthworm module parameters

STEP 8. Start Earthworm

Figure A-4. Eight steps for Earthworm installation

# Earthworm Schema



Installation ID

Installation name

Module ID

Module name

Message Type

Message name(waveform, PICK, LOCATION, HeartBeat)

Ring Name

Shared memory name

Figure A-5. Earthworm naming system

# Earthworm Definition

Earthworm.d

Define RING NAME, MODULE ID, MESSAGE TYPE

Earthworm\_global.d

Defien INSTALLATION ID, MESSAGE TYPE

Startstop.d

Describe modules and rings used in the system

ew\_nt.cmd

Describe path and installation ID

Figure A-6. Definition files in the Earthworm

Figure A-7 shows the second example that the Earthworm receives data from IRIS data center and serves waveform data using WaveServer. In this example, we use slink2ew module to receive real-time data from seedlink server. From WaveServer we display waveform using WaveViewer and archive data using Waveman2disk. We can use programs like “findwave” and “sniffwave” to check if real-time data coming into the WAVE\_RING. In addition, the program “getmenu” can help us to check if the WaveServer can serve waveform data.

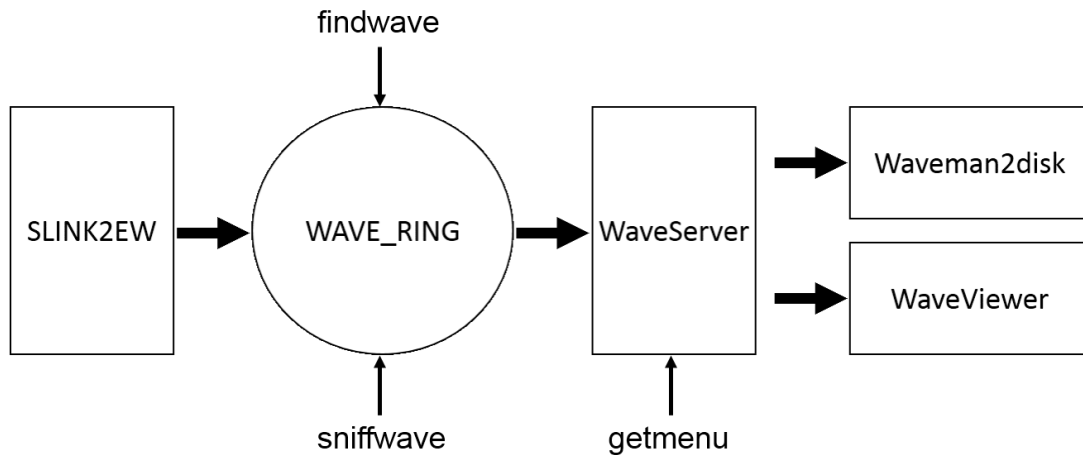


Figure A-7 The Earthworm diagram of waveform receive, display and archive.



## A.2 Earthworm Features

1. **Data Input:** The Earthworm software supports different kinds of commercial sensors for receiving data streams from them, such as Geotech SmartGeoHub, Guralp scream, Quanterra Q330, Nanometrics Appolo Server and Seedlink server, shown as Figure A-8.

### Earthworm functions

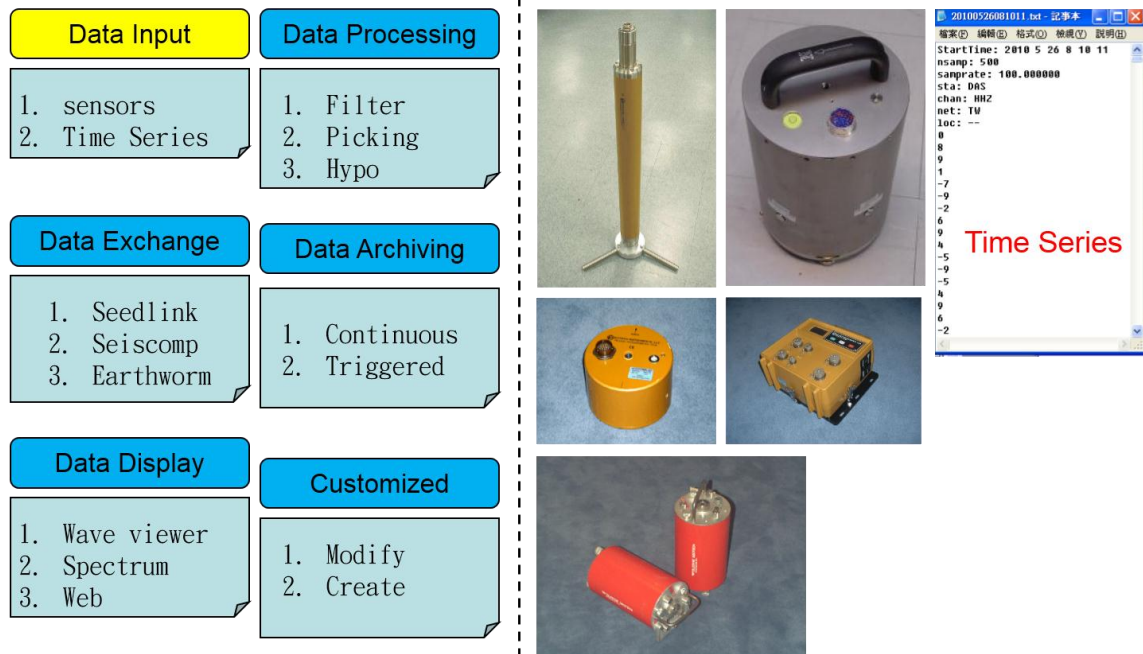


Figure A-8. The Earthworm features of data input.

2. **Data Exchange:** The Earthworm software use import/export modules to exchange real-time data in waveforms or some parameters. For example, one Earthworm system may have functions for picking P-wave arrivals. This system can only send picks to other Earthworms. In this way, we do not need to send massive waveform data to data center. We can have P-wave auto picking in sub centers and send only picks to the data center. As a result, the limited band width between data center and sub centers can be saved. In addition, the Earthworm software can receive data from other software used in other data centers, such as Antelope and Seiscomp, shown as in Figure A-9.

## Earthworm functions

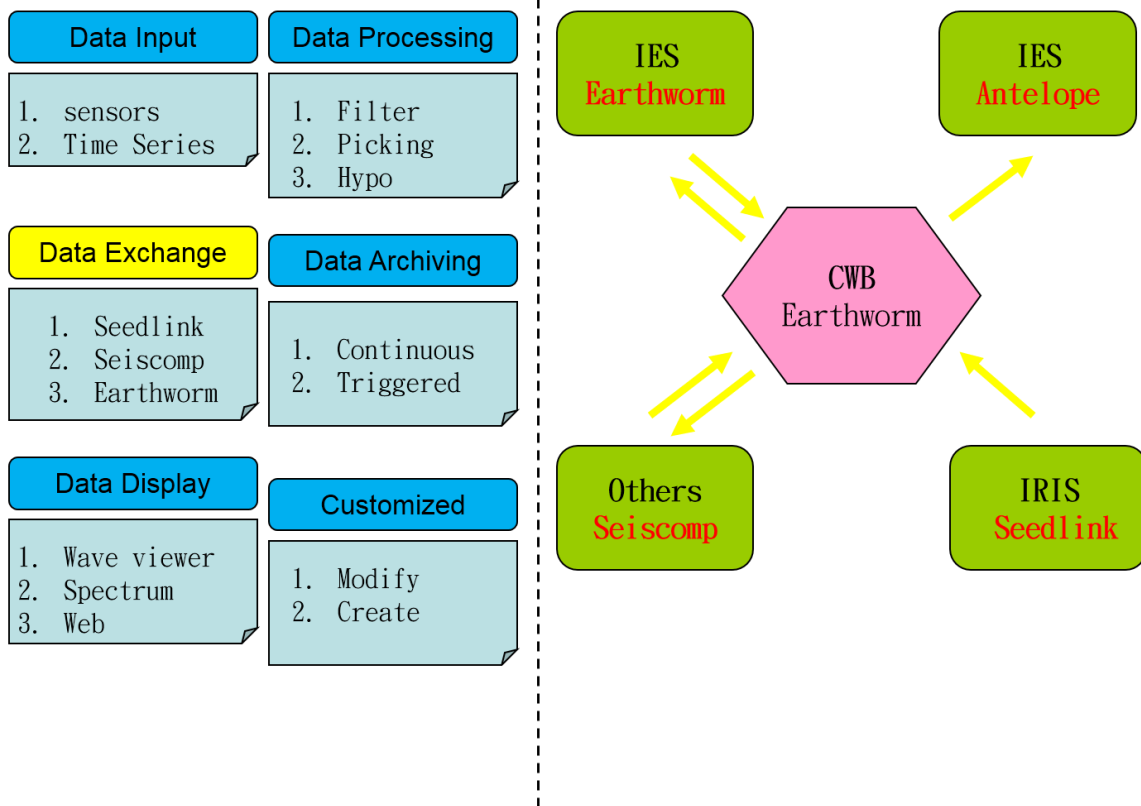
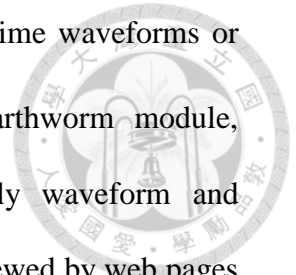


Figure A-9. The Earthworm features of data exchange.

3. **Data Display:** The Earthworm software can display real-time waveforms or passed waveforms as long as they are stored in the Earthworm module, WaveserverV. In addition, the Earthworm can have daily waveform and time-frequency plots for each channel. The pictures will be viewed by web pages, shown as in Figure A-10.



## Earthworm functions

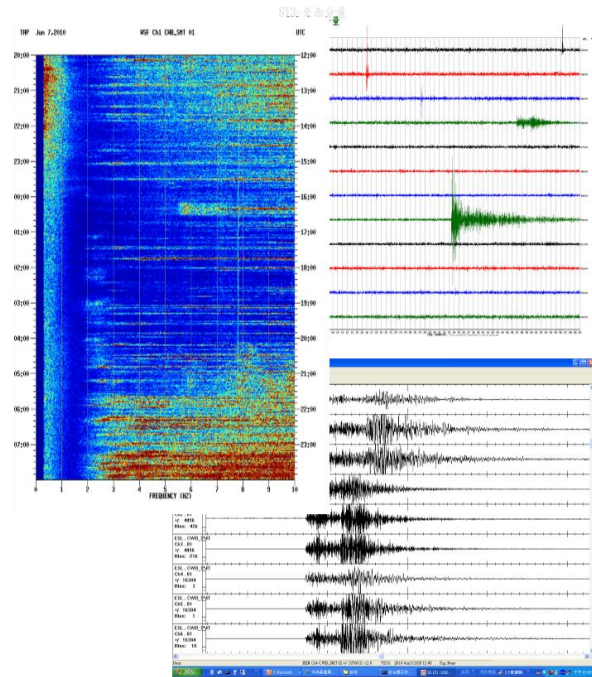
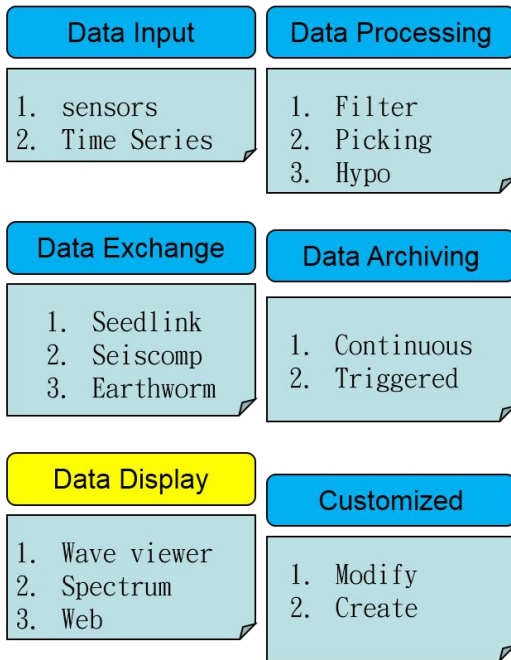
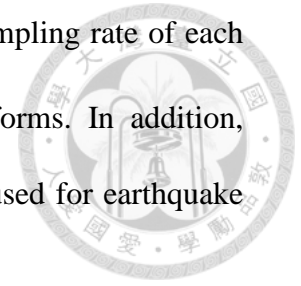


Figure A-10. The Earthworm features of data display.

4. **Data Processing:** The Earthworm software can reduce sampling rate of each channels and also can apply different filters to the waveforms. In addition, P-wave auto picking can be applied and those picks can be used for earthquake location, shown as in Figure A-11.



## Earthworm functions

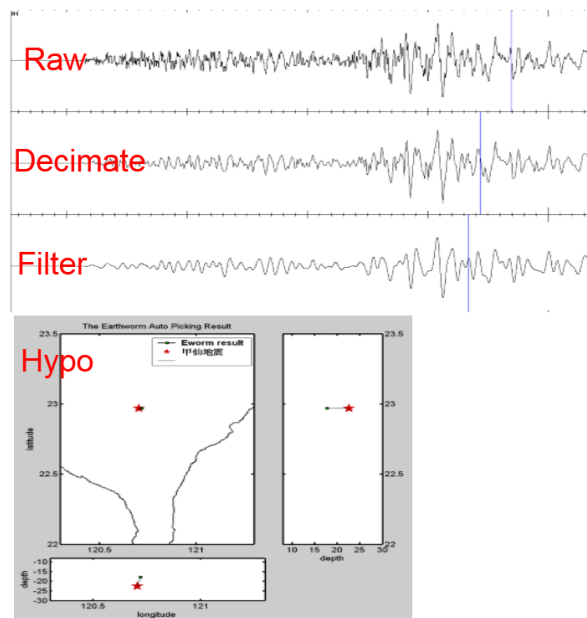
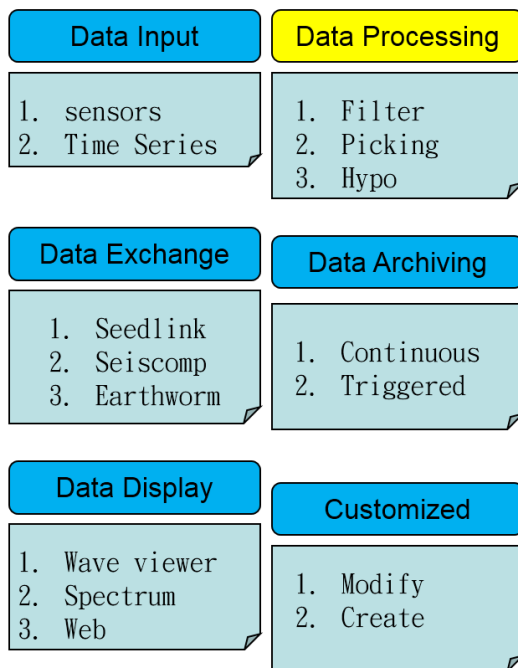
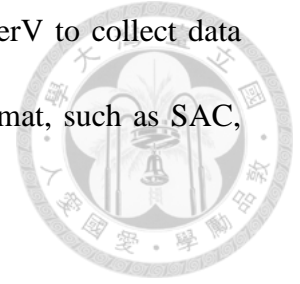
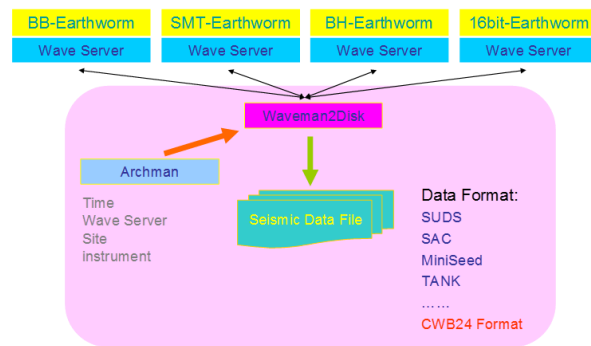
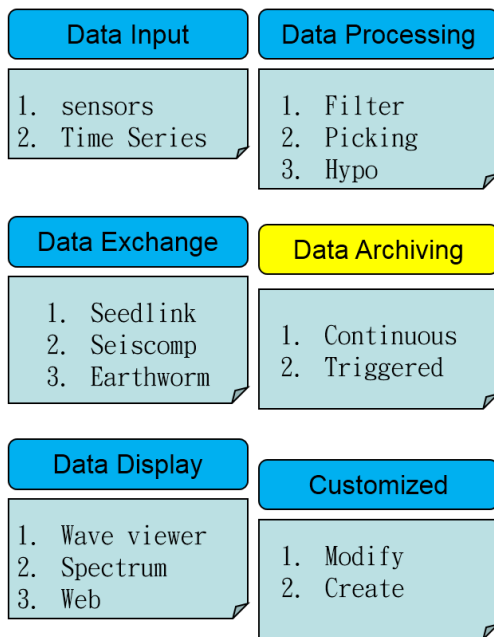


Figure A-11. The Earthworm features of data processing.

5. Data Archiving: The Earthworm software use WaveServerV to collect data for some time period. Users can archive data in different format, such as SAC, miniseed or SUDS, etc., shown as in Figure A-12.



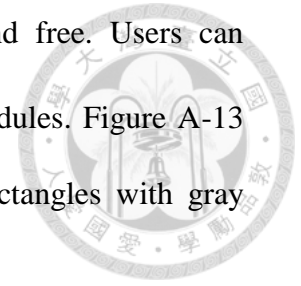
## Earthworm functions



**Data Format:  
SAC, MiniSeed, SUDS, ...**

Figure A-12. The Earthworm features of data archiving.

6. **Customize:** The Earthworm software is open source and free. Users can modify codes and compile them for creating customized modules. Figure A-13 shows an example for developing Earthworm modules. Rectangles with gray colors represent modules created in this study.



## Earthworm functions

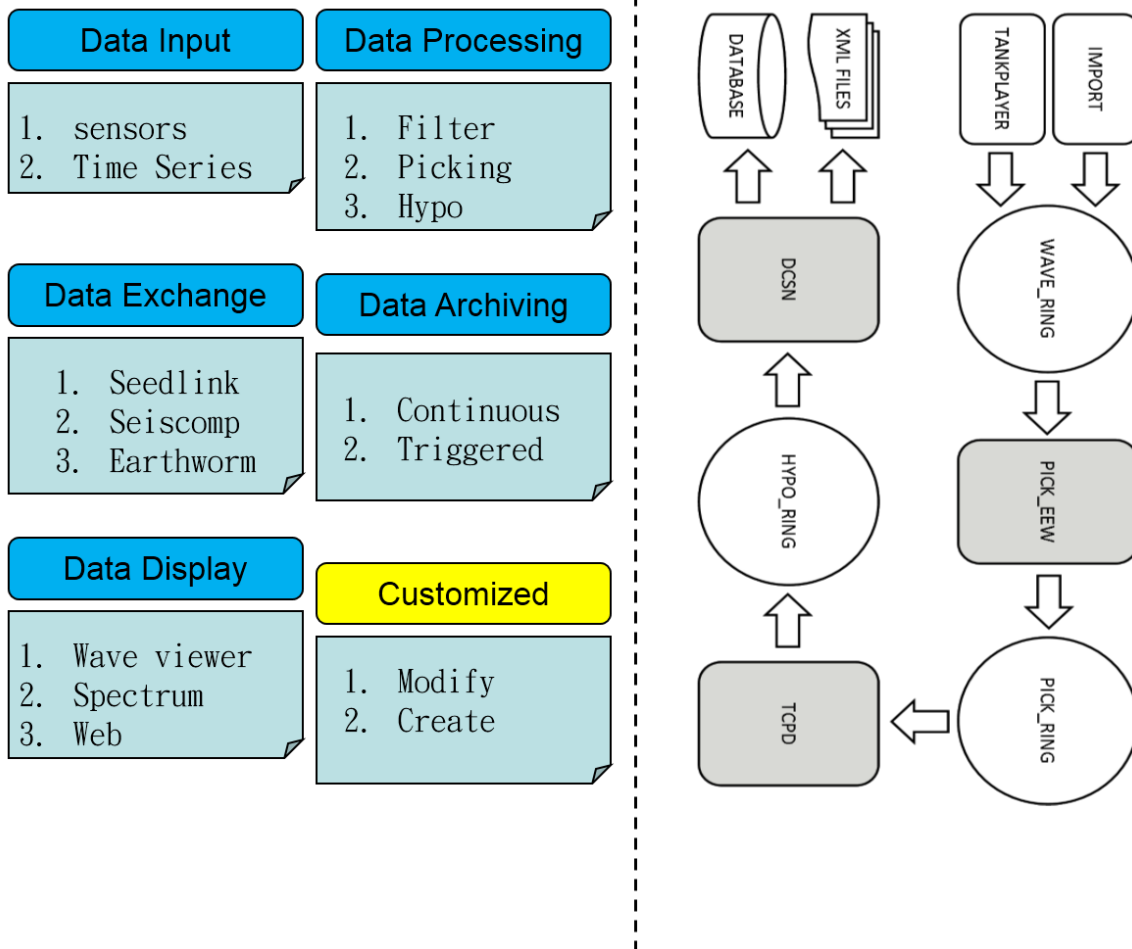


Figure A-13. The Earthworm features of customized modules.

# Appendix B.

## CWB24 Format



File Header	Port Header	Data (Component , Port , Points)
24 bytes	32 bytes * (number of ports)	4 bytes * 3 (components) * (number of port) * Points (File length * Sample rate)

### File Header (24 bytes)

	內容	資料型態	範例 / 說明
1	<b>System ID</b>	<b>4 Bytes Char</b>	<b>CWBN for 24 bit system</b>
2	Year	2 bytes Int	2009
3	Milli-second	2 bytes Int	0，一般情況由整秒紀錄
4	File length (sec)	2 bytes Int	檔案紀錄長度，(File Length * Sample Rate=點數)
5	Month	1 byte Int	11
6	Day	1 byte Int	24
7	Hour	1 byte Int	10
8	Minute	1 byte Int	55
9	Second	1 byte Int	20
10	<b>Sample Rate</b>	<b>1 byte unsigned Int</b>	<b>100 for 24 bit system</b>
11	<b>Number of Port</b>	<b>2 bytes Int</b>	總共多少 Port (1 個port =1套儀器，並非站數) 目前為 <b>200</b> ，未來6年估算將約為： <b>414</b> <b>SMT (SP+FBA) = 71+71 = 142</b> <b>BH (BB+2 FBA) = 9 * 3 = 27</b> <b>CWB-BB = 36</b> <b>IES (BB+YMS) = 21 + 5</b> <b>IRIS-JPN = 3</b> 未來BH = <b>6*10*3 = 180</b>
12	Null (Empty)	6 bytes Int	第一站站名(方便定位使用)

### Port Header (32 Bytes each port)

	內容	資料型態	範例 / 說明
1	Station	4 Bytes Char	TAP1, HWA, CHN5, .....
2	<b>Instrument</b>	<b>4 bytes Char</b>	<b>FBA</b> ：強震儀， <b>SP</b> ：短週期， <b>BB</b> ：寬頻
3	Component Order	3 bytes Char	VNE
4	<b>GPS status</b>	<b>1 bytes Int</b>	<b>0</b> ：unlock， <b>1</b> ：lock， <b>2</b> ：unknown， <b>3</b> ：broken
5	Null (Empty)	2 bytes Int	未使用
6	Number of Comp	1 bytes Int	3
7	<b>Location</b>	<b>1 bytes Int</b>	<b>1</b> ：地表， <b>2</b> ：井下， <b>3</b> ：海底
8	<b>Net Name</b>	<b>4 bytes Char</b>	<b>SMT</b> ：smart24 網 <b>BB</b> ：寬頻觀測網 <b>BH</b> ：井下觀測網 <b>JPN</b> ：IRIS 日本網 <b>YMS</b> ：中研院陽明山 <b>BATS</b> ：中研院寬頻 ( <b>RTD / S13</b> ：專線之舊系統)
9	Null (Empty)	12 bytes Int	未使用

Data (Component , Port , Points) column major structure

(1,1,1)	(2,1,1)	(3,1,1)	(1,2,1)	(2,2,1)	(3,2,1)	.....	(1,M,1)	(1,M,1)	(3,M,1)
4 bytes	4 bytes	4 bytes	4 bytes	4 bytes	4 bytes	.....	4 bytes	4 bytes	4 bytes
第 1 port 第 1 點 UD	第 1 port 第 1 點 NS	第 1 port 第 1 點 EW	第 2 port 第 1 點 UD	第 2 port 第 1 點 NS	第 2 port 第 1 點 EW	.....	第 M port 第 1 點 UD	第 M port 第 1 點 NS	第 M port 第 1 點 EW

(1,1,2)	(2,1,2)	(3,1,2)	(1,2,2)	(2,2,2)	(3,2,2)	.....	(1,M,2)	(1,M,2)	(3,M,2)
4 bytes	4 bytes	4 bytes	4 bytes	4 bytes	4 bytes	.....	4 bytes	4 bytes	4 bytes
第 1 port 第 2 點 UD	第 1 port 第 2 點 NS	第 1 port 第 2 點 EW	第 2 port 第 2 點 UD	第 2 port 第 2 點 NS	第 2 port 第 2 點 EW	.....	第 M port 第 2 點 UD	第 M port 第 2 點 NS	第 M port 第 2 點 EW

.....

(1,1,N)	(2,1,N)	(3,1,N)	(1,2,N)	(2,2,N)	(3,2,N)	.....	(1,M,N)	(1,M,N)	(3,M,N)
4 bytes	4 bytes	4 bytes	4 bytes	4 bytes	4 bytes	.....	4 bytes	4 bytes	4 bytes
第 1 port 第 N 點 UD	第 1 port 第 N 點 NS	第 1 port 第 N 點 EW	第 2 port 第 N 點 UD	第 2 port 第 N 點 NS	第 2 port 第 N 點 EW	.....	第 M port 第 N 點 UD	第 M port 第 N 點 NS	第 M port 第 N 點 EW

$$\text{Total Bytes} = 4 * M * N$$

M : Number of Ports

N : Number of Points = File Length \* Sample Rate

Example:

4-min file with 200 stations

Number of Ports = 200    File length = 240    Sample Rate = 100

<b>File Header</b>	<b>Port Header</b>	<b>Data (Component , Port , Points)</b>
24	32 * 200 = 6400	4 * 3 * 200 * 240 * 100 = 57600000



# Appendix C.

## Configure files of EEW modules



```
#
# Pick_ew's Configuration File
#
MyModId      MOD_PICK_EW_BB      # This instance of pick_ew

StaFile      "pick_cwb24_Z"      # File containing station name/pin# info

InRing       EXPPT_RING_BB      # Transport ring to find waveform data on,
OutRing      PICK_RING         # Transport ring to write output to,
HeartbeatInt 30                # Heartbeat interval, in seconds,
RestartLength 100              # Number of samples to process for restart
MaxGap       15                # Maximum gap to interpolate
Debug        0                 # If 1, print debugging message

StorePicks 1                    # If 1, store picks
Ignore_weight 5                 # Ignore picks with weight #num, If -1, disable this function.

EEWFile      sta_CWB24_Z

# Specify which messages to look at with Getlogo commands.
#   GetLogo <installation_id> <module_id> <message_type>
# The message_type must be either TYPE_TRACEBUF or TYPE_TRACEBUF2.
# Use as many GetLogo commands as you need.
# If no GetLogo commands are given, pick_ew will look at all
# TYPE_TRACEBUF and TYPE_TRACEBUF2 messages in InRing.
#-----
GetLogo INST_WILDCARD MOD_WILDCARD TYPE_TRACEBUF2
```



```
#
#
#
MyModuleId      MOD_TCPD  # module id for this instance of template
RingName        PICK_RING  # shared memory ring for input/output
RingName_out    EEW_RING  # shared memory ring for input/output
LogFile         0          # 0 to turn off disk log file; 1 to turn it on
HeartBeatInterval 15      # seconds between heartbeats
MagMin 0.5      # Min magnitude
MagMax 10       # Max magnitude
Ignore_weight_P 2        # include 3
Ignore_weight_S 2
Mark 231 # 3 characters for identify system

MagReject       CHGB HHZ BS 01      # ignore magnitude
MagReject       TATO HHZ IU 01      # ignore magnitude

Trig_tm_win     40.0      # The P wave arrival time between each triggered station
Trig_dis_win    180.0     # Distances between each triggered station
Active_parr_win 45.0     # Survival time of each station (sec) , between the P wave arrival time
and current time

Term_num        50          # The last report should be less than this number.
Show_Report     1          # 0: Disable, 1:Enable

#----- P-wave velocity model
Boundary_P      40.0       # boundary of shallow and deep layers
SwP_V           5.10298    # initial velocity in shallow layer
SwP_VG          0.06659    # gradient velocity in shallow layer
DpP_V           7.80479    # initial velocity in deep layer
DpP_VG          0.00457    # gradient velocity in deep layer
GetEventsFrom  INST_WILDCARD  MOD_WILDCARD  TYPE_EEW
```



## Dcsn\_XML's Configuration File

```
#
#
#
MyModuleId      MOD_DCSN_XML  # module id for this instance of template
RingName        EEW_RING   # shared memory ring for input/output
LogFile         1          # 0 to turn off disk log file; 1 to turn it on
                  # to log to module log but not stderr/stdout
HeartBeatInterval 15       # seconds between heartbeats

Magnitude 4.0
Pro_time 60.0
Show_Report_Num 50      # no larger than this number

XML_DIR         D:\Earthworm\xml      # where we store XML files for EEW client program
XML_DIR_LOCAL   D:\Earthworm\xml\xml  # where we store XML files for message
InfoType Exercise          # Actual: for real case, Exercise: for drill, default: Exercise

# List the message logos to grab from transport ring
#           Installation      Module          Message Types
GetEventsFrom INST_WILDCARD   MOD_WILDCARD
```

## Dcsn\_DB's Configuration File



```
#
#
MyModuleId      MOD_DCSN_DB  # module id for this instance of template
RingName        EEW_RING  # shared memory ring for input/output
LogFile         1          # 0 to turn off disk log file; 1 to turn it on
                  # to log to module log but not stderr/stdout
HeartBeatInterval 15      # seconds between heartbeats

Magnitude 1.5
Pro_time 60.0
Show_Report_Num 50      # no larger than this number

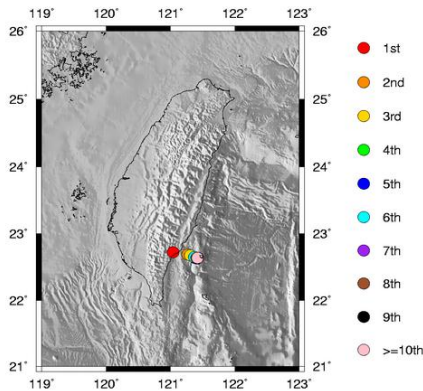
MySQL_Host      192.168.20.234

InfoType  Exercise          # Actual: for real case, Exercise: for drill, default: Exercise

# List the message logos to grab from transport ring
#           Installation      Module          Message Types
GetEventsFrom INST_WILDCARD    MOD_WILDCARD
```

# Appendix D.

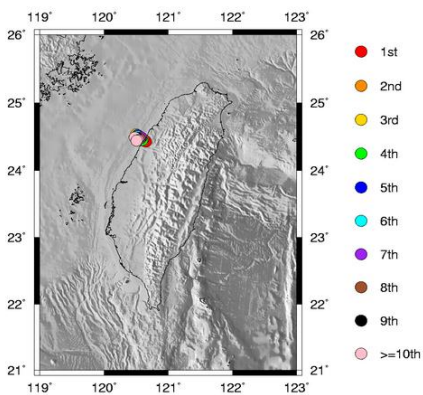
## Online Display of EEW system



報數	報告發送時間	處理時間 (sec)	緯度	經度	深度 (km)	規模	使用測站數	與RTD誤差 (km/mag)
1	2015-02-14 04:06:48	13.3	22.72	121.04	40	6	8	40.51/-0.3
2	2015-02-14 04:06:49	16.1	22.69	121.27	20	6.3	13	14.81/0
3	2015-02-14 04:06:49	16.7	22.68	121.31	50	6.4	18	10.23/0.1
4	2015-02-14 04:06:51	20.1	22.64	121.41	30	6.3	22	2.48/0
5	2015-02-14 04:06:54	21.2	22.63	121.39	40	6.5	25	3.51/0.2
6	2015-02-14 04:06:54	22.9	22.65	121.37	20	6.5	34	3.51/0.2
7	2015-02-14 04:06:56	25.3	22.63	121.43	20	6.6	41	4.71/0.3
8	2015-02-14 04:06:58	27	22.64	121.41	20	6.7	46	2.48/0.4
9	2015-02-14 04:07:00	28.7	22.64	121.43	20	6.7	48	4/0.4
10	2015-02-14 04:07:00	29.4	22.64	121.42	20	6.7	48	3.14/0.4
11	2015-02-14 04:07:00	29.6	22.64	121.42	10	6.6	52	3.14/0.3

Updated Earthquake location in EEW system. Different colors represent different report.

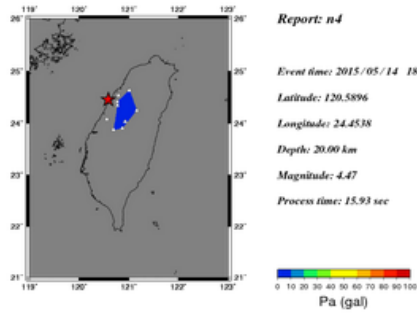
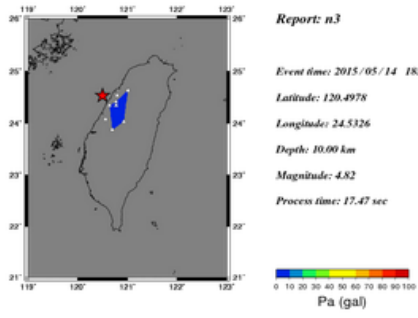
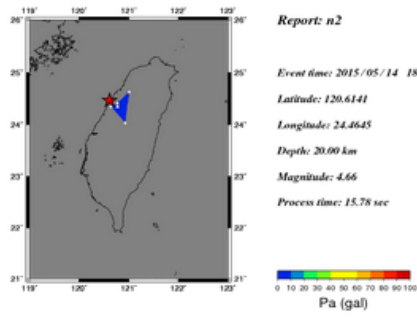
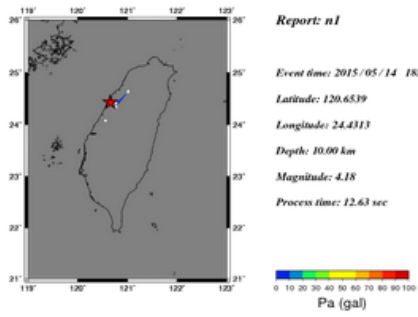
There are 11 reports in this case.



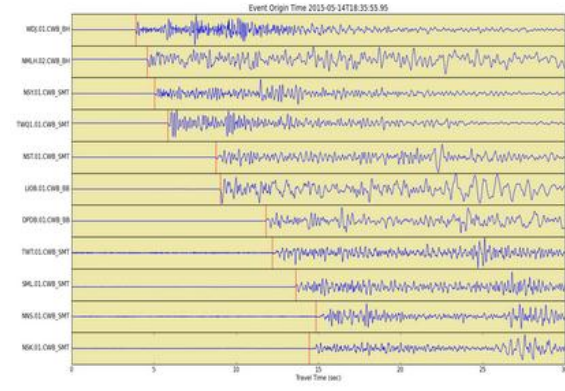
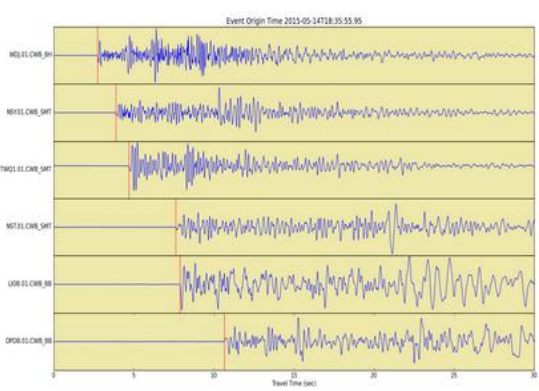
報數	報告發送時間	處理時間 (sec)	緯度	經度	深度 (km)	規模	使用測站數	與RTD誤差 (km/mag)
1	2015-05-15 02:36:05	12.6	24.43	120.65	10	4.2	6	---/---
2	2015-05-15 02:36:09	15.8	24.46	120.61	20	4.7	7	---/---
3	2015-05-15 02:36:09	17.5	24.53	120.5	10	4.8	10	---/---
4	2015-05-15 02:36:09	15.9	24.45	120.59	20	4.5	11	---/---
5	2015-05-15 02:36:11	19.4	24.52	120.52	20	4.6	13	---/---
6	2015-05-15 02:36:11	20.2	24.51	120.52	10	4.5	17	---/---
7	2015-05-15 02:36:13	20.9	24.49	120.58	20	4.5	22	---/---
8	2015-05-15 02:36:13	21.4	24.47	120.56	20	4.6	25	---/---
9	2015-05-15 02:36:18	26.2	24.49	120.5	30	4.8	27	---/---
10	2015-05-15 02:36:18	26.9	24.49	120.48	30	4.6	30	---/---
11	2015-05-15 02:36:19	26.9	24.45	120.53	30	4.6	31	---/---
12	2015-05-15 02:36:32	40.1	24.44	120.51	20	4.7	39	---/---

Updated Earthquake location in EEW system. Different colors represent different report.

There are 12 reports in this case.



Updated Earthquake information in EEW system. Pa values are adopted within 3-sec time window after P-wave arrival.



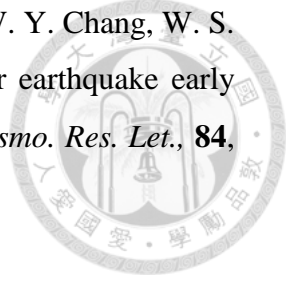
The red lines represent the P-wave arrival picked by the EEW system. The figures are generated by the ObsPy (Beyreuther et al., 2010).

# Appendix E.

## Publications at National Taiwan University



1. Hsiao, N. C.\*, Y. M. Wu, L. Zhao, **D. Y. Chen**, W. T. Huang, K. H. Kuo, T. C. Shin, and P. L. Leu, 2011, A new prototype system for earthquake early warning in Taiwan, *Soil Dyn. Earthquake Eng.*, **31**, 201-208.
2. Lin, T. L., Y. M. Wu\*, **D. Y. Chen**, N. C. Hsiao, and C. H. Chang, 2011, Magnitude estimations in earthquake early warning for the 2010 JiaSian earthquake, Taiwan, *Seismo. Res. Lett.*, **82**, 201-206.
3. Lin, T. L., Y. M. Wu\*, and **D. Y. Chen**, 2011, Magnitude estimation using initial P-wave amplitude and its spatial distribution in earthquake early warning in Taiwan, *Geophys. Res. Lett.*, **38**, L09303.
4. **Chen, D. Y.**, T. L. Lin, Y. M. Wu\*, and Nai-Chi Hsiao, 2012, Testing a P-wave Earthquake Early Warning System by Simulating the 1999 Chi-Chi, Taiwan, Mw 7.6 Earthquake, *Seismo. Res. Lett.*, **83**, 103-108.
5. Hsieh, C. Y., T. L. Lin\*, Y. M. Wu, and **D. Y. Chen**, 2012, Source Uncertainty Estimation in Seismic Intensity Determination of the Taiwan Region, *Bull. Seism. Soc. Am.*, **102**, 848-853.
6. Chang, C. H., Y. M. Wu\*, **D. Y. Chen**, T. C. Shin, T. L. Chin, and W. Y. Chang, 2012, An Examination of Telemetry Delay in the Central Weather Bureau Seismic Network, *Terr. Atmos. Ocean. Sci.*, **23**, 261-268.

- 
7. Wu, Y. M.\*, **D. Y. Chen**, T. L. Lin, C. Y. Hsieh, T. L. Chin, W. Y. Chang, W. S. Li, and S. H. Ker, 2013, A high density seismic network for earthquake early warning in Taiwan based on low cost sensors, accepted by *Seismo. Res. Let.*, **84**, 1048-1054.
  8. Hsieh, C. Y., Y. M. Wu\*, T. L. Chin, K. H. Kuo, **D. Y. Chen**, K. S. Wang, Y. T. Chan, W. Y. Chang, W. S. Li, and S. H. Ker, 2014, Low Cost Seismic Network Practical Applications for Producing Quick Shaking Maps in Taiwan, *Terr. Atmos. Ocean. Sci.*, **25**, 617-624.
  9. **Chen, D. Y.**, N. C. Hsiao, and Y. M. Wu, 2015: The Earthworm based earthquake alarm reporting system in Taiwan. *Bull. Seismol. Soc. Am.*, **105**, 568-579.
  10. **Chen, D. Y.**, Y. M. Wu\*, T. L. and Chin, 2015, Incorporating Low-Cost Seismometers into the Central Weather Bureau Seismic Network for Earthquake Early Warning in Taiwan, *Terr. Atmos. Ocean. Sci.*, **25**, 617-624.